Traceability of Measurements in Optical Coordinate Measuring Machines

by
Zamokuhle Luthuli

Thesis presented in partial fulfilment of the requirements for the degree of Master of Engineering (Mechanical) in the Faculty of Engineering at Stellenbosch University

Supervisor: Prof K Schreve

December 2020

DECLARATION

By submitting this thesis electronically, I declare that the entirety of the work contained therein is my own, original work, that I am the sole author thereof (save to the extent explicitly otherwise stated), that reproduction and publication thereof by Stellenbosch University will not infringe any third party rights and that I have not previously in its entirety or in part submitted it for obtaining any qualification.

Date: .....

Signature: .....

Abstract

Optical coordinate measurement systems (photogrammetry or fringe projection) are gaining acceptance in the measurement industry. Their portability, scalability and ability to scan large areas instantaneously make them very attractive to the industry. Measurements on these systems can be taken with any type of camera, from a compact cell phone camera to high-end digital cameras. Basic triangulation can be accomplished with simple programs and there are many open-source packages available. For high-quality measurements, the cost of such a system can be very significant.

Despite the growing use of these optical systems in various industry sectors, there is currently no internationally accepted standard to establish their traceability to the length standard. The VDI/VDE (German standard) standard is widely used for verification of these systems using non-complex artefacts that are easy to measure and have already been calibrated with other traceable measuring machines, e.g. the sphere, gauge-blocks, etc.

Achieving traceability of measurements in optical systems is a very big challenge. This is because camera-based measurements are fraught with many challenges, e.g. changing camera settings or moving cameras relative to each other completely changes the configuration of the system and normally requires an entirely new calibration. Changes in light conditions can also affect the measurements over and above the normal ambient effects. Based on a survey and literature review, the state of the art of optical coordinate measurement systems and the challenges to establishing a traceability standard were investigated in this research. The urgent need for such a standard in the South African industry was also demonstrated by this research.

Owing to the wide range of uncertainty contributors, it is a time consuming and difficult task to set up a robust uncertainty analysis for optical CMMs. The Virtual CMM technique offers a better solution to such a problem. The Virtual CMM technique has only been applied to tactile CMMs and articulated arm optical CMMs, also known as discrete point systems since they measure one point at a time. The development and application of the Virtual CMM technology to stereovision scanning optical CMMs was demonstrated in this research. Finally, successful measurements that conform with other measurement systems were taken with the developed stereovision system using the Virtual CMM technique.

Opsomming

Optiese-koördinaat-meetmasjiene (fotogrammetrie of randprojeksie) word toenemend in die metrologie industrie aanvaar. Hul draagbaarheid, vermoë om te skaleer en vermoë om groot areas oombliklik te skandeer, maak hulle aantreklik vir die industrie. Enige tipe kamera, van ’n kompakte selfoonkamera tot hoëvlak digitale kameras, kan gebruik word vir hierdie meetstelsels. Eenvoudige programme kan basiese driehoeksmeting doen en daar is heelwat vryelik beskikbare programmatuur beskikbaar. Die koste van so ’n stelsel vir hoë kwaliteit metings kan egter baie beduidend wees.

Ten spyte van die toenemende gebruik van hierdie optiese-stelsels in verskeie industriesektore, is daar tans geen internasionaal aanvaarde standaard om die naspeurbaarheid tot die lengtestandaard te bevestig nie. Die VDI/VDE (Duitse standaard) standaard word wyd gebruik vir verifikasie van hierdie stelsels deur van eenvoudige artefakte gebruik te maak, wat maklik is om te meet en wat reeds gekalibreer is met ’n ander naspeurbare meetmasjien, bv. ’n sfeer, maatblokkies, ens.

Dit is baie moeilik om naspeurbaarheid van optiese-stelsels te behaal. Dit is omdat kamera gebaseerde metings belaai is met uitdagings, bv. die verandering van die kamera instellings, of deur die kameras relatief tot mekaar te beweeg, verander die konfigurasie van die stelsels en vereis normaalweg dat die stelsel weer gekalibreer moet word. Bo en behalwe die normale omgewingsfaktore kan veranderinge in die lig kondisies ook die metings beïnvloed. Die jongste stand van optiese-koördinaat-meetmasjiene en die uitdagings tot gestandaardiseerde naspeurbaarheid is hier ondersoek deur ’n opname en literatuuroorsig. Die dringende behoefte vir so ’n standaard in die Suid Afrikaanse industrie is ook deur hierdie navorsing gedemonstreer.

Die wye verskeidendheid van onsekerheidsfaktore maak dit baie tydrowend en moeilik om ’n robuuste onsekerheidsanalise op te stel vir optiese-koördinaat-meetmasjiene. Die virtuele KMM (koördinaat-meetmasjien) tegniek bied ’n beter oplossing vir die probleem. Die virtuele KMM tegniek is tot nou nog net op kontak KMM’s en geartikuleerde arm optiese KMM’s, ook bekend as diskrete punt stelsels omdat hulle een punt op ’n slag meet, gebruik. Die ontwikkeling en toepassing van virtuele KMM tegnologie op stereovisie skandering optiese KMM’s is gedemonstreer in hierdie navorsing. Laastens is suksesvolle metings, wat ooreenstem met ander meetstelsels, geneem met die ontwikkelde stereovisie stelsel en die virtuele KMM tegniek.

Dedication

To my family and friends, without their encouragement and prayers to Shembe uNyazilwezulu, this thesis would not have been possible.

Acknowledgment

I would like to express my deepest gratitude to the following individuals and institutions for their contributions towards this research:

- My Heavenly Father (Shembe uNyazilwezulu) without him this dissertation would not have been possible.
- My supervisor Professor Kristiaan Schreve for his unwavering support, collegiality and mentorship throughout this project.
- My family and friends for their non-failing sympathy and encouragement.
- Stellenbosch Mechanical Engineering workshop staff for their collegial guidance and support throughout this project.
- My sponsor NMISA for sponsoring the whole research study.
- Finally, the following NMISA workers for their collegial guidance, constructive criticism and support over the period of this project:
    - K. Tilholoe in the HR department.
    - O.A. Kruger, the head of the Length department.
    - P. Greeff in the Length department.
    - K. Manana in the Length department.
    - P. Kuduntwane in the Length department.

Table of Contents

List of Figures

List of Tables

Nomenclature

CMM	Coordinate Measurement Machine or Coordinate Metrology Machine
DLT	Direct Linear Transform
GUM	Guide to the Expression of Uncertainty in Measurements
ISO	International Standardization Organisation
NMISA	National Metrology Institute of South Africa
PTB	National Metrology Institute of Germany
UMM	Universal Measuring Machines
VAACMM	Virtual Articulated Arm Coordinate Measuring Machine
VCMM	Virtual Coordinate Measurement Machine
NIST	American Metrology Institute
NSAI	National Standards Authority of Ireland

Chapter 1: Introduction

1.1 Subject and Motivation

This thesis is concerned with the investigation of traceability of measurements in optical coordinate measuring machines in various South African industries and developing a virtual optical coordinate measuring machine to establish traceability.

1.2 Background of the Report

The National Metrology Institute of South Africa also referred to as NMISA was established in 1947. "*NMISA is part of the department of trade and industries family of technical infrastructure institutes. Metrology standards, procedures and regulations are some of the family responsibilities. The family is also responsible for accreditation in South Africa for the purpose of confidence in goods and products. The accreditation ensures prosecution in cases of non-compliance. The mission and vision of NMISA is to be a measurement centre of excellence inspired to deliver outstanding, innovative and internationally comparable measurement solutions that support the country's trade and people's quality of life*" [1].

The Length Section at NMISA maintains and disseminates the standards for length measurements in South Africa. As part of the dissemination, the section investigates new types of measuring equipment used in the metrology industry. One of the growing areas is the field of optical coordinate measuring machines. The growing popularity of these systems is due to their mobility and portability, scalability, and the ability to scan a large area instantaneously. Figure 1 is a traceability chart of NMISA which shows the position of optical coordinate measuring machines in the NMISA traceability chain. Traceability refers to the property of measurement results whereby it can be related to stated references, usually national or international standards through an unbroken chain of comparisons, all having stated uncertainties [2]. This will be further discussed later in Section 2.5.

In this report, Coordinate Measuring Machine is abbreviated as CMM. Optical CMMs refers to all the non-contact 3D scanners that use cameras or camera images to realize measurements, e.g. passive light non-contact 3D scanners, structured light non-contact 3D scanners, stereovision 3D scanners, photogrammetry 3D scanners, etc. In cases where the report refers to all the non-contact 3D scanners in general or it refers to a specific type of optical CMM, this will be specified. On the other hand, all contact 3D scanners are referred to as tactile CMMs in this report.

It is a difficult and challenging task to achieve traceability in optical CMMs. In these systems, any type of camera can be used when taking measurements, from a compact cell phone camera to high-end digital cameras, with the best quantitative and qualitative results depending on the type of imaging sensor, the software used and the shape of the workpiece [3]. For high-quality measurements, the cost of such an optical CMM can be very high and the system must be inspected on installation and during operation to ensure that traceability of measurements is achieved [4].

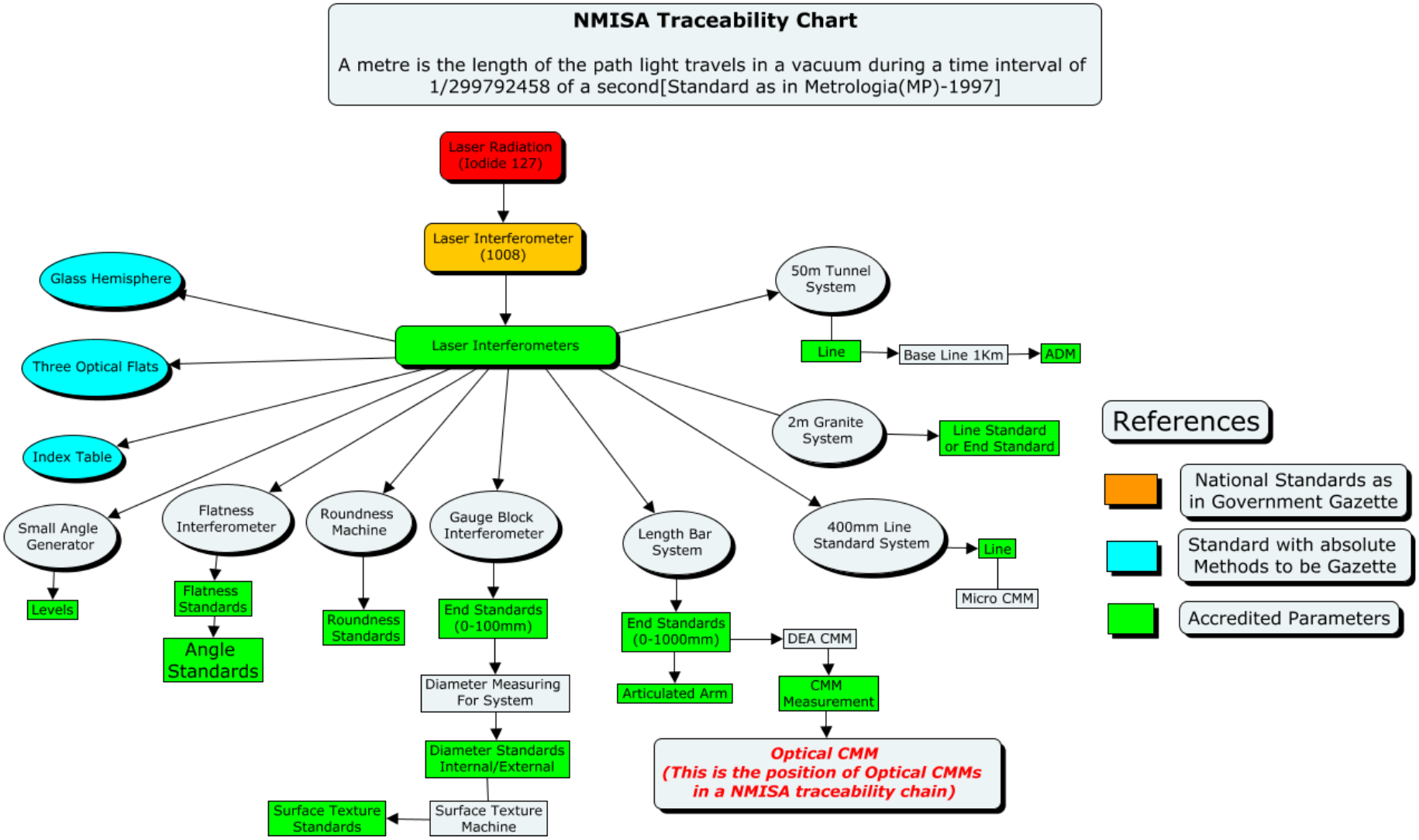

Figure 1: Flowchart of the NMISA traceability chain in 2018 [5]

Although these optical CMMs can be very accurate systems, their users are faced with many challenges other than cost and installation check-ups [4]. For instance, changing the camera size or moving cameras relative to each other completely changes the geometric configuration of the system [6]. This change normally requires an entirely new calibration of the system. Changes in light conditions can also affect the measurements over and above the normal ambient effects. Light interacts differently with optical CMMs compared to the way it interacts with tactile CMMs. When using an optical CMM, the user is required to understand the measurement situation in terms of light absorption, transmission, reflection scattering and diffraction [7].

The chart in Figure 2 shows all the 3D scanner groups that are available. A lot of research has been done to achieve traceability in most of the 3D scanners shown, but for optical CMMs, there is currently no internationally accepted traceability standard [8]. Standards applicable to each CMM type are shown in the chart in Figure 3.

To limit the scope of this research, the focus of this report will be on the camera-based 3D scanners, i.e. optical CMMs. In some countries, there are published traceability procedures and national standards that are available for optical CMMs, e.g. Germany has a VDI/VDE standard. South Africa has not yet established any national standard or procedure. Not having the international standard or national standard, limits the use of these optical CMMs as quality control tools in the South African industry. Considering the fact that optical CMMs can be designed as portable machines and they can take more data points at a faster rate than tactile CMMs, a factory may use only one optical CMM to do all of its measurements [4]. This shows that the economic impact of these systems can potentially be very significant for South Africa.

The effort of the International Standardization Organisation (ISO) to have such a standard has not been successful yet. Without a standard to demonstrate measurement uncertainty, these systems cannot be used for quality control in a globally competitive manufacturing world and companies must revert to possibly slower and more expensive measurement methods. An acceptable standard could unlock the economic potential of optical CMMs in South Africa.

1.3 Research Question

South Africa is one of many countries without a traceability standard or procedure for optical CMMs. Therefore, the first question to ask is how companies in various South African industrial sectors currently achieve traceability of measurements in optical CMMs, and secondly, how can traceability of measurements from optical CMMs be achieved?

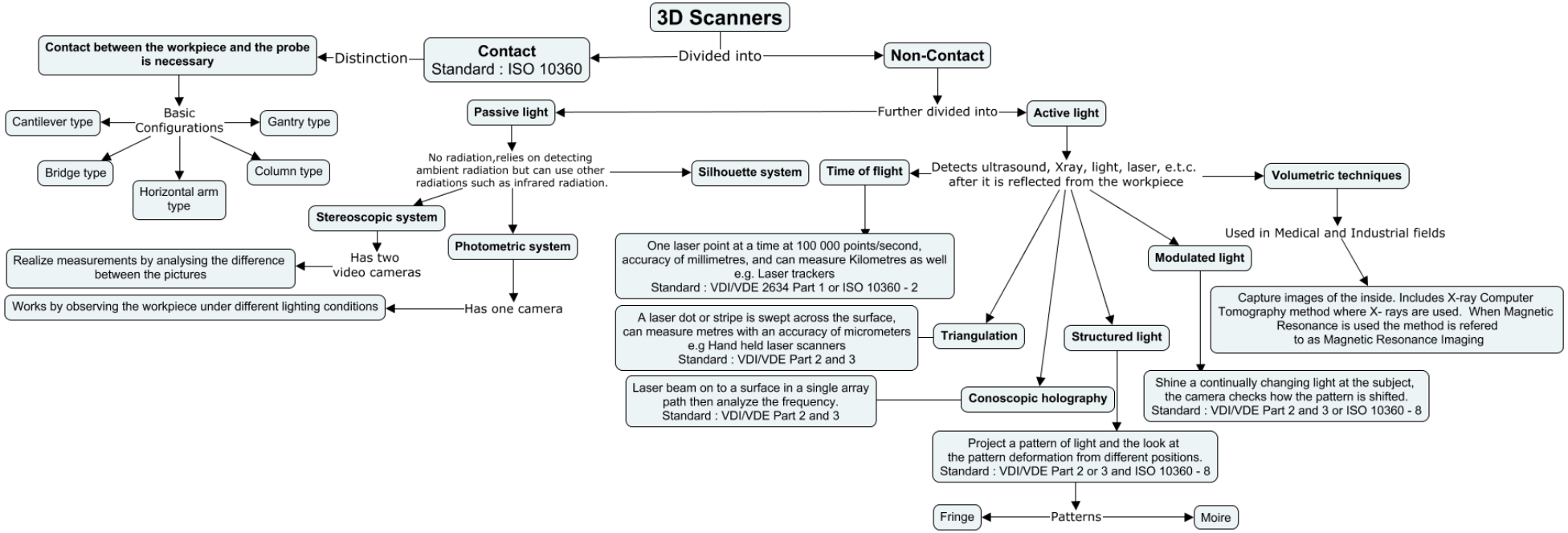

Figure 2: Flowchart of all types of 3D scanners

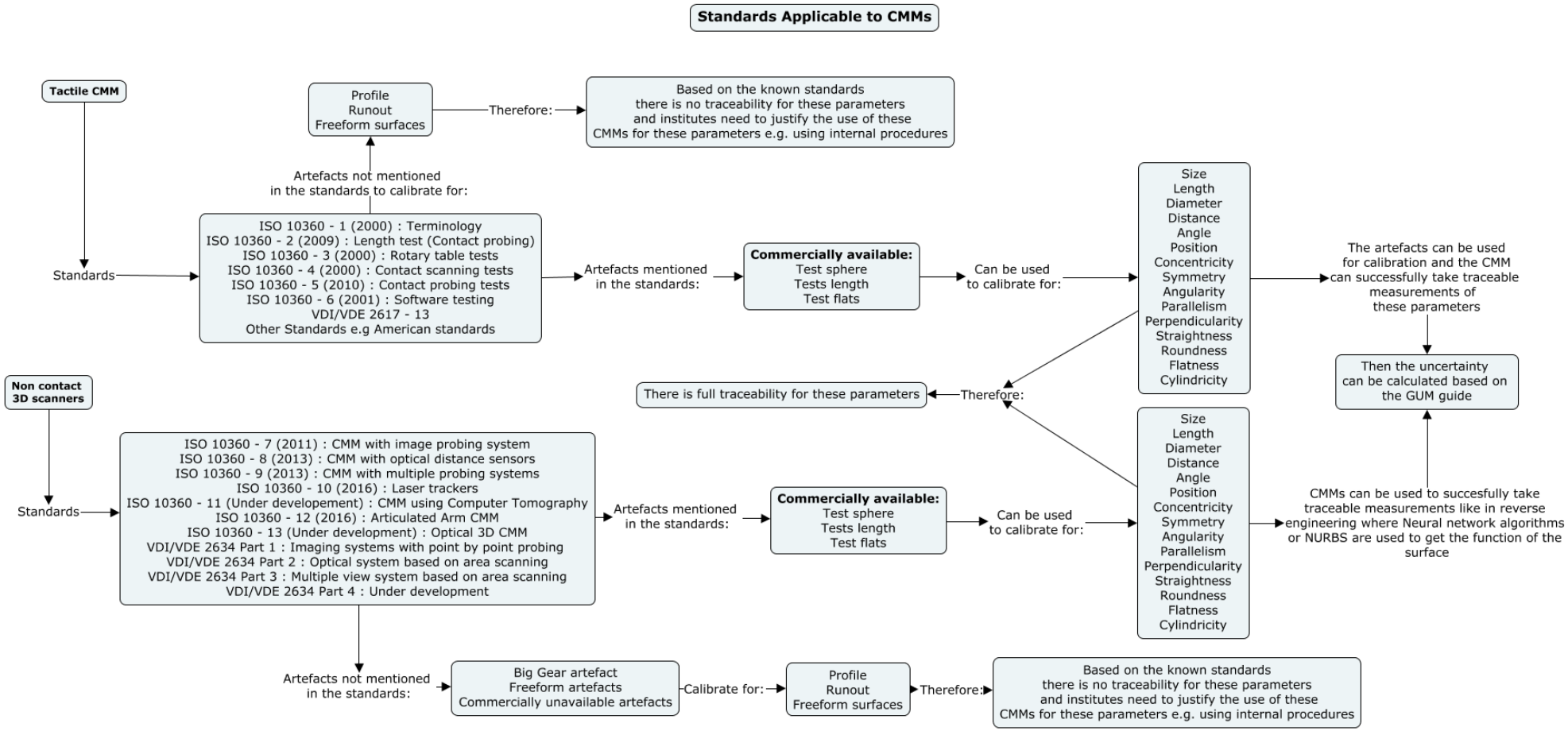

Figure 3: Flowchart of all standards applicable to various 3D scanners

1.4 Objectives

The main goals of this project are to evaluate how traceability is currently achieved in the South African industry and to develop a new procedure to achieve traceability in optical CMMs. These goals will be achieved based on the following objectives.

- The review of literature related to optical CMMs.
- The review of existing traceability standards in the field of optical CMMs.
- The comparison between the existing standards and procedures.
- A survey on the use of CMMs in various South African industries, paying more attention to the use of optical CMMs.
- Investigation of the challenges faced by optical CMM users and the effect of these challenges on the traceability of measurements.
- Comparison study of an optical CMM and a tactile CMM using a calibrated artifact.
- Develop and make a Virtual CMM to address the traceability challenges in optical CMMs. A Virtual CMM is a CMM that performs a point by point simulation of measurements, emulating the measurement strategy and the physical behaviour of the CMM with the dominating uncertainty contributors disturbing the measurement [9]. This will be further discussed in Section 2.8.
- Conclusions and recommendations will be made based on all the above objectives.

1.5 Thesis Outline

The main objective of this thesis is to achieve traceability in optical CMMs. Therefore, it is important to review the existing literature and traceability standards related to these systems. Chapters 2 and 3 are the main body of the thesis. Chapter 2 reviews the related literature which includes an investigation of traceability challenges in optical CMMs and in Chapter 3 measurements using different systems are taken. In Chapter 4, a Virtual CMM is developed, tested and used to take measurements of a known artefact. After a discussion of the results from Chapter 3 and 4, the thesis is ended with a conclusion.

Chapter 2: Literature Review

2.1 Introduction

A lot of research and development has been done in the field of coordinate metrology systems. This chapter intends to briefly review the relevant literature. In one of the sections of this chapter, a survey on the use of coordinate measuring machines in the South African industry was done. A section on the challenges faced by users when using optical CMMs is also included.

2.2 Metrology in General

Metrology is defined by the National Standards Authority of Ireland (NSAI) as the science of measurements [10]. National metrology institutions around the world ensure that measurement instruments in use are fit for the purpose. The basic activities of any metrology institute include defining internationally acceptable units of measurements (SI), the realization of the units of measurements in practice (e.g. realization of a meter by establishing a gauge block), and establishing traceability of these measurements [11]. When taking measurements, a number relating the item under investigation and the referenced unit is acquired. It is imperative that there is a comparison between the referenced unit and the number acquired to ensure accuracy, precision and traceability of the measurement.

Measurement instruments, like any other instrument, are subject to many degrees of instrument error and uncertainty. The measurements taken with these devices are of great importance to the engineering and scientific communities. These measurements are used in different industries, e.g. to ensure the safety and effectiveness of health care diagnosis and treatment or to get accurate and precise results in a scientific research. This emphasizes the need to ensure that all measurements are correct and can be traceable to the same measurement standard.

The field of metrology is generally divided into the scientific or fundamental metrology, applied (technical or industrial) metrology and legal metrology [12]. Scientific metrology is concerned with the establishment of quantity systems, unit systems and units of measurements, the development of new measurement systems and methods, the realization of measurement standards and ensuring that traceability is transferred from the standards to the users in the society [12].

The industrial metrology subfield deals with the application of measurement science to the manufacturing processes [12]. It ensures the suitability of measurement instruments, their calibration and quality control of products. The emphasis here is on the measurements themselves and the traceability of these measurements to ensure that there is more confidence in the measurements taken by any measuring instrument.

The legal metrology subfield deals with activities that result from statutory requirements [12]. It concerns the legal requirements of the measurement process. It establishes necessary rules and regulations on the quality and control of measuring instruments and their use. Legal metrology also helps to detect fraudulent measurements.

There are also other subfields of metrology that have more to do with the application of metrology like forensic metrology and nanometrology. In forensic metrology, numerous measurements and tests are performed to support both criminal and civil legal actions. Whereas in nanometrology, nanoprobes are used to measure nanoparticle characteristics. Figure 4 shows all the subdivisions of the metrology field.

The work done in the metrology field is very important and other industries depend on this work. For instance, the goal in the manufacturing industry is to provide quality products and services to customers. The quality product must meet the requirements of the user and have the stipulated dimensions. Measurements cannot be perfect, but the user needs to have confidence in the measured results. This confidence is dependent on the measuring instrument's accuracy, which must be investigated via calibration of the instrument. Calibration needs to be carried out as per standard. Several calibration laboratories at different levels exist, e.g. the in-house calibration labs, the professional calibration labs and the national physical labs like NMISA. These labs help to ensure that all measurements are traceable [12].

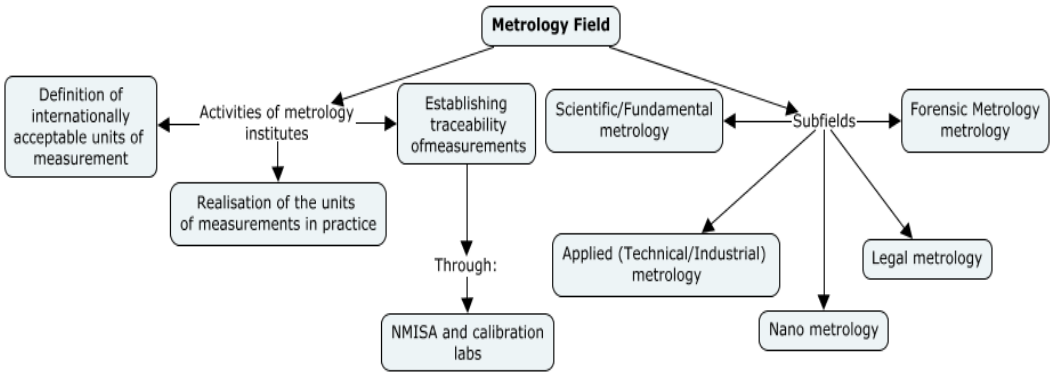

Figure 4: Flowchart of Metrology subfields [11]

2.3 Coordinate Measuring Machines

Universal Measuring Machines (UMM), e.g. micrometers, can be used to quantify inside or outside dimensions, angles and threads. There has been a transition in the metrology industry from using UMMs to using CMMs due to the need for devices that can do faster first piece inspection with a high turnaround. CMMs play an important role in the mechanization of the inspection process and can generally be divided into two types; contact CMMs and non-contact CMMs [13]. Generally, contact CMMs can also be referred to as tactile CMMs whereas non-contact CMMs can also be referred to as optical CMMs. But in this report as mentioned in Section 1.2, "non-contact 3D scanners" refers to all types of optical CMMs in general, and "optical CMMs" is reserved for camera-based non-contact 3D scanners.

2.3.1 Contact Type Coordinate Measuring Machines

Like UMMs, tactile CMMs measure the physical characteristics of an object and contact between the workpiece and the instrument is required to realize the measurement. An operator can manually control these machines or they can be computer-controlled. The data collection system typically includes a machine controller, a desktop computer and a software application. A probe attached to the third moving z axes of the machine takes the measurements [13]. These CMMs consist of a platform worktable to place the workpiece. Figure 5 shows an example of a tactile CMM.

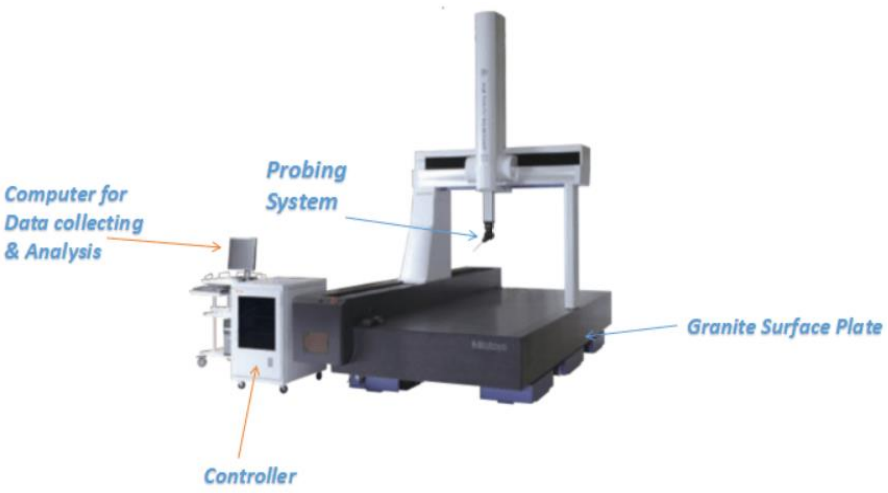

Figure 5: Example of a tactile CMM [14]

They are versatile in their ability to record measurements of complex profiles with high sensitivity (0.25 micrometers) and speed [11]. These systems have a rugged design to resist environmental effects in manufacturing plants such as temperature fluctuations, vibration and dust. All the moving members, the bridge structure, z axes carriage and z column are made of hollow box construction. This is done to ensure maximum rigidity of the machine without excessive weight [15]. Each axes has a scale system that shows the location of that axes.

The machine will read the input from the probe as directed by the user or CNC program. Then the machine uses the x y z coordinates of each of the points read by the probe to calculate the size and position of the workpiece with micrometer precision [15]. In some cases, an accuracy of 24 nanometres has been achieved [16]. These machines can be designed to have air bearings, ensuring a frictionless travel. In these air bearings, compressed air is forced through a series of small holes in a flat bearing surface to provide a smoothly controlled air cushion on which the CMM can move without friction [15].

In the case of a complicated workpiece, there are rotary tables that can be used to improve the movement of the measuring probe when it approaches the workpiece. Some CMMs have their own computer which consists of an interactive dialogue facility and a friendly software. Systematic errors in the machine are built up and fed into the computer system so that the software automatically compensates for the errors which increase the accuracy and precision of the CMM [15].

In the manual operation mode, the CMM has a free-floating probe. The operator moves the x y and z axes to establish contact with the workpiece. In the manual computer-assisted operation mode, electronic digital displays are incorporated into the CMM to make zero settings, to select units and to print data in the standard format [11].

These electronic digital displays save time, minimize calculations and reduce errors. In motorized computer-assisted CMMs, the machine axes are controlled with a joystick. The operator brings the probe into contact with the workpiece through a series of manipulations of the joystick. Whereas a direct computer-controlled CMM is fully programmable, the CMM uses the workpiece CAD data to decide where the probe makes contact with the workpiece and then collect the measurement data [15].

A fully automated CMM allows the user to place the workpiece on a table, run the CNC program, gather all the data and generate an output report [15]. There are different types of tactile CMM arrangements available, with the main parts of each arrangement being the main structure, machine control unit, probing system, automatic stylus changer, environment monitoring system, computer with CNC software and accessories. All of these configurations have a method of moving the probe along the three axes relative to the workpiece. The five-basic tactile CMM arrangements are the cantilever, the bridge, the horizontal arm, the column and the gantry type of CMM arrangement. Refer to [11] for more information on these CMM arrangements.

2.3.2 Coordinate Metrology Machine Probes

The basic CMM configurations can be fitted with different types of probe designs which can be grouped into four different types as follows [13]:

- The touch trigger probe
- The scanning probe
- The five-axis probe
- And the optical/vision probe

In the touch-trigger probe design as the probe makes contact with the workpiece, the electric circuit breaks. The computer records coordinate of this point of discontinuity. An LED (Light Emitting Diode) light and an audible signal indicate the contact between the stylus and the workpiece. Touch trigger probes measure discrete points, making them ideal for the inspection of 3D geometric parts [17]**.** In the case of scanning probe design, the stylus remains in contact with the part surface as it moves. This probe design is generally used when measuring contour surfaces or complex and irregular shapes. The probes are miniature-measuring machines that can measure hundreds of surface points each second. Scanning probes can also similarly measure discrete points as a touch-trigger probe [17].

The CMM structure makes all the necessary movements required to acquire the surface data in conventional CMM measurement methods. CMM structure acceleration induces inertial deflection into the machine frame which in turn causes measurement errors [11]. Techniques have been developed to mitigate these dynamic errors, but there is an upper-speed limit imposed by the machine and servo system stiffness beyond which measurements cannot be taken with reliability.

A five-axis probe system was developed to address this issue. It uses an articulating head that moves in two rotary axes during the measurement process which allows the CMM to move at a constant velocity in a single vector while measuring [11]. This probe head is lighter and more dynamic than the CMM structure. The probe has the ability to quickly notice and follow changes in the geometry of the workpiece without inducing harmful dynamic errors.

This results in fast speeds on the surface of the workpiece and shorter measurement cycles. Five-axes scanning technology allows the operator to achieve extraordinary levels of throughput [11]. In a motorized five-axes probe head, an integral LCD allows for easy programming of the probe location. Multiple stylus heads are also possible and a stylus is selected based on the application.

These advanced probe heads increase inspection throughput up to three times using faster infinite rotary positioning and unique head touch capability [13]. The type and size of the stylus used depends on the feature to be inspected. However, the maximum rigidity of the stylus and perfect sphericity of the tip is always very important. The performance of gauging can be degraded if a stylus used is with poor ball roundness, poor ball location and bad thread fit or a compromised design that allows excessive bending during measurement [13]. Accuracy at the point of contact is achieved by keeping the stylus short, having a minimum number of joints and the stylus ball must be as large as possible [13]. A stylus is usually calibrated with a master ball calibration location before use. There are many other artefact shapes available for the calibration of tactile CMMs which will be discussed later.

When utilizing touch probes to determine the CMM scanning probe error, a sphere of diameter 25 mm with an insignificant certified form error is scanned along four recommended scanning lines [18]. The time required for this test must be stated since speed has a huge influence on the results. Calibration can also be done using a laser or using slip gauges. If the workpiece is complex, the stylus must be changed to suit the different measurement tasks, e.g. accessing deep features that require a long or complex stylus, as well as using different stylus tips like spheres or discs or cylinders [13]. A stylus should be optimized for the application to ensure sound measurement results. A stylus can be changed manually using a threaded connection, but recalibration is required when changing the stylus if the probe system is not with a repeatable and automated means to switch the stylus.

With the help of an optical probe also known as a vision probe, a CMM can be used as a microscope for electronic circuits, micro holes and elastic bodies. The image captured by the optical probe has various edge detections performed by the dedicated CMM software which also performs the necessary calculations such as calculation of dimensions and geometric deviations [11]. An automatic probe changer can be used to mount the optical probe, allowing fully automated measurement including both contact and non-contact type of measurements. When an optical probe is used, the CMM is no longer referred to as a tactile CMM but an optical CMM.

With powerful image processing tools, an optical probe can detect the various forms of edges at a very high speed. It can determine measurements in the height direction utilizing its autofocus function and save the captured image. In ordinary microform measurements, it is often difficult to remove burrs and dust from the objective workpiece resulting in an inevitable measuring error. However, the advanced optical probe software can recognize these obstructions and bypass them during measurements [19].

The combination of a 3D vision system and a touch trigger probe with its ability to reach undercuts and similar features not accessible to the camera results in an extremely productive machine on most workpieces due to its high intensity LED stroboscopic image capturing technique that operates while the stage is moving [20]. This combination eliminates the time required to accelerate, decelerate and then hold the stage stationary while taking the measurement. There is a lot more that has been done to optimize CMMs like programmable ring lighting to provide flexibility in the lighting orientation and intensity to achieve maximum surface contrast for best image resolution.

2.3.3 Non-Contact Type Coordinate Measuring Machines

The other types of CMMs are referred to as non-contact CMMs or optical CMMs. These CMMs typically consist of a dual-camera system, optical probe (non-contact/wireless), data acquisition system, storage, processing system and display system. The camera monitors both the probe and the workpiece. Optical CMMs are used in the production lines of big industries like automotive, aerospace and manufacturing industries. These systems are highly efficient in measuring parts that cannot be moved to a worktable, and they are ideal for geometric and surface quality control [21]. These systems can also be used for scanning purposes and they can successfully measure most types of materials like soft or porous materials. To measure a shiny or transparent material, spraying of the workpiece is necessary. This introduces an error due to the spray thickness on the workpiece measurements, this will be further discussed later in this report.

Cameras in an optical CMM can simultaneously observe the target's position on the probe and the workpiece, this makes it possible to calculate the workpiece dimensions using the optical triangulation technique [21]. Arm free probing systems give total freedom of movement and significantly increases productivity. The sensors of the dual cameras are fitted with high-quality optics and special lighting to enable them to measure all reflectors placed on the workpiece within their operating space [21].

The dedicated software in the case of optical CMMs does more than just help to efficiently run the system. The software guides the operator every step throughout the measurement process. It clearly and instantly advises the operators to take more images if necessary. This increases the accuracy of measurements. Real time visualization and validation of the positioning model allows the operator to see the rebuilt volume and all estimated points with accuracy [21]. The software measures and precomputes all the identified points each time an image is captured.

It is possible to create a virtual metrology lab by connecting up to four optical CMMs in a single network [22]. This allows seamless probing and 3D scanning operations using the probe or 3D scanner and optical CMMs without having to manoeuvre the optical tracker to the workpiece.

Another type of non-contact 3D scanning system is the laser scanner. This system can take between 100 and 1000 images per second and it is normally used in weld joint preparation check-ups [19]. The vision system moves along with the processing machine for inspection. This 3D contour digitization detects small weld defects and gets enough data to track the joint at a speed of 1 to 20 meters per minute which is compatible with the welding speed [19]. Laser vision sensors are used in conjunction with robots for seam tracking on components ranging from the chassis to the body of a vehicle. They can also be used to automatically visually inspect pipes, tubes and pipeline welding.

2.4 Optical Measurement Techniques

The development of automation in all the fields of industry and on the consumer market is associated with the development of technologies to make a machine conscious of its environment and its location in that environment [23]. This three-dimensional environmental consciousness is realized by using 3D vision technologies.

Several different technologies are available today for 3D vision, mainly based on one of the following three operating principles [23].

1. Structured light
2. Stereovision
3. Time of flight

The structured light principle works by projecting a known pattern onto a scene, then observing the way this pattern is deformed, giving us information to calculate the distance. However, this technology has limitations in bright sunlight conditions or when high resolution is needed as it requires expensive and large projectors and a lot of computation afterward to get the distance data [23].

Stereovision is based on the use of two cameras that need to be accurately positioned relative to each other. When correlating the two images from these cameras, it is possible to generate the depth map using the triangulation technique [23]. This technology for 3D vision has an advantage of the relatively low cost of the sensors and a good resolution. But all of this depends a lot on the lighting conditions of the observed scene. Unfortunately, it has a high computer processing cost and it might require significant space due to the distance between the two cameras [23].

Indirect time of flight technology works by illuminating a scene using modulated light and measuring the phase delay of the returning light after it has been reflected by the workpiece [23]. The phase delay is then measured and converted to a distance measurement. The advantages of indirect time of flight technology are high frame rate due to low computation required and a relatively low cost [23]. The technique of optical triangulation is a process of determining the location of a point in space by forming triangles to it from pre-determined points. The process is also used in optical 3D measuring systems where there will be two sensors observing the item [19]. Typically, one of the sensors is a digital camera device and the other sensor can also be a camera or a light projector as shown in Figure 6.

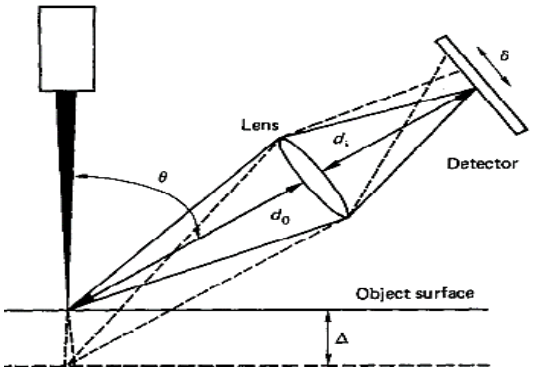

Figure 6: Diagram showing the optical triangulation technique [19]

The projection centres of the cameras and the considered point on the workpiece surface define a triangle. Within this triangle, the distance between the sensors is known and referred to as a base. The intersection point in a 3D space is calculated from triangular relations by defining the angles between the projection rays of the sensors and the base [19]. Systems based on this technique can measure multiple 3D points at the same time.

There are many other optical measurement techniques that are not covered in this report used in non-contact 3D scanning technology like interferometry and Moiré projection. Interferometry realizes measurements through the interference of light [24]. In optics, Moiré refers to a beat pattern produced between two gratings of approximately equal spacing [25]. When these patterns are superimposed, they form what is referred to as fringe patterns. Fringe projection entails projecting a fringe pattern on a workpiece and viewing it from different directions.

Fringe projection is associated with optical triangulation using a single point of light and light sectioning where a single line is projected onto an object and viewed from different angles to determine the surface contour. Fringe projection is a convenient technique for contouring objects that are too rough to be measured with the standard interferometry technique. Moiré and fringe projection interferometry complements conventional holographic interferometry, especially for testing optics to be used at long wavelengths [25].

2.5 Traceability of Length Measurements in Optical CMMs

One of the main activities of metrology is ensuring that all measurements are traceable and that measuring instruments are fit for their purpose. Traceability of measurements is ensured by developing standards as well as artefacts that can be used as a means of ensuring that the traceability chain is not broken. ISO 9001 [26], ISO 17025 [27] and ISO 14253-1 [28] are some of the international standards that make traceability of measurements a requirement. These traceability standards need to have comprehensive test procedures (capable of detecting errors) and should be practical (in terms of time and effort involved in realizing them) [29].

According to the international vocabulary of metrology, *"traceability is the property of the result of a measurement or the value of a standard whereby it can be related to stated references, usually national or international standards, through an unbroken chain of comparisons, all having stated uncertainties"* [2]. This means that for any measuring instrument to be traceable, the measurement results obtained by the instrument have to be traceable to the SI units through a chain of calibrations achieved through an acceptance criteria and reverification of the instrument measurements at regular intervals [20]. This responsibility of ensuring the traceability of measurements lies with the manufacturer (The manufacturer determines the maximum possible error and makes recommendations on the calibration interval) and the users of the measuring instrument.

In the case of CMMs, all the tactile CMMs and CMMs in the mid - long range category of CMMs described in Appendix A.3 have internationally recognized standards that are used to ensure traceability of measurements in these systems even though there are still some developments and improvements being done on these standards.

In the case of optical CMMs in the close-range category described in Appendix A.2, it is widely accepted that no internationally recognized standard ensures traceability of measurements. The German VDI/VDE standard is currently the most developed in this regard.

Although optical CMMs are very efficient machines and many companies are moving towards using these machines as quality control tools, these machines are fraught with many traceability challenges and error sources, with most of them mentioned below:

- In photogrammetric systems, changing the camera size requires recalibration of the system.
- In photogrammetric systems, moving cameras relative to each other completely changes the geometric configuration of the system.
- Changes in camera settings require recalibration of the system.
- Changes in light conditions (too much light or less light or change in a light colour) or taking measurements in different light conditions requires recalibration of the system.
- Light intensity changes occurring in the measurement process influences the measurement uncertainty.
- Any type of camera can be used to do the measurements which makes it difficult:
    - For a traceability standard to cover all types of cameras.
    - For the user to calibrate the optical system for all types of cameras.
    - For the user to do the uncertainty analysis.
- A user needs to understand a measurement situation in terms of light absorption, transmission, reflection, scattering and diffraction [30]. This can be time-consuming and difficult for some materials.
- It is not possible to make conclusions only from measured error components of the CMM on the uncertainties of the measured results [30].
- It is impossible to relate the spot check results obtained in the acceptance test (with calibrated measurement standard) to the measuring results even of any similar measuring task [30].
- Most 3D imaging systems cannot measure a single point and can only scan a region and produce a point cloud, this brings up two issues which are sources of error [29]:
    - The fact that the points are inherently noisy.
    - And the question of which point in the point cloud to use.
- Range discontinuity on a surface affects the measurement accuracy of 3D imaging systems [31].
- Continuity between surfaces may affect the profile measuring capability of a 3D imaging system [6].

These above error sources make it difficult to calculate the uncertainties when dealing with optical CMMs. Thus, making it difficult to achieve traceability of measurements in optical CMM. Generally, there are two steps in metrology that are necessary for checking the accuracy of the CMM and for obtaining measurement traceability [32]. Firstly, the metrological performance verification and testing. Secondly, the assessment of a task specific measurement uncertainty.

The first step is described in the German guideline VDI/VDE 2617-13 that is intended for tactile CMMs, but the step description can also be applied to optical CMMs. In close reliance on ISO 10360-2, the VDI/VDE 2617-13 guideline describes the procedure for acceptable testing and for the monitoring of length measurement error.

In the second step described in the Guide to the Expression of Uncertainty in Measurements, i.e. the GUM Guide [33], a model is required that covers all the variables influencing the value being measured and that describes the effect of changes in these variables on the measurand. The same guide also describes a procedure for evaluating and reporting on uncertainty. The evaluation and expression of uncertainty are done in eight steps described in [33] as follows:

- *Step 1:* Mathematically express the relationship between the measurand Y and the input quantities X_i on which it depends: $Y = f(X_1, X_2, \ldots, X_n)$. The function f should contain every quantity, including all corrections and correction factors that can contribute a significant component of uncertainty to the measurement.
- *Step 2:* Determine x_i, the estimated value of input quantity X_i, either based on the statistical analysis of a series of observations or by other means.
- *Step 3:* Evaluate the standard uncertainty $u(x_i)$ of each input estimate x_i. For an estimate obtained from the statistical analysis of series of observations, the standard uncertainty is evaluated using Type A evaluation method, whereas if the input estimate is obtained by other means Type B evaluation method is used. The types of standard uncertainty evaluation methods are described in more detail in the GUM guide.
- *Step 4:* Evaluate the covariances associated with any input estimates that are correlated.
- *Step 5:* Calculate the results of the measurement, that is, the estimate y of the measurand Y, from the functional relationship f, using for the input quantities X_i the estimate x_i obtained in *step 2*.
- *Step 6:* Calculate the combined standard uncertainty $u_c(y)$ of the measurement results y from the standard uncertainties and covariance associated with the input estimates. If the measurement determines simultaneously more than one output quantity, calculate their covariances.
- *Step 7:* If it is necessary to give an expanded uncertainty U, whose purpose is to provide an interval $(y - U)$ to $(y + U)$ that may be expected to incorporate a large fraction of the distribution of the values that could reasonably be attributed to the measurand Y, multiply the combined standard uncertainty $u_c(y)$ by a coverage factor k.
- *Step 8:* Report the results of the measurement y together with its combined standard uncertainty $u_c(y)$ or expanded uncertainty U.

The GUM Guide is an internationally accepted guide for evaluating and expressing the uncertainty of measurements. In the case of optical CMMs, measurement uncertainty analysis must contain a clear definition of the measurand to be determined. According to [32], measurement traceability in optical CMMs can be achieved by developing a reference object, understanding the influence of all factors on the measurement and assessing methods for determining the measurement uncertainty. As can be seen in Figure 7, traceability is established in a multi-step process going back in an unbroken sequence to national or international standards [34]. Like all measurement instruments, measurements taken by using optical CMMs need to be traceable to a meter which is a recognized unit in the international system of units [35].

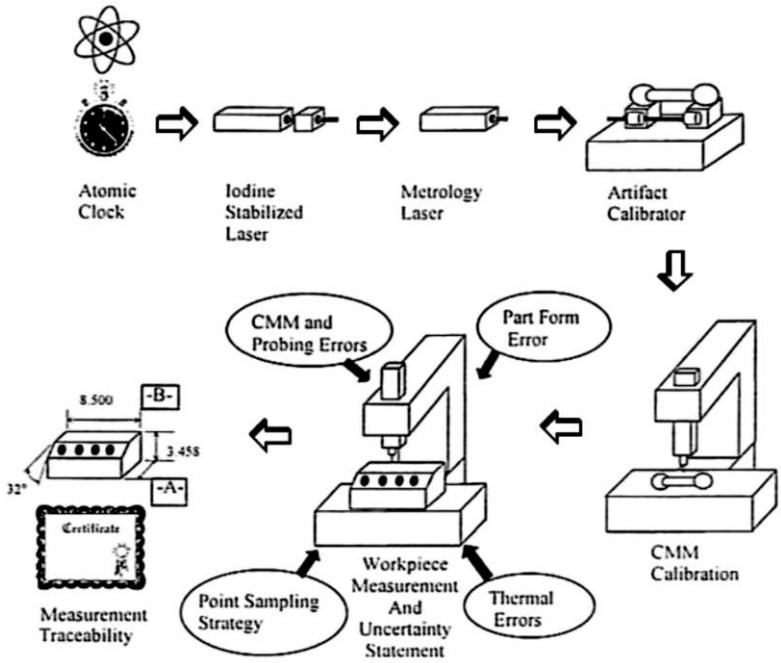

Figure 7: Flow diagram of typical traceability chain in CMMs [32]

It is very difficult to establish traceability of measurements from optical CMMs due to their versatility and complexity as measurement instruments. Achieving traceability requires a documented standard procedure and verification artefacts. Like in the case of tactile CMMs, ISO 10360 is the documented standard procedure and Figure 8 shows some of the available artefacts for these machines. It can be seen in Figure 8 that the artefacts are generally a combination of spheres, the length bar, cylinders and ring gauges.

Figure 8: Some of the existing artefacts (physical standards) for tactile CMMs [36]

On the other hand, verification procedures and more specifically verification artefacts for optical-based systems (all ranges) are still in their early stages, especially in South Africa. Some verification artefacts for these machines are shown in Figure 9. Furthermore, industries seek traceability in 3D measurements of high precision components, e.g. the need for highly accurate measurements of gears with diameters up to 1000 mm for gearboxes of wind turbines [36].

Figure 9: Some of the existing artefacts (physical standards) for optical CMMs [36]

In a research paper from the University of Maribor [36], three different types of artefacts were developed as a way of trying to achieve traceability when using optical CMMs. The paper describes the three artefacts that were developed during the project, namely tetrahedron artefacts for determining the basic measurement capability of optical 3D devices, freeform verification artefacts for testing the capability of measuring complex geometry and a large gear artefact for task-related calibration of several types of optical CMMs [36]. In addition, artefact calibration data with associated measurement uncertainties and international inter-comparisons were presented in the paper. Such developments are of considerable value to end-users, calibration laboratories and manufacturers of optical and tactile CMMs.

For the developments in [36], an internal performance verification procedure of non-contact measurement systems, SOP-36, was used and not the VDI/VDE standard. This is further discussed in Chapter 3. Another research and development project that has taken place over the years is the European project “EASYTRAC” with its main objective to significantly reduce efforts associated with the traceability of industrial dimensional metrology laboratories by means of the almost exclusive use of CMMs in combination with laser interferometers [37].

2.6 Survey of the South African Industry

The literature review shows that there are different procedures and standards that are available to be used as a way of ensuring that traceability is achieved when using optical CMMs. The German standard series (VDE/VDI 2634) seems to be the most developed of all the standards in this regard.

As a result, the expectation of a survey that was done by the author on the distribution of CMMs and the main calibration/measurement requirements was that most optical CMM users in South Africa are using the German standard to ensure the traceability of their measurements. Optical CMMs are very expensive machines and only those users in the industry that are well established can afford to buy and maintain such systems. Such users would be the educational institutions and big companies that are concerned with meeting the high-quality standards of their products. Therefore, it was also expected that most users are aware of the need for traceability of measurements and the need to calibrate their machines according to the time intervals recommended by the CMM manufacturers.

2.6.1 Methodology

The survey was done using the online Survey Monkey platform. All feedback was treated confidentially. The author only reported on the overall results of the survey. The results were reported based on the category in the survey – results based on specific CMM models and company names were not reported or mentioned. The survey was distributed as widely as possible amongst South African users and distributors of CMMs using emails and a link.

The purpose of the survey was to investigate the distribution of contact, laser and optical CMMs and to evaluate the main calibration or measurement requirements of the users. Questions that were used in the online platform to achieve the purpose of the survey can be found in Appendix B.

2.6.2 Survey Results of the South African Industry

Based on the information given by distributors of CMMs to NMISA and the online survey it is estimated that there are more than 504 CMMs in the South African industry as shown in Figure 10 [8]. These are complete CMM structures with each CMM capable of being fitted with different types of probes depending on the application.

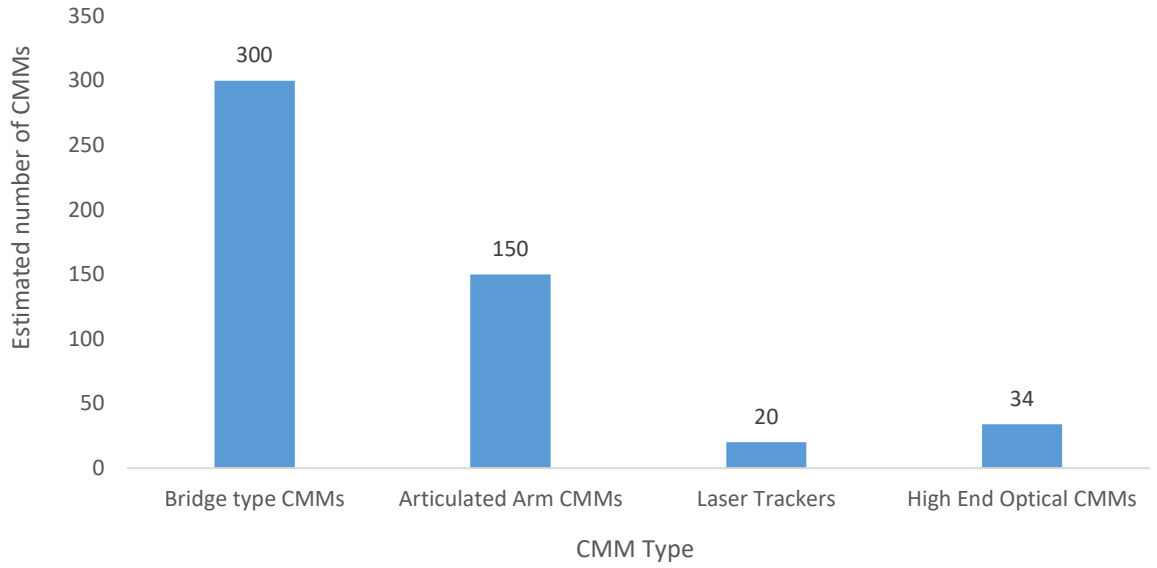

Figure 10: Histogram showing the number of CMMs in the South African industry [38]

The response to the online survey was very small, only 8.57% of the users responded to the survey. The survey shows that the users are aware of the importance of traceability of their measurements since they ensure that their CMMs are always calibrated. The users generally use CMMs for educational purposes, training, reverse engineering, quality control and inspection. Most users require a mobile system for the CMMs and they measure components ranging from 10 mm to 1000 mm with an accuracy requirement ranging from 0.005 mm to 1.000 mm, this is in the close-range category of CMMs as described in Appendix A.2.

2.6.3 Conclusion Based on the Literature Review and Survey

It is not easy to draw conclusions from the small response on the state of the South African industry regarding optical CMMs. Based on the survey, there are at least 34 high-end optical CMMs in the country. This is definitely a conservative estimate and excludes the plethora of hand-held scanners and photogrammetry systems. However, it already shows a significant uptake of these systems in the country. Considering that a single high-end system can serve the inspection needs of a reasonably sized manufacturing company in South Africa and the fact that traceability is not negotiable in an internationally competitive manufacturing firm, it is clear that their economic impact may be larger than the number of systems in the country seem to indicate. It is therefore clear that an acceptable national standard is needed to support the activities of the companies already using optical CMMs.

2.7 Freeform Surfaces

In the sections above it was made clear that to achieve traceability of measurements in any type of system, a standard procedure and a certified artefact are required. The need for calibration of the CMMs was also emphasized as a way of ensuring that measurements are traceable. There are many different standards and artefacts that can be used for calibrating and testing the performance of CMMs. Artefacts can be used on their own or in different combinations. Most of these artefacts consist of basic spatial or planar configurations [39]. In most cases, such artefacts are equipped with external and internal balls. An example of an artefact is a ball which is the most common element used for determining metrological characteristics of optical 3D measurement systems such as fringe projection systems, laser scanners, photogrammetric systems and other similar optical systems [39].

The VDI/VDE standard is the most suitable standard for optical CMMs. However, the standard does not extend to fully address performance verification when freeform surfaces are measured using optical CMMs. Freeform surfaces can be defined as surfaces with no axes of rotational invariance (within or beyond the part). They may appear to have an arbitrary shape and regular or irregular shape structures. Freeform surfaces have a broad application prospect in various areas such as aerospace, illumination and biomedical engineering. But these surfaces offer new opportunities to the designers and new challenges for the optical manufacturing and measuring industry [40]. Designing and machining of freeform surfaces require an accurate mathematical description. The most common ways to describe freeform surfaces are:

- Freeform surfaces expressed with a specific mathematical formula, e.g. double sinusoidal surface described with sine and cosine function.
- Surfaces described with general xy polynomials, as has been used routinely in commercial optical design software.
- Surfaces described using Non-Uniform Rational Basis Splines (NURBS) or Neural Networks suitable for CAD modeling software. Commercial optical design software also supports this data format [41].

Optical surface measurement techniques (including imaging) and interferometric techniques provide non-contact measurement of freeform surfaces and it is possible to measure the entire surface in a single measurement [39]. These techniques can be performed quickly with low uncertainty, but they are sensitive to environmental influences as well as to disturbances caused by the workpiece itself. Further limits can arise from certain surface structures like steps or high surface curvature. Steps can lead to optical edge artefact, so-called batwings, and high surface curvature. In some interferometric systems, these steps can lead to phase jumps or so-called ghost steps [40].

A few things to point out from this section are that it is very difficult to achieve traceability of freeform surfaces due to the lack of physical standards for those particular form of surfaces, available standard documentation does not cater for freeform surfaces and since there are different freeform surfaces, it is impossible to have a physical standard for each and every type of freeform surface. Therefore, a better method is required in order to achieve traceability of freeform surfaces when using CMMs. This is further discussed in Section 2.8.

2.8 Virtual CMM Technology

Rules in the ISO 14253 standard state that in order to demonstrate conformance with specifications, the measurement result must have an associated measurement uncertainty [28]. The GUM guide gives some general guidance on calculating measurement uncertainties [42]. However, for a CMM, except in the most trivial cases, the calculations are complex and the measurement task generally includes a number of different geometrical features and a datum that cannot be easily described by classical uncertainty budgets. This and other pitfalls mentioned in [42] make it difficult to directly use the GUM guide in CMM measurements.

An alternative method is needed. In the case of CMMs especially optical CMMs, it is a task particularly difficult and not always straightforward to determine the uncertainty of these machines since they are fraught with many sources of uncertainty as shown in Figure 11. Therefore, users and manufacturers of these machines often overlook the problem of measurement accuracy giving in exchange the accuracy of the measuring device [43].

One option that is widely used but not necessarily recommended, is to use the CMM manufacturer's specified value for the maximum permissible error of length measurement. This error is expressed as $A + L/K$, where A and K are constants and L is the measured length [43]. This method does not apply when measuring inner feature distances and angles, when reporting geometric form or when using a long stylus. This is because machine specification only applies for a specific case and it is not an uncertainty. This error is determined for a selected task as a measurement of distance and is given as a maximum permissible error by the manufacturer. Thus defined, it is significantly different from the accuracy of the real measuring task at hand and can results in bad decisions in the determination of compliance with the product specifications.

Moreover, when the maximum permissible error is used instead of task specific error, all measurement tasks are simplified to the measurement of distance, which is not consistent with the nature of coordinate measurement techniques [43].

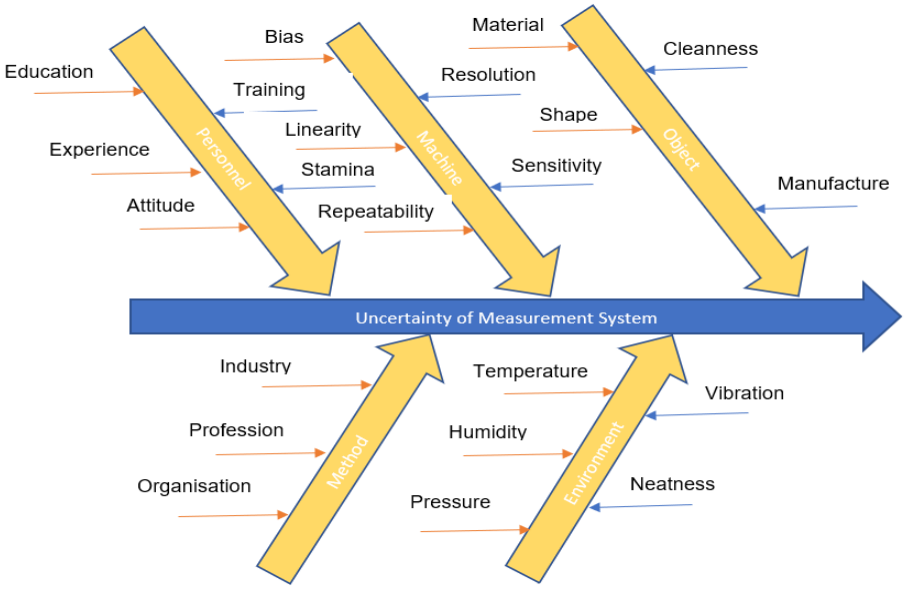

Figure 11: Fishbone diagram of CMM uncertainty contributors [43]

The conventional methods to determine uncertainty described in [44] are generally difficult to perform, require knowledge and experience in the field of measurement and are time consuming [45]. A better alternative is to use the method described in ISO 15530-3 [44], i.e. the method of substitution. This method works very well but relies on the availability of suitable referenced standards that meets the similarity conditions listed in clause 5.2. To quote the standard: *"The aim of this part of ISO 15530 is to provide an experimental technique for simplifying the uncertainty evaluation of CMM measurements"*. In this experimental approach, i.e. the substitution method, measurements are carried out similar to the actual measurements, but with calibrated workpieces or measurement standards of similar dimension and geometry instead of the unknown objects to be measured.

Another method that can be used is the multiple measurements method which requires a lot of measurements to be taken, making it a time consuming and impractical process. These methods still do not help users to achieve traceability of measurements in freeform surfaces, since they depend on the availability of physical standards that are similar to the workpiece being measured. Another group of methods consists of analytical methods based on calculations of the uncertainty of indirect measurement. It uses geometrical relationships and the analysis is performed similarly to the classical uncertainty of measurement done by a micrometer. However, these methods are difficult to use in practice and they present an approach similar to methods based on expert's knowledge [44].

A valuable alternative from the above-mentioned methods is the use of Monte Carlo simulations to calculate the measurement uncertainties. This idea was first introduced by researchers from the National Metrology Institute of Germany (PTB) [9]. They called their concept the Virtual Coordinate Measuring Machine (VCMM) and described it as follows "*The Virtual CMM performs a point by point simulation of measurements, emulating the measurement strategy and the physical behaviour of the CMM with the dominating uncertainty contributions disturbing the measurement*". They designed a software tool based on the VCMM specifically for tactile CMMs. After the successful development of the software, a CMM manufacturer ZEISS was able to offer an optional module to their Calypso CMM software called OVCMM (Offline Virtual Coordinate Measuring Machine) to calculate measurement uncertainty. The module is based on the VCMM engine of PTB. The VCMM technique is currently the best method for determining the uncertainty in tactile CMMs.

The VCMM method has also been successfully applied to Articulated Arm CMM technology and other discrete point measurement systems [46]. The trend in accuracy estimation is currently moving towards these simulative methods. In practice, the development of the so-called Virtual measuring machine used to evaluate the accuracy of the measurement is required. Currently, these methods are the most accurate since they are based on the reproducibility of the measuring point idea and because of it, they are consistent with the nature of coordinate measuring techniques. This preferred technique to establish the uncertainty of measurements is the use of uncertainty evaluating software (UES) that makes use of Monte Carlo methods.

Monte Carlo methods are a class of computational algorithms that rely on repeated random sampling to compute their results [47]. In effect, they run the CMM program multiple times on a Virtual CMM.

There are several commercial implementations of EUS including those that are optional extras for ZEISS Calypso and Leitz Quindos, and the stand-alone package Metrosage Pundit. In ISO 15530-4, a technique for calculating task specific measurement uncertainties using simulation is outlined [47].

Initially, when implementing a Virtual CMM in practice, the residual error field must be measured [9]. These are stochastic uncertainty contributors that can be changed before each VCMM run. They can be varied depending on the real CMM specified uncertainty, e.g. maximum permissible error given as $A + L/K$. This measurement is usually performed by the manufacturer. Next, temperature gradients are measured around the machine. Finally, the kinematic chain of the machine must be described.

This information describes the real CMM to the simulation software in use. Further input parameters are needed to describe all relevant error contributors of the CMM. Some of the contributors are related to the environment, some related to the probing process and some are related to the workpiece itself. These steps are shown in Figure 12 and the application of this method in optical CMMs is deferred until Chapter 4.

Once all these input parameters have been determined, the software repeatedly simulates collecting individual points with a Gaussian spread and propagates these values through all the calculations necessary to produce the desired result [9]. The output is all the characteristics requested by the user, each printed out with an associated measurement uncertainty and stored on the software as representative samples of potential measurement results.

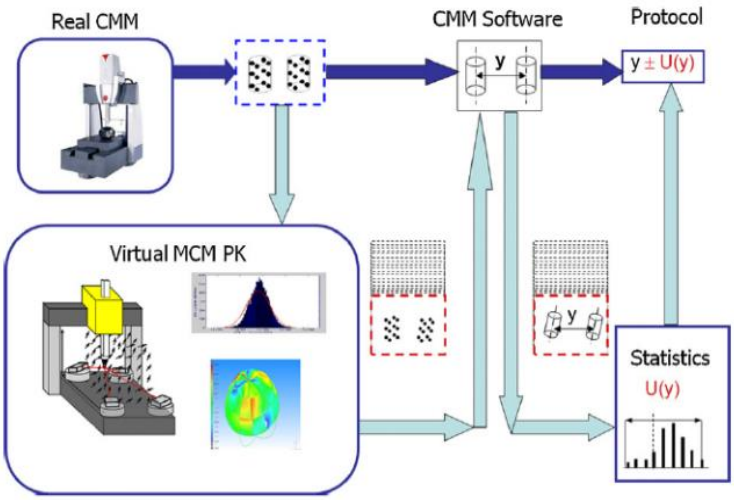

Figure 12: Algorithm of workings of the Virtual CMM [9]

From the samples, a statistical routine calculates an interval that includes more than 95% of all the results for the measurand. The measurement report of the CMM software states the actual measured value and the associated uncertainty. The advantage of this method is that, as long as the operational conditions do not change, the Monte Carlo simulation only has to be performed once for a particular component. A further advantage of the technique is that it allows “what if” calculations to be performed [9].

For the application of this method in a calibration lab, there must be a correspondence between the assumptions made for creating the Virtual CMM input parameters and the actual conditions. This is realized by regularly monitoring measurements of calibrated artefacts in order to verify the entire system as a “black box” [9].

The measurement task has to be fast and simple but at the same time sensitive to all the significant uncertainty contributors such as changes of scale factor due to temperature, changes of squareness due to changing temperatures gradients or collisions and de-adjustment of the probing system [9]. Two procedures complying with these requirements are the measurement of ball plates in two closed positions (according to VDI 2617 sheet 5) and the measurement of the so-called ball cube. The decision of whether the Virtual CMM still calculates the “correct” uncertainty can be determined through the comparison of results of the actual test with the calibrated values.

The Virtual CMM simulation software can calculate reliable uncertainties for all of the measured or derived features and therefore the process of measurement and simulation can be regarded as calibration [9]. In [43], the developed Virtual CMM model was tested according to the VDI/VDE guidelines presented in [48]. Then the same model was tested by performing the common metrological tasks such as measurements of the point to point distance, the plane to plane distance, the diameter of a sphere, the form error of the sphere and the distance between the centres of two spheres. Then for each measurement, the standard uncertainty was calculated according to the methodology used in the classical methods of determining the accuracy of measurements. The uncertainty determined classically was successfully compared with the uncertainty obtained by the developed simulative Virtual CMM model [43].

In [49], the idea of Virtual Articulated Arm Coordinate Measuring Machine (VAACMM) allows for a near real-time determination of single measurement results along with its uncertainty. This eliminates the need for multiple repetitions of measurements and significantly reduces the cost associated with the measurement procedure. The paper [45] describes the development of VAACMMs used in the automotive industry for quality control purposes.

These simulative methods currently have only been applied to discrete point CMMs (these are CMMs that measure one point at a time) and not optical CMMs [45]. Refer to Appendix A.2 for more information on discrete point CMMs. The VCMM technique has allowed for full traceability in CMM measurements in discrete point CMMs, even when measuring freeform surfaces, full traceability can be achieved since the point uncertainty can be propagated to any type of shape or surface function. This will be further discussed and demonstrated in Chapter 4. The GUM guide has also been improved to include Monte Carlo simulations. Similarly, the American Metrology Institute (NIST) has developed an online uncertainty program that is based on the GUM guide and Monte Carlo simulations [50]. There seems to be no ongoing work to apply the VCMM technique in optical CMMs, thus the need for this research.

2.9 Optical CMM Technology

The following is a short background on multiple view geometry based on the book by Hartley and Zisserman [51]. In multiple view geometry, the pinhole camera projection model is used. The model assumes that images are projected onto a camera image plane using a perspective projection, i.e. all projection lines meet at the camera centre as shown in Figure 13.

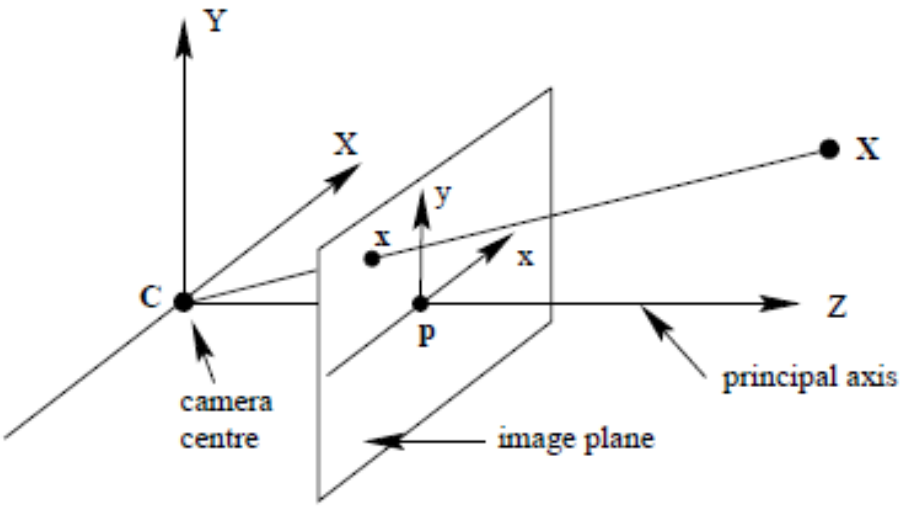

Figure 13: Pinhole camera model [51]

The geometry of this model is represented in perspective space as opposed to normal Euclidian space. In perspective space points are represented as homogeneous coordinates. A function often performed in vision applications is transforming images. Homographies are used to do these transformations. The transformation involves the change of scale, straightening a skewed image, rotation, etc. The transformation from the world coordinates to camera coordinates is required in multiple view geometry and this is done through camera matrices.

$$x = PX \tag{1}$$

Where x are camera image coordinates, X are the world coordinates and P is the camera matrix. The camera matrix incorporates both the intrinsic and extrinsic camera parameters. There are numerous algorithms for calculating the camera matrix like the Direct Linear Transform (DLT) method which assumes a linear camera model (pinhole camera model) [51]. This means that the world point, image point and optical centre are collinear.

In practice, when real camera lenses are used, the linear camera model assumption does not hold. The most important deviation is generally the radial distortion and it becomes more significant as the focal length of the lens decreases. The cure for this distortion is specified by Hartley and Zisserman [51] "*The cure for lens distortion is to correct the image measurements to those that would have been obtained under a perfect linear camera action, then the camera is then effectively again a linear device*". The following Equation (2) can be used to calculate the camera matrix:

$$P = KR[I \mid -C] \tag{2}$$

Where C is the camera centre, I is the identity matrix, R is the rotation matrix and K is the calibration matrix. The calibration matrix for a CCD camera is derived in [51], the matrix contains all the intrinsic parameters of the camera.

$$K = \begin{bmatrix} \propto_x & s & x_o \\ 0 & \propto_y & y_o \\ 0 & 0 & 1 \end{bmatrix} \tag{3}$$

Where $\propto_x$ and $\propto_y$ denote the focal length of the camera in terms of pixel dimensions in the x and y direction respectively. They are scaling factors taking into account the fact the CCD pixels may not be square. Then $x_o = m_x\, p_x$ and $y_o = m_y\, p_y$ are offsets of the principle point from the image centre and s is a skewness parameter. The camera matrix is very sensitive to noise [52] especially the temperature.

Most materials behave differently at different temperature conditions. The camera matrix can capture the change in behaviour of the optical system under different temperature conditions. Analysis of the camera matrix is beyond the scope of this thesis, but knowing how camera sensors behave at different temperatures will be beneficial in analysing the uncertainty of the camera system measurements and developing an Optical Virtual CMM programme which will be discussed in Chapter 4.

Most sources of camera noise are well documented in literature, e.g. flicker noise. Camera noise is exhibited as spatial (inter-pixel) and temporal (intra-pixel) variations of pixel values. One of the significant contributors to image noise is heat within the sensor, where fluctuations in thermally induced currents result in the variation of measured pixel intensity values. These fluctuations can have a severe impact on the robustness of applications that process the resultant image [53]. Temperature can have a significant effect on the level of noise present in the captured image with some noise sources like dark current shot noise doubling with an 8 ℃ rise in temperature [54]. The following are some types of camera noises available for both CCD and CMOS sensors [54]:

- SN_{ph} Photon shot noise
- $PRNU$ Photon-response non uniformly
- SN_{dark} Dark-current shot noise
- FPN Fixed pattern noise
- N_R Reset
- N_{therm} Thermal noise (Johnson – Nyquist)
- N_{other} Minor contributors such as flicker noise and conductor shot noise
- $AFPN_{gain}$ Active gain FPN (CMOS only)
- $AFPN_{off}$ Active offset FPN (CMOS only)
- $CFPN_{gain}$ Column gain FPN (CMOS only)
- $CFPN_{gain}$ Column offset FPN (CMOS only)
- N_D Demosaicing effects (colour filter array sensors only)
- N_{flit} Filtering effects (e.g. gamma, gain, etc)
- N_Q Quantization noise

The noise path is quite complex, especially for CMOS sensors. A detailed description of all the above sources can be found in the literature [54]. In [53], four different camera sensors were tested for their noise characteristics from 21 ℃ to 55 ℃.

Results showed that the camera noise is highly temperature dependent, varies significantly between camera models and sensors and can have unexpected characteristics. In [55], an analytical expression of uncertainty characterizing the results of image processing software was derived. The expression is based on the GUM guide and is as follows:

$$\widehat{U}_I^2 = K_{\triangleq} U_A^2(i,j) + K_{\triangleq} U_B^2(i,j) + 2\, C_F\, |U_A(i,j)|\, |U_B(i,j)| + U_C^2(i,j) + U_q^2 \quad (4)$$

Where $\widehat{U}_I$ is the uncertainty of the pixel intensity and the other variables are calculated using the following equations:

$$U_A(i,j) = (dI(i,j)/dx)/U_x \quad (5)$$

$$U_B(i,j) = (dI(i,j)/dy)/U_y \quad (6)$$

with $U_x = \Delta x/\sqrt{12}$ and $U_y = \Delta y/\sqrt{12}$ standard deviations of a triangular distribution defined in $\pm\Delta x = dx$ (pixel width) and $\pm\Delta y = dy$ (pixel height), respectively. C_F is a correlation factor, which lies in the range $[-1, +1]$.

$$U_c(i,j) = K_C\, I(i,j) \quad (7)$$

$$U_q = \sqrt{\left(U_V^2 + K_Q/2^N\right)} \quad (8)$$

U_q is a constant for a given image, where U_v is the standard deviation due to vibrations and N is the number of grey levels. $K_{\triangleq}$, K_C and K_q are constant weights that depend on image characteristics. In [53], the uncertainty expression was used to test the uncertainty of the Canny edge detector algorithm.

This pixel uncertainty expression was developed as a code on Python by the author and used to calculate the uncertainty associated with the Canny edge detector algorithm. This will further be discussed in Chapter 4 when developing the VCMM for optical CMMs. The results of this section show and emphasize the complexity involved in the establishment of traceability in optical measurement systems.

2.10 Challenges in Optical CMMs

From a metrological point of view, every measurement must be traceable to the SI unit and have stated measurement uncertainty. Since optical systems are fraught with many challenges that affect the measurement uncertainty (e.g. illumination, edge effects, the operator and non-idealities of the workpiece), achieving traceability in such systems can be a very big challenge as explained in the sections above. In this section, challenges in optical systems and how their effect on the measurement uncertainty can be mitigated were investigated by the author. Some of the solutions were suggested by the manufacturer of the HP 3D scanner in their specification document [56]. All of this is represented in Table 1 below.

Table 1: Optical CMM challenges and proposed solutions

Challenge	Influence on measurements	Solution
Vibrating Surfaces	• Damage the internal components of the system. • Cause battery leakage. • It affects the calibration as well as measurements being taken.	• Measure when there is less vibration or negligible vibration. • Move the measuring instrument and object to a place with no vibrations.
Humid environment	• Damages the internal parts of the scanner. • Affect the images i.e. blurry images. • It can cause the expansion of the workpiece.	• Dehumidify the room or move to a less humid place.
Scans are noisy and with rough surfaces	• Inaccurate measurements.	• Adjust the camera aperture. • Maximize the projector's brightness. • Increase the camera viewing angle and the distance between the camera and object. • Reduce ambient light.
The colour texture does not look good	• Inaccurate measurements.	• Perform a white balance of the system.
Complex surfaces with high sloped surfaces	• The system cannot measure high sloped surfaces leading to inaccurate measurements.	• Use a portable CMM and move it around the workpiece to cover all the surfaces.
Scans contain irregular distortions/Outliers	• Inaccurate measurements	• Make sure ambient light is constant. • Make sure nothing moves in view of the cameras when scanning, i.e. no shadows are casted on the workpiece. • Spray shiny surfaces. • Use a dark background that reflects no light. • If you cannot avoid outliers use the software to clean them.

Table 2: Table 1 continued

Challenge	Influence on measurements	Solution
Scans show a regular wave pattern	• Inaccurate measurements.	• Reduce ambient light. • Avoid flickering light sources as well as fluorescent lights. • On shiny objects, avoid direct reflection of the light projector in the camera, the object must be matted with spray. • Make sure the exposure time of the camera fits the frame rate of the projector (usually 60Hz). This ensures that the camera image does not flicker. • During the scan, nothing is allowed to move (scanner or workpiece).
Fine details are missing on the scan	• Inaccurate measurements.	• The shorter the distance between the scanner and the object the more detailed the scans are. • Set up the scanner at the smallest possible working distance so that the scan size is just sufficient. • Make sure the distance between the scanner and the object is the same as during the calibration. • Make sure that both the projector and camera are well focused on the scanner object.

Optical CMMs have many more uncertainty contributors that influence their measurement results than tactile CMMs. Therefore, it is imperative that every time measurements are taken, the system is calibrated for the specific measurement conditions and that attention is given to all factors influencing the measurements. There are many methods, with some of them already discussed in Section 2.5, that can possibly be used to determine the task specific uncertainty of measurements in optical CMMs as described in [42]:

- Use of multiple measurement strategies without calibrated workpiece or standard (ISO/TS 15530 - 2).
- Use of multiple measurement strategies with the calibrated workpiece or standard (ISO/TS 15530 - 3).
- Use of computer simulations (ISO/TS 15530 - 3).

- Use of expert judgment.

In [42], the unsuitability of the conventional GUM guide for optical CMM measurements is discussed, thus the development of the above methods which are designed and mostly applied in discrete measurement systems. One of the many reasons given that make the GUM guide unsuitable for CMM measurements is that the method assumes that the measurand can be written as an analytical function of a set of output quantities with associated uncertainties. The sensitivity coefficient cannot be determined if this analytical function is not available. Alternatively, the sensitivity coefficient could be determined experimentally but this is a time-consuming process and only possible for a limited set of problems.

It is difficult to define an analytical relationship between all the uncertainty contributors and the measurand due to the complexity of the measurement process of optical CMMs with all the different uncertainty contributors. Besides that, most CMM measurement results are obtained by using iterative fitting algorithms that do not provide an analytical relationship [42].

These above-mentioned observations from [42] are accurate but one can argue that the main purpose of the GUM guide is to offer a general guide to calculating measurement uncertainty. It is not intended to be a specific guide for any particular measurements. This means the user still needs to develop a measurement uncertainty procedure for their instrument even if they have the GUM guide. Their procedure must be based on the GUM guide. With so many challenges in the case of optical CMMs, this is a particularly difficult task and requires more research and development in order to achieve full traceability in optical CMMs as in tactile CMMs.

2.11 Conclusion

It has been established that the field of optical CMMs is a growing industry in South Africa and these systems have a significant economic impact in the country. Despite this growth and impact, full traceability of measurements from optical CMMs cannot currently be achieved, since optical CMMs are fraught with many uncertainty contributors [56]. There is currently no internationally recognized traceability standard for optical CMMs systems and the VDI/VDE standard is the most developed in this regard [8]. Freeform surfaces are very difficult to measure but the Virtual CMM technique has been used to achieve full measurement traceability of freeform surfaces in tactile CMMs and offers a viable solution in the case of optical CMMs which will be demonstrated by this research [9].

Chapter 3: Optical CMM Traceability Standards

3.1 Introduction

The German VDI/VDE standard describes performance verification procedures to be performed in optical CMMs in order to achieve traceability of measurements, i.e. acceptance and reverification procedures. However, the standard does not cover the performance verification of freeform surfaces as discussed in Section 2.7. In the association of the European project iMERA plus JRP T3J2.2 NIMTech project [36], different types of performance verification procedures and corresponding artefacts were developed for verifying the freeform measurement capability of optical and tactile CMMs. One of the procedures, the SOP-36, was developed specifically for measuring tetrahedron artefacts using optical CMMs.

In Chapter 2 it was established that the VDI/VDE 2634 standard is the most developed traceability standard for optical CMMs, this is further investigated in this chapter by evaluating both the VDI/VDE standard and the SOP-36 procedure in more details. The VDI/VDE 2634 standard will also be used in Chapter 4 to verify the performance of an optical CMM developed by the author.

3.2 VDI/VDE 2634 Standard

Part 1 of this standard describes the acceptance and reverification methods for the evaluation of the accuracy of optical 3D measuring imaging systems with point by point probing. The standard describes the type of artefact that must be used when implementing the standard. This artefact must have features that are suitable for tactile or optical probing. Firstly, the artefact needs to be calibrated for the desired dimensions. Then quality parameters need to be defined, in this case the three-dimensional length measurement error (Δl). During the acceptance or reverification test, this error is defined as the difference between the measured distance (l_m) and the calibrated distance (l_k) between two points.

$$\Delta l = l_m - l_k \tag{9}$$

The maximum permissible error specified by the manufacturer is the limiting value for the length measurement error when executing acceptance tests. Whereas in the case of reverification tests, the limiting value can be specified by the user. The user also needs to define a measurement volume and at least five different test lengths shall be tested inside the defined volume. The quality parameter must never exceed the specification for the acceptance or reverification criteria to be satisfied.

Part 2 of the standard applies to optical CMMs based on area scanning. This part applies to the measuring of 3D objects in a single elementary measuring process (single view). The optical CMM and the workpiece shall not be moved relative to each other during the measurement process. In this case, the quality parameters are the probing error, sphere spacing error and flatness measurement error. It is very important to record the operating conditions for these measurements. As it was discussed in Chapter 2, optical CMM behaviour can change significantly with a small change in the operating conditions.

The probing error parameter is defined in Chapter 2. The probing error depends on different factors such as digitizing error, phase measuring error, pixel and image coordinate measuring errors, lateral structural resolution, etc. In this case, a sphere artefact is used and at least ten arbitrary positions of the artefact within the measuring volume must be sampled.

The specification of probing error can only be satisfied if the determined values of the quality parameters do not exceed the related limit value at any measuring position. The sphere spacing error parameter serves to verify the length measuring capability of the system and to ensure traceability. This is determined from the difference between the measured and calibrated values of the distance between the centres of the spheres. The parameter limits specified by the manufacturer shall be observed within the entire measuring volume regardless of the arrangement of the artefacts. Seven different positions need to be sampled. The resulting sphere spacing error (SD) is calculated using equation (10) below, where L_a is the actual measured length between the spheres and L_r is the calibrated value.

$$SD = L_a - L_r \tag{10}$$

The measurement limits are specified by the manufacturer or the user. The last quality parameter is the flatness measurement error. This is the range of distances of the measuring points from the best-fit plane calculated according to the least-squares method. In this case, parallelepiped artefacts are used. The artefact positions and the number of points are specified in the standard document. The procedure for reverification is always analogous to the acceptance procedure, but the user specifies the limits and number of measurements to be taken. The guide further instructs the estimation of test uncertainty for both the acceptance test and the reverification test procedure. The uncertainty estimation is dependent on the artefact material and other uncertainty contributors mentioned in the standard document.

Similar to Part 2 of the standard, Part 3 also applies to optical CMMs based on area scanning. But in addition to Part 2, it defines necessary supplements for the measurement of objects using multiple images. In this part of the standard, the optical CMM and workpiece can be moved relative to each other. The different single images of the workpiece are transformed into a uniform object coordinate system for instance by a transformation of the single images through suitable reference markers. There are also other methods for doing the transformation discussed in the standard document.

In addition to acceptance testing and reverification described in Part 2, Part 3 also checks what effects repositioning of the sensor or the workpiece exerts on the quality parameters. For the testing of the quality parameter probing error described in Part 2, it is also tested whether the measuring system can transform several single images captured independently of each other into a common coordinate system.

For the quality parameter sphere spacing error, the measured spacing is derived from measurement values from several area scans. Another quality parameter, the length measurement error, is measured. This parameter describes the three-dimensional error behaviour of the measuring volume. The reverification procedure is analogous to the acceptance procedure, but the limits are specified by the user, not the manufacturer. More details on the above can be found on the VDI/VDE 2634 standard document.

3.3 SOP-36 Procedure

As mentioned in the introduction, there is another performance verification procedure specifically developed for testing the tetrahedron artefacts, the SOP-36 [36]. This is not an international or a national standard but an internal procedure from the University of Maribor. The best way to describe the procedure is to use it and perform the actual measurements based on the procedure. The following is a description of performance verification tests done on an HP 3D scanner using the SOP-36 procedure.

3.3.1 Apparatus

The first CMM used was the HP 3D Structured light scanner. The scanner properties are available on their website [56]. According to the HP 3D Structured light scanner specification document, the accuracy of the system was tested using the VDI/VDE 2634 standard.

The second CMM used is the NMISA tactile CMM with volume dimensions as; x = 900 mm, y = 2000 mm and z = 900 mm. The tactile CMM is calibrated annually using the ISO 10360 standard and NMISA uses the system to calibrate other instruments to ensure traceability of their measurements. This system was used to calibrate the tetrahedron artefact which was used during the application of the SOP-36 procedure.

The measurement deviation, that is the difference between a measured dimension and the nominal dimension, of the NMISA tactile system depends on the position of the measured point in the 3D space. Micrometer deviations from nominal dimensions can be achieved with the NMISA tactile system as shown in Figure 14.

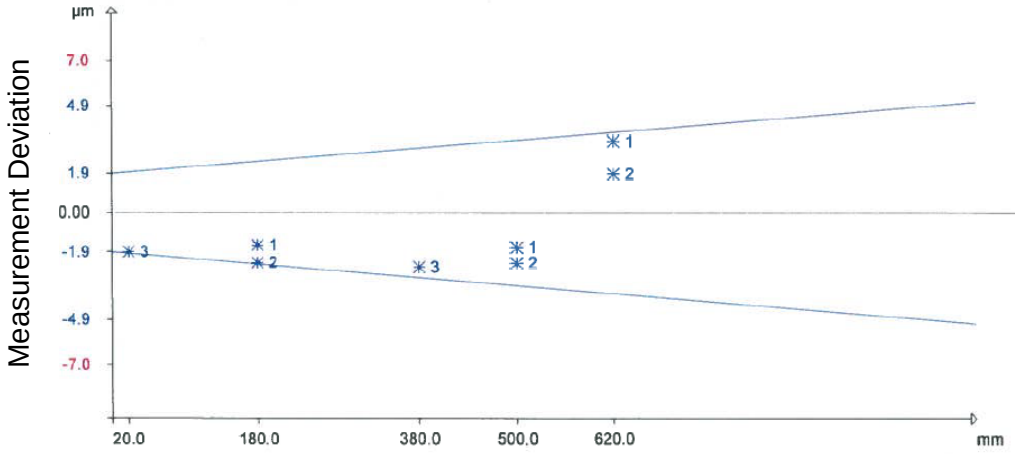

Figure 14: NMISA tactile CMM full volume accuracy from their 2018 calibration certificate

The tetrahedron artefact obtained from NMISA is shown in Figure 15 and it was measured using the above two CMMs. This is further explained later in this chapter. Results from the tactile CMM were used as calibration results and measurements on the HP scanner were done based on the SOP-36 procedure. All of this is further described in the remaining sections of this chapter.

Figure 15: Tetrahedron artefact

3.3.2 Calibration of the Tetrahedron Artefact

The tactile CMM measurements were taken by the author at a workpiece temperature of 18.69 ℃. Table 3 shows all the results of the measurements. The table shows the actual measured dimensions (calibrated measurements) from the NMISA tactile CMM and the nominal dimensions of the artefact. Dimensions measured are the diameters of the spheres and the distances between two sphere centres. The nominal dimension refers to the measurement that is used for general identification of the artefact dimension. These nominal dimensions are dimensions that were specified by the manufacturer of the artefact. In this case, these were measured with the NMISA tactile CMM when the artefact was manufactured.

Table 3 also shows the deviation of the calibrated measurements from the nominal dimensions. These calibrated measurements will be used later when calculating the measurement uncertainty based on the SOP-36 procedure. Each calibrated measurement is an average of three measurements for that particular dimension.

Table 3: Tetrahedron artefact measurement results from the NMISA tactile CMM

Item	Calibrated (mm)	Nominal(mm)	Deviation(mm)
Sphere 1 to 2	299.823	299.851	0.028
Sphere 1 to 3	300.257	300.264	0.007
Sphere 1 to 4	299.852	299.887	0.022
Sphere 2 to 3	299.775	299.800	0.026
Sphere 2 to 4	300.143	300.124	0.019
Sphere 3 to 4	300.031	300.060	0.029
Sphere diameter 1	25.013	25.000	0.013
Sphere diameter 2	25.004	25.000	0.004
Sphere diameter 3	25.006	25.000	0.006
Sphere diameter 4	25.019	25.000	0.019

Figure 16 shows the positioning of the spheres as numbered in Table 3.

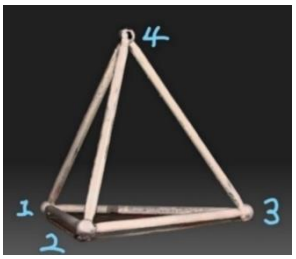

Figure 16: Tetrahedron scan with sphere references

3.3.3 Measurement of the Tetrahedron Artefact Using the SOP-36 Procedure

Measurements in this section and the uncertainty analysis in the next section are all based on the SOP-36 procedure, which was designed and used for performance verification of non-contact measuring systems using a tetrahedron artefact by the University of Maribor [36].In this optical measurement experiment, the same dimensions measured in Table 3 using a tactile CMM were measured using the HP 3D structured light scanner.

Then the measurement uncertainty was calculated based on the SOP-36 procedure [57]. During the measurements, the surface roughness of the spheres was neglected as recommended by the SOP-36 procedure. A room temperature of 23.90 ℃ was measured using a thermometer. Then using a hygrometer, a wet-bulb temperature of 22.80 ℃ was measured. This gives a relative humidity of 95% when using the psychometric chart for the elevation of Stellenbosch in the Western Cape province of South Africa [58]. This room temperature is different from the temperature measured during the calibration of the artefact.

This change in environmental conditions when measurements are performed especially the temperature, from 18.69 ℃ to 23.90 ℃, influences the measurements and it will be discussed later when doing the uncertainty analysis. Other environmental conditions have changed and will affect the measurements like the change in humidity, but investigating all of the environmental conditions that have changed is a time-consuming process and it is beyond the scope of this chapter as well as beyond the scope of the SOP-36 procedure. The effect of these environmental changes on the measurements will be discussed later in Chapter 4.

The SOP-36 procedure specifies two ways of scanning the artefact; the single scan procedure and the multiple scans procedure. Both procedures were used and will be reported in this section. The measurement uncertainty calculation procedure described later in this chapter is the same for both scanning procedures. One of the authors of the SOP-36 procedure specified in email correspondences that this procedure can always be improved to include more error sources associated with optical system measurements [57]. This improvement of the SOP-36 procedure is beyond the scope of this research. Therefore, the procedure was applied without any improvements.

Due to the shiny nature of the surface of the tetrahedron artefact, it was necessary to coat the surface with a thin layer of light-diffusing powder before measurements were performed. The thickness of the powder used is close to 10 micrometres [36], the significance of this error on the measurement uncertainty will be discussed later in the uncertainty analysis.

Single Scan Procedure Results

The following are results from the single scan procedure. The measurements were taken using the HP 3D scanner. Five single scans were taken for the tetrahedron structure without moving the scanner and Figure 17 shows the resultant scan with the spheres labelled as in Figure 16.

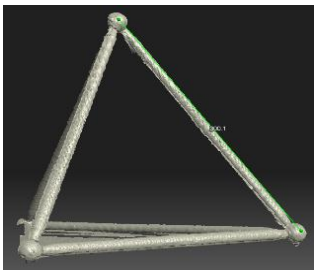

Figure 17: Screenshot of the final result of the single scan procedure

The HP scanner dedicated software allows the user to take measurements between two points. These measurements are dependent on the point selected by the user. Therefore, the measurement method is prone to human error. In the case of measuring the diameter, it is difficult to take measurements since the scan does not show the whole sphere, e.g. sphere 1 in Figure 17.

A better scan is required and a better method for calculating dimensions from the scan is also required. A multiple scans procedure seems to be a better way since it allows the artefact to be scanned from different positions, resulting in a rotatable final artefact scan. The downside of taking multiple scans is that the scan requires a lot of post-processing and cleaning of the scan to ensure that the layers of the scan from the different scanning positions are perfectly aligned.

Multiple Scan Results

The setup when applying the multiple scans procedure was the same as in the single scan procedure. But in this case, the scanner and the artefact were allowed to move relative to each other. Five single scans were taken in each scanning position. There were three scanning positions in total as described in the SOP-36 procedure. Figure 18 shows a screenshot of the final scan from the multiple scan procedure and the final scan from the single scan procedure. As seen, the scanning results from the multiple scan procedure are better than results from the single scan procedure.

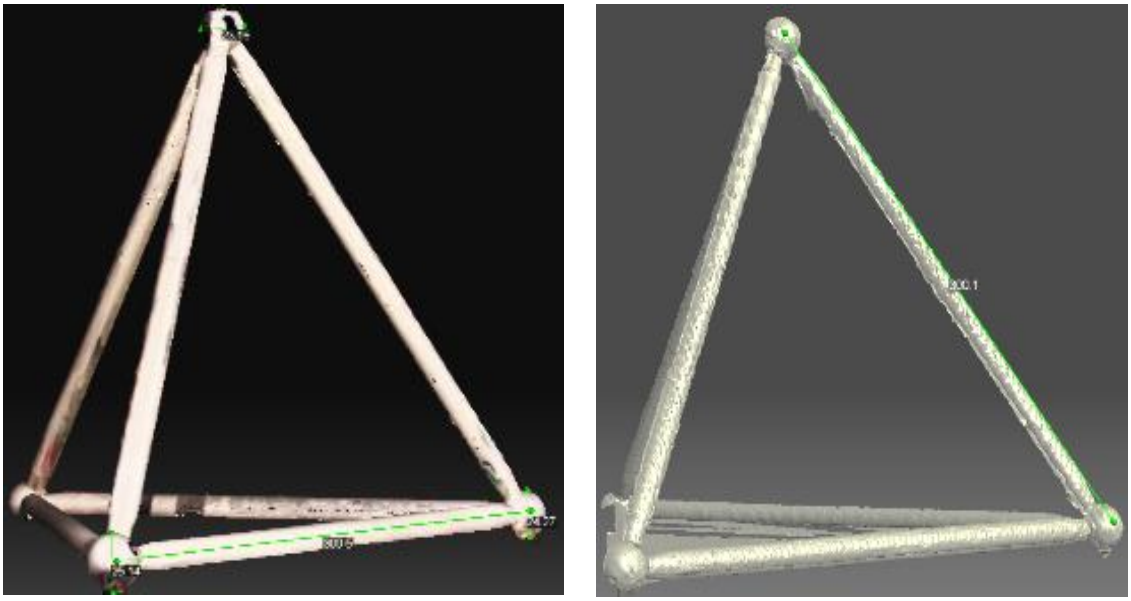

Figure 18: Screenshot of the final result of the multiple scan procedure (left) and a screenshot of the final scan results from the single scan procedure(right)

The scan from the multiple scan procedure in Figure 18 was exported to the Fusion 360 software and then all the measurements were done from the Fusion 360 sculpts models function to get the dimensions. The measurements taken from point to point using the Fusion 360 software gives an idea of how big the measurements must be, but they cannot be used in an uncertainty budget since they are extremely prone to human error.

A better solution is to export the scan as a text file using the Meshmixer software. The exported file gives the artefact scan as nodes in a 3D space. These nodes are specified as x, y and z coordinates. A least-squares sphere fit code was developed in Python by the author based on an existing Python code [59]. The code takes 3D points that lie on a sphere surface and fit a sphere on those points.

The output of the code is the sphere diameter and the sphere centre point coordinates. Using two sphere centre points, the code calculates a 3D distance between two spheres. Table 4 shows the deviations of the code results from the calibrated measurements from the tactile CMM in Table 3. Each measurement (code) result in the table is an average of five measurements from the code for that particular dimension.

Table 4: Tetrahedron artefact measurement results from the HP 3D scanner

Item	Measurement(mm)	Calibrated(mm)	Deviation(mm)
Sphere 1 to 2	300.175	299.823	0.352
Sphere 1 to 3	299.089	300.257	1.168
Sphere 1 to 4	300.111	299.852	0.259
Sphere 2 to 3	300.383	299.775	0.608
Sphere 2 to 4	300.504	300.143	0.361
Sphere 3 to 4	299.052	300.031	0.979
Sphere diameter 1	24.459	25.013	0.554
Sphere diameter 2	24.381	25.004	0.623
Sphere diameter 3	23.985	25.006	1.021
Sphere diameter 4	25.077	25.019	0.058

The measurement results in Table 4 were measured at a different temperature from the calibrated measurements in Table 3 and no temperature compensations were allowed on the measurements by the Python code. This will be discussed in the following section. The deviations in Table 4 were included to give an indication of the accuracy of the HP 3D scanner compared to the tactile CMM that was used to calibrate the tetrahedron artefact in Section 3.3.2.

3.3.4 Uncertainty Analysis

The uncertainty analysis in this section was done according to the SOP-36 performance verification procedure. Uncertainty contributors, like the error due to powder thickness and uncertainty due to changes in temperature or humidity in the laboratory where measurements were taken, are not fully discussed in the SOP-36 procedure (only the temperature is discussed) and will be discussed later in Chapter 4 of this report.

The SOP-36 procedure specifies that the HP 3D scanner measurement results must be compared with the calibration results from the tactile CMM, both of these results are shown in Table 4 and the specification of the limiting values is similar to the one described in the VDI/VDE standard, i.e. specified by the manufacturer when doing acceptance tests and specified by the user when doing the reverification tests. The following are the uncertainty contributors that are considered in the SOP-36 procedure when doing the uncertainty analysis:

1. Uncertainty of optical measurement machine reading $u(L_{om})$
2. Uncertainty of the standard's length $u(L_m)$
3. Uncertainty of the standard's linear temperature expansion coefficient $u(\alpha_m)$
4. Uncertainty due to the standard's temperature deviation $u(\theta_m)$
5. Total uncertainty $u_c(e)$

1. Uncertainty of optical measurement machine reading $u(L_{om})$:

The uncertainty of an optical measurement machine output is a result of resolution and repeatability limitations. According to the SOP-36 procedure, an optical measurement machine resolution of 0.010 mm causes an error interval of ∓5.000 µm. When a rectangular distribution of the reading is assumed, which is a more conservative distribution than a triangular distribution or a normal distribution, the uncertainty due to the resolution limitation is:

$$u(L_L) = \frac{5}{\sqrt{3}} = 2.9\ \mu\text{m} \tag{11}$$

According to the HP 3D scanner specifications document, the HP 3D scanner has a resolution of 0.1% of the measured size. The longest measurement that could be taken during this experiment was 415.692 mm, which is the longest diagonal inside a cube with a volume of 240 x 240 x 240 mm. Therefore, the resolution was 0.416 mm, causing an error interval of 0.208 mm. The uncertainty due to resolution limitation was calculated as:

$$u(L_L) = \frac{0.208}{\sqrt{3}} = 0.120\ \text{mm} \tag{12}$$

According to the SOP-36 procedure, repeatability of measurements is established during the calibration by measuring one of the rods (distance between two sphere centres) five times. In this case, the distance between sphere 1 and sphere 3 was measured. Any spheres could have been chosen to demonstrate the calculations, but the distance between sphere 1 and sphere 3 was chosen because as seen in Table 4 it has the biggest deviation from the calibrated results. This will lead to a calculation of the most conservative measurement uncertainty since some uncertainty contributors are dependent on the measured distance and deviation.

Table 5 below shows the results for the average distance measured between the spheres using the HP 3D scanner, as well as the deviation of the measurements from the calibrated distance of 300.257 mm measured from the NMISA tactile CMM, and the average deviation (e). The measurements were repeated 5 times as recommended by the SOP-36 procedure. The least-squares sphere fit Python code developed by the author uses only twenty points of the many points exported from the Meshmixer software to realize the measurements. For each measurement, different points were used thus the difference in the measurements in Table 5.

Table 5: Repeatability of the HP 3D scanner

Measurement Number	Measurement(mm)	Deviation(mm)
1	299.085	1.172
2	300.010	0.247
3	299.106	1.151
4	299.072	1.185
5	299.089	1.168
Average	**299.272**	**0.985**

From the limitation due to resolution and the average deviation in Table 5, the uncertainty of the HP 3D scanner measurement reading can be calculated as follows:

$$u(L_{om}) = \sqrt{(u(L_L))^2 + (e/\sqrt{3})^2} \tag{13}$$

$u(L_L)$ in the above equation (13) is 0.120 mm and e is 0.985 mm which gives an HP scanner reading uncertainty of 0.581 mm.

2. Uncertainty of the standard's length $u(L_m)$:

The SOP-36 procedure also includes the error of the calibrated measurements as another uncertainty contributor. According to the NMISA tactile CMM calibration certificate, the maximum possible error of length measurements from the CMM can be calculated with the following equation:

$$u(L_m) = \left(1.9e^{-3} + \frac{L}{333}\right) \text{ mm} \tag{14}$$

Where L is the calibrated length in millimetres, the uncertainties of the tetrahedron structure measurements using equation (14) are as follows:

For the rod (Sphere 1 to 3): $u(L_m) =$ 0.903 mm

And for the sphere (Sphere 3): $u(L_m) =$ 0.077 mm

The uncertainty calculations for sphere 1 are similar to the calculations for sphere 3. Therefore, they are not included in this uncertainty analysis.

3. Uncertainty of the standard's linear temperature expansion coefficient $u(\alpha_m)$:

The tubes of the tetrahedron artefact described in the SOP-36 procedure were constructed from a composite material consisting of carbon fibre in an epoxy matrix. The SOP-36 procedure specifies that the tetrahedron tube's linear temperature expansion coefficient is $2.200e^{-6}\ \frac{\text{m}}{\text{m}}°\text{C}^{-1}$, this was established by extensive tests on the tubes described in [36]. This linear temperature expansion coefficient for the tubes was also used by the author because the material of the tetrahedron tubes that were used by the author is similar to the one described in the SOP-36 procedure and material testing of the tubes used here is beyond the scope of this project. The linear temperature expansion coefficient leads to an estimated interval of $\pm 1.100e^{-6}\ \frac{\text{m}}{\text{m}}°\text{C}^{-1}$. The standard uncertainty at supposed rectangular distribution for the tubes is:

$$u(\alpha_m) = \frac{1.100e^{-6}}{\sqrt{3}} = 0.635e^{-6}\ \frac{\text{m}}{\text{m}}°\text{C}^{-1} \tag{15}$$

The spherical balls of the tetrahedron artefact are made of carbon steel. The linear temperature expansion coefficient of carbon steel is $11.700e^{-6}\ \frac{\text{m}}{\text{m}}°\text{C}^{-1}$ [58]. An interval of $\pm 5.850e^{-6}\ \frac{\text{m}}{\text{m}}°\text{C}^{-1}$ is estimated. The standard uncertainty at supposed rectangular distribution for the spheres is:

$$u(\alpha_m) = \frac{5.850e^{-6}}{\sqrt{3}} = 3.378e^{-6}\ \frac{\text{m}}{\text{m}}°\text{C}^{-1} \tag{16}$$

The spheres are connected to the tubes using magnets that are inside the tubes to form the tetrahedron artefact structure as shown in Figure 15. These magnets do not have any effect on the length of the tubes or the diameter of the spheres and they are excluded in this uncertainty analysis.

4. Uncertainty due to the standard's temperature deviation $u(\theta_m)$:

During calibration, the lab measured temperature was 18.69 ℃, and when the HP 3D scanner was used the lab measured temperature was 23.90 ℃. Therefore, temperature deviations in the lab are estimated to be ∓5.21 ℃. Standard uncertainty assuming a rectangular distribution was:

$$u(\theta_m) = \frac{5.21}{\sqrt{3}} = 3.008\ ℃ \tag{17}$$

This is how the SOP-36 procedure recommends the temperature deviations should be included in the uncertainty analysis. Other methods for doing such calculations will be discussed in Chapter 4.

5. Total uncertainty:

The last step of this uncertainty analysis for the HP 3D scanner measurements is to calculate the total uncertainty. This is done by combining all the above calculated uncertainties from different uncertainty contributors as shown in Table 6.

Table 6: Total uncertainty contributors based on the SOP-36 procedure

Symbol	Rod Standard uncertainty	Sphere Standard uncertainty	Distribution	Sensitivity coefficient	Contribution Uncertainty(mm)		Significance (%)	
					Rod	Sphere	Rod	Sphere
L_{om}	0.581 mm	0.581 mm	Rectangular	1	0.581	0.581	39.067	88.133
L_m	0.903 mm	0.077 mm	Rectangular	1	0.903	0.077	60.734	11.675
α_m	$0.635e^{-6}$ ℃$^{-1}$	$3.378e^{-6}$ ℃$^{-1}$	Rectangular	5.21 ℃ L	$3.308e^{-6}L$	$1.760e^{-5}L$	0.067	0.064
θ_m	3.008 ℃	3.008 ℃	Rectangular	$2.200e^{-6}$ ℃^{-1}L Or $11.700e^{-6}$ ℃^{-1}L	$6.618e^{-6}L$	$3.519e^{-5}L$	0.133	0.128

Therefore, the total uncertainty is:

$$u_c(e) = \sqrt{(u(L_{om}))^2 + (u(L_m))^2 + (u(\alpha_m))^2 + (u(\theta_m))^2} \tag{18}$$

$$u_c(rod) = \pm 1.074\ \text{mm}$$

$$u_c(sphere) = \pm 0.586\ \text{mm}$$

Based on the above calculations using equation (18), the uncertainty of the rod measurement is 1.074 mm and the uncertainty of the sphere diameter measurement is 0.586 mm.

This can also be reported as an expanded uncertainty of 2.149 mm for the rod and 1.173 mm for the sphere both at a 95% confidence level, i.e. at a coverage factor of $k = 2$. Table 6 also shows the significance of each uncertainty contributor compared to other contributors. This shows that most of the uncertainty of the HP 3D scanner comes from the limitations due to machine readings and also from the length of the standard. This was anticipated since the machine readings are dependent on the user and the type of software used to get the readings from the scan, this process is prone to human error and can lead to big uncertainties if a bad software is used or the optical system has a big limitation due to resolution.

Additional to the significance of the machine reading uncertainty contributor, it is evident in the uncertainty analysis that the uncertainty of machine readings is not dependent on the measured length. This is the same for both the rod and sphere measurements. This leads to the total uncertainty of the two measurements being closer to each other even though there is a big difference between the sphere diameter and the length of the rod.

After the uncertainty calculations, both the VDI/VDE standard and the SOP-36 procedure specify that comparison is required between the specified maximum limit and the calculated value. This will be done in Chapter 4. The SOP-36 procedure specifies that if the maximum value is exceeded, the measurement in which the limit has been exceeded must be repeated three times. In the repeated measurements, the limit must not be exceeded again. Otherwise, the performance verification test is regarded as unsuccessful.

3.4 Conclusion

The main objective of this chapter was to differentiate between the VDI/VDE standard and the SOP - 36 performance verification procedure. This has been done by describing how the tests are implemented using each of the methods and the following are the main differences pointed out between the two methods:

- There are a lot of measurements to be performed when using the VDI/VDE standard compared to the SOP-36 procedure, the verification approach of the VDI/VDE standard can be extremely time consuming and can result in high costs.
- The SOP-36 procedure only calibrates for the length dimension whereas the VDI/VDE standard also calibrates for more dimensions like probing error as described in Section 3.2.
- Both guidelines still do not cover performance verification of freeform surface measuring systems and the SOP-36 needs to be improved to include more uncertainty contributors when performing the uncertainty calculations.
- The purpose of the SOP-36 procedure and the tetrahedron artefact was to demonstrate the dimensional measurement capability of the selected optical-based 3D measurement technologies to measure specific forms and various surface conditions, rather than to be a universal standard.

From the above analysis and discussion, it can be seen that the SOP-36 procedure was developed based on the VDI/VDE standard. Its uncertainty analysis is based on the GUM guide as seen in the GUM guide uncertainty calculation recommended steps mentioned in Section 2.5. The purpose of the SOP-36 procedure is to minimize the verification time and still comply with the VDI/VDE standard by combining the advantages of both ball cube and ball bar artefacts [36]. Despite the fact that there is still room for improvement of the VDI/VDE standard, the standard is still the most developed traceability standard for optical CMMs and will be used in the next chapter for performance verification of an optical CMM.

Chapter 4: Virtual CMM Technique in Optical CMMs

4.1 Introduction

In Chapter 2 it was established that for full traceability of 3D measurements, in both tactile and optical CMMs, two procedures need to be completed using the CMM before the actual measurements can be taken. That is the performance verification tests and task related calibration. For even better measurement results, the Virtual CMM technique discussed in Section 2.8 can be applied when doing task-related calibration and when performing the actual measurements.

Performance verification confirms the measurement uncertainty declared by the manufacturer through standards employed for performing such tests, e.g. the VDI/VDE standard for optical CMMs [36]. In this chapter, the performance verification of a stereovision system made by the author will be done based on the VDI/VDE 2634 standard.

Task-related calibration employs the comparator principle, here certain quantities are measured or calibrated to high accuracy. The measured quantity is then compared with a calibrated standard of similar form and dimension [36]. Performance verification procedures and task-related calibration currently cannot be used for complex forms due to many reasons mentioned in the literature review of this report, one of the reasons mentioned is that performance verification standards do not cover freeform surfaces.

As discussed in Section 2.8, the VCMM technique has made it possible to perform task related calibration of tactile CMMs using complex artefacts and to also take measurements of freeform surfaces. The technique has never been applied to optical CMMs, but it offers a viable solution to the optical CMM challenges mentioned in Section 2.5. In this chapter, a Virtual CMM programme and a stereovision system were developed to perform measurements on a tetrahedron artefact, the same artefact used in Chapter 3.

The VCMM programme was developed on Python and is based on the pyMulticam programme [60]. The purpose of these developments is to apply the VCMM technique in an optical CMM and to demonstrate the achievement of full traceability of measurements in optical CMMs including measurement of freeform surfaces.

4.2 Stereovision System Performance Verification

A stereovision system developed and used in [61] was modified by the author to be able to fit a bigger calibration plate and use cameras with a better resolution. The original system is shown in Figure 19. The modified system consisted of a Canon camera (model EOS 4000D), a Nikon camera (model D750) and a laser (model CL 805). A frame as seen in Figure 19 was used to adjust the distance between the two cameras as well as the distance between the cameras and the clamp/workpiece.

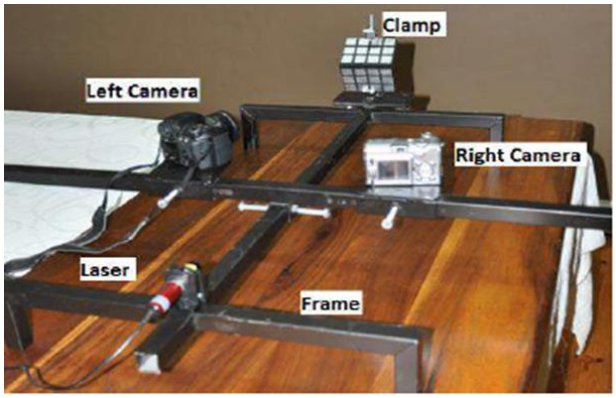

Figure 19: Stereovision system for experiments [61]

The performance verification testing of the developed system was done by following Part 3 of the VDI/VDE 2634 standard since the system meets the application specific requirements of the standard. That is, the developed stereovision system must be based on area scanning which operates on the triangulation principle, measurements must be taken using multiple images and the system can be moved relative to the workpiece when taking measurements.

The standard then specifies the requirements to be met by the artefacts that can be used for performance verification. That is, artefacts within the scope of the standard are linear, planar and spherical. Any arrangement of spherical, planar and linear artefacts within a measurement volume is also within the scope of the VDI/VDE standard. The tetrahedron artefact meets these requirements of the VDI/VDE standard. It is also important to ensure that the artefact has been calibrated with regards to the required dimensions before the standard can be applied. The tetrahedron artefact has already been calibrated for the distances between spheres and the diameters of the spheres in Chapter 3 using the NMISA tactile CMM.

Then to assess the accuracy of the developed stereovision system, quality parameters need to be specified. In this case, only the sphere spacing error quality parameter will be verified because that is what has been calibrated on the tetrahedron artefact. Sphere spacing refers to a distance between two points within the measurement volume. In these tests, the distance between two sphere centres is measured as distances between two points thus the verification of only the sphere spacing error quality parameter. The author did not have the right artefacts to verify the other quality parameters specified by the VDI/VDE standard in Section 3.2, e.g. the flatness measurement error requires a parallelepiped artefact which was not available. Verification of all the quality parameters is beyond the scope of this project.

Generally, limits are specified for the quality parameter before the tests can be performed, but in this case, the stereovision system was manufactured by the author. Therefore, performance verification will be used to determine the limits of the developed system. These limits will then be compared with reverification results from the HP 3D scanner done in Chapter 3. It is understandable to compare these two systems since both systems were used to take measurements of the same dimensions of the tetrahedron artefact. The design of the stereovision system is similar to the HP 3D scanner design and the mode of operation when using the stereovision system will be the same as when the HP 3D scanner was used.

A similar mode of operation when measurements are taken is a very important requirement of the VDI/VDE standard to ensure the comparability of the measurement results. According to Part 3 of the VDI/VDE 2634 standard, it is important to define the measurement volume. In this case, a volume of 350 mm was chosen, which is 350 mm in each of the axes direction, i.e. (350 x 350 x 350) mm. This volume is enough to fit the whole tetrahedron artefact.

4.2.1 Sphere Spacing Error

According to Part 3 of the VDI/VDE 2634 standard, the quality parameter “sphere spacing error” serves to test the capability of the measuring system for performing length measurements from several different single images. This parameter is obtained as the difference between the measured value and the calibrated value of the spacing of the centres of two spheres. The spheres of the tetrahedron artefact are made from carbon steel which was matted with white powder during the test to ensure the spheres are visible to the cameras.

The VDI/VDE standard specifies that the roughness of the artefacts should be negligibly small. In [36], the thickness of the powder was measured to be 10 micrometers. Assuming a rectangular distribution of this error due to powder thickness and comparing it to other uncertainty contributors in Section 3.3.4, the uncertainty due to powder thickness has an insignificant contribution to the uncertainty of the measurement from the HP 3D scanner. It was therefore decided to exclude the error due to the roughness of the spheres and the thickness of the powder used to coat the artefact in this performance verification since the structural design of the stereovision system is similar to the HP 3D scanner.

Calibrated distances between spheres of the artefact are shown in Table 3 with their deviations from their nominal dimensions. The sphere diameters are also measured in the same fashion as the distance between sphere centres and are also included in Table 3.

The VDI/VDE 2634 standard specifies that within the whole measuring volume, any arrangement of the artefact must comply with the sphere spacing error. This is done by measuring the quality parameter at different random positions within the specified volume. The standard further elaborates on the positions that should be measured. The tetrahedron artefact gives a total of six different positions, i.e. six different distances between spheres. The following image in Figure 20 is one of the artefact images taken during testing with the stereovision system.

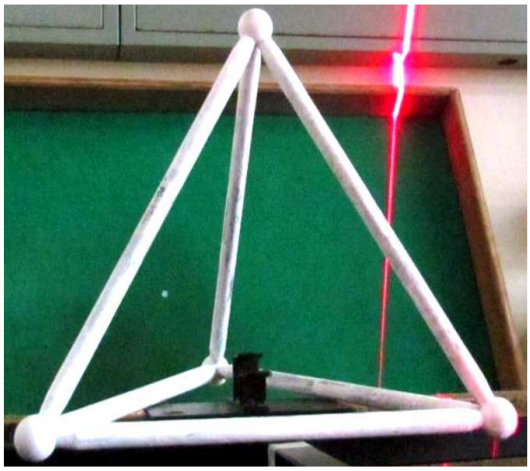

Figure 20: Tetrahedron artefact during performance verification

The stereovision system was used to take the artefact images. For each system position, both cameras were used to take the images of that artefact position. The following are steps followed by a program developed by the author to take measurements from the stereovision system images:

- *Step 1:* Set up the stereovision system as shown in Figure 19. In the position of the clamp, the tetrahedron artefact was placed. Then for each scanning position, it was ensured that the artefact is visible to both cameras. It is always recommended to have a background that does not reflect light for better images, e.g. a green background. This also makes it easy to post-process the images. In this step, it is also important to ensure that the operating conditions of the stereovision system are similar to operating conditions when the HP 3D scanner was used since results from both systems will be compared later in this chapter.
- *Step 2:* The laser was projected on a sphere of the tetrahedron artefact. Both cameras were then used to simultaneously take the pictures of the artefact. This was repeated for all the spheres. The position of the tetrahedron artefact within the volume can be changed in between the scans. This is allowed as long as there is a minimum of two spheres with the laser line visible to ensure that at least one distance between two spheres can be calculated for that specific artefact position.
- *Step 3:* As described in [61], OpenCV and Python were used to:
  - Take a picture with camera 1 (Image 1) and apply the Canny edge detection and Gaussian noise removal functions to get the laser line that lies on the sphere.
  - Select a corresponding image from camera 2 (image 2). The corresponding image is the image of the same artefact position that was taken simultaneously with camera 1.
  - Then the Canny edge detection and Gaussian noise removal functions are applied to image 2 to get the laser line that lies on the same sphere.
  - A point that lies on the image 1 laser line is selected.
  - Then an epipolar line corresponding to the point selected from image 1 was drawn on image 2.
  - The intersection point on image 2 of the epipolar line and image 2 laser line is the image point corresponding to the point selected on the image 1.
- *Step 4*: The image points above and camera matrices were used to triangulate the image points to get the corresponding world points that lie on the sphere.
- *Step 5*: The above steps were repeated many times to get as many world points as possible that lie on the sphere.
- *Step 6*: According to the VDI/VDE standard, the least-squares method [59] must be used to fit a sphere on the above world points. Maximally 3% of the measuring points may be rejected when calculating the fitting sphere. Therefore, a Python code that does this was developed by the author. The code calculates the sphere centre, the sphere diameter and the distance between two selected spheres using the following equations:

$$Sphere\ radius = \sqrt{(x - x_i)^2 + (y - y_i)^2 + (z - z_i)^2} \tag{19}$$

  Where x_i, y_i and z_i are center points of the sphere and x, y, and z are points that lie on the surface of the sphere.

$$Distance\ between\ two\ spheres = \sqrt{(x_2 - x_1)^2 + (y_2 - y_1)^2 + (z_2 - z_1)^2} \tag{20}$$

  Where x_i, y_i and z_i are center points of the spheres with i representing the sphere number.
- *Step 7*: The above steps were also done for all the other spheres of the tetrahedron artefact.

These steps are shown in a flow diagram in Appendix C.1 and more information on how the camera matrices described in *step 4* above were calculated is available in Section 2.9.

The VDI/VDE standard specifies that the sphere spacing error (SD) for each measurement is the difference between the measured value (L_{ka}) and the calibrated value (L_{kr}) of the tested length. This is represented by the following equation:

$$SD = L_{ka} - L_{kr} \tag{21}$$

Table 7 shows the results of the measurements from the stereovision system performed as described in the above steps as well as the calibrated measurements from the NMISA tactile CMM and sphere spacing errors for each measurement which were calculated using equation (21).

Table 7: Measurements from the developed stereovision system

Item	Measurement(mm)	Calibrated(mm)	Spacing error (mm)
Sphere 1 to 2	300.044	299.823	0.221
Sphere 1 to 3	299.369	300.257	0.888
Sphere 1 to 4	299.810	299.852	0.043
Sphere 2 to 3	299.790	299.775	0.015
Sphere 2 to 4	299.722	300.143	0.421
Sphere 3 to 4	299.691	300.031	0.340
Sphere diameter 1	25.029	25.013	0.016
Sphere diameter 2	25.033	25.004	0.029
Sphere diameter 3	24.888	25.006	0.118
Sphere diameter 4	25.043	25.019	0.024

Comparing the deviation of HP 3D scanner measurements in Table 4 with the sphere spacing error of measurements from the developed stereovision system in Table 7, it can be seen that the developed stereovision system generally has less error from the calibrated measurements. This is due to the type of software used. In the developed stereovision system, the author had more control over the points used in the least-squares sphere fit algorithm, and points that do not lie on the sphere were easily discarded. On the other hand, the HP 3D scanner points were exported from the Meshmixer software directly to the least-squares sphere fit algorithm. Some points were discarded when the scan was cleaned, but after exporting the scan to get the 3D coordinate points, it is a difficult and time-consuming process to select and discard points that do not lie on the sphere.

The VDI/VDE standard specifies that when comparing the sphere spacing error with the maximum possible error which is being calculated in this case, it is important to account for the expanded uncertainty of the test method used to get the measurements. Therefore, the following is the uncertainty analysis of the test method for the tests done on the stereovision system.

4.2.2 Uncertainty of Measurements from the Stereovision System

The VDI/VDE standard specifies that the determination of sphere spacing error is essentially influenced by; the uncertainty of calibration of length artefact, the uncertainty of the coefficient of linear thermal expansion, the uncertainty of the temperature of the artefact and the uncertainty of the setup and mounting of the artefact. These are the same uncertainty contributors used in the case of HP 3D scanner uncertainty analysis. For the sake of comparison of results from the HP 3D scanner and the developed stereovision system, it was ensured that the operating conditions were the same for both systems.

Compensations will also be included in this uncertainty analysis for cases where the operating conditions were different. The following are the uncertainty contributors included in this uncertainty analysis:

1. Uncertainty of optical measurement machine reading $u(L_{om})$
2. Uncertainty of the standard's length $u(L_m)$
3. Uncertainty of the standard's linear temperature expansion coefficient $u(\alpha_m)$
4. Uncertainty due to the standard's temperature deviation $u(\theta_m)$
5. Total uncertainty $u_c(e)$

1. Uncertainty of optical measurement machine reading $u(L_{om})$:

The developed stereovision system uses cameras with better resolution than the HP 3D scanner cameras, the camera sensor size was 2934 x 2731 pixels. The longest measurement that could be taken during this experiment was 606.218 mm, that is the longest diagonal length in a volume of 350 x 350 x 350 mm. This gives an estimated system resolution of 0.222 mm, causing an error interval of ∓0.111 mm. The uncertainty due to the resolution limitation, assuming a rectangular distribution, was calculated as:

$$u(L_L) = \frac{0.111}{\sqrt{3}} = 0.064 \text{ mm} \tag{22}$$

Repeatability of measurements is established during the calibration by measuring one of the rods (distance between two sphere centres) five times. In this case, the distance between sphere 1 and sphere 3 was measured. Any spheres could have been chosen to demonstrate the calculations, but sphere 1 and 3 were chosen because they were also used in the uncertainty analysis of the HP 3D scanner measurements. Table 8 shows the results for the average distance measured between the spheres using the stereovision system, as well as the sphere spacing error for each measurement which was calculated based on equation (21). The measurements were repeated 5 times and the averages are included in Table 8. The symbol e is used to denote the average sphere spacing error in this section.

The Python code described in Section 4.2.1 calculates more than a hundred points that lie on each sphere. The least-squares sphere fit Python code uses only twenty points to realize the measurements. For each measurement, different points were used thus the difference in the measurements in Table 8.

Table 8: Repeatability of the stereovision system

Measurement number	Measurement (mm)	Sphere spacing error (mm)
1	300.277	0.020
2	299.644	0.613
3	300.146	0.111
4	299.576	0.681
5	300.082	0.175
Average	**299.945**	**0.320**

From the limitation due to resolution and the average spacing error in Table 8 an uncertainty of the stereovision system measurement reading can be calculated using equation (15), where $u(L_L)$ is 0.064 mm and e is 0.320 mm which gives a stereovision system reading uncertainty of 0.196 mm.

2. Uncertainty of the standard's length $u(L_m)$:

The calculation of this uncertainty contributor has been done in Chapter 3. Therefore, the same results were used in this case:

For the rod (Sphere 1 to 3): $u(L_m) =$ 0.903 mm

And for the sphere (Sphere 3): $u(L_m) = 0.077$ mm

3. Uncertainty of the standard's linear temperature expansion coefficient $u(\alpha_m)$:

This contributor is also the same calculations done in Chapter 3. Therefore, the standard uncertainty for the tubes of the tetrahedron artefact was:

$$u(\alpha_m) = \frac{1.100e^{-6}}{\sqrt{3}} = 0.635e^{-6}\ \frac{\text{m}}{\text{m}}\text{°C}^{-1} \tag{23}$$

and the standard uncertainty for the spheres balls was:

$$u(\alpha_m) = \frac{5.850e^{-6}}{\sqrt{3}} = 3.378e^{-6}\ \frac{\text{m}}{\text{m}}\text{°C}^{-1} \tag{24}$$

Similar to the analysis in Chapter 3, the magnets in the artefact do not have any effect on the length of the tubes or the diameter of the spheres and they are therefore excluded in this uncertainty analysis.

4. Uncertainty due to the standard's temperature deviation $u(\theta_m)$:

During calibration, the lab measured temperature was 18.69 °C and when the stereovision system was used, the lab temperature was 21.50 °C. Therefore, temperature deviations in the lab are estimated to be ∓2.81 °C. Standard uncertainty at proposed rectangular distribution was:

$$u(\theta_m) = \frac{2.81}{\sqrt{3}} = 1.62\ \text{°C} \tag{25}$$

This uncertainty contributor unit is converted to millimetres using the sensitivity coefficient of the standard as shown in Table 9. These methods of calculating the uncertainty contributors are used in the SOP-36 procedure described in Chapter 3. They are also described in more detail in the DIN ISO/TS 23165 standard and the GUM guide.

5. Total uncertainty $u_c(e)$:

The last step of this uncertainty analysis is to calculate the total uncertainty. This is done by combining all the above calculated uncertainties from the different uncertainty contributors as shown in Table 9.

Table 9: Total uncertainty contributors to the stereovision system measurements

Symbol	Rod Standard uncertainty	Sphere Standard uncertainty	Distribution	Sensitivity coefficient	Contribution Uncertainty(mm)		Significance (%)	
					Rod	Sphere	Rod	Sphere
L_{om}	0.196 mm	0.195 mm	Rectangular	1	0.195	0.195	17.766	71.564
L_m	0.903 mm	0.077 mm	Rectangular	1	0.903	0.077	82.089	28.176
α_m	$0.635e^{-6}$ °C^{-1}	$3.378e^{-6}$ °C^{-1}	Rectangular	2.81 °C L	$1.784e^{-6}L$	$9.492e^{-6}L$	0.049	0.086
θ_m	1.622 °C	1.622 °C	Rectangular	$2.200e^{-6}$ °C^{-1}L Or $11.700e^{-6}$ °C^{-1}L	$3.569e^{-6}L$	$1.898e^{-5}L$	0.097	0.173

Therefore, the total uncertainty is:

$$u_c(e) = \sqrt{(u(L_{om}))^2 + (u(L_m))^2 + (u(\alpha_m))^2 + (u(\theta_m))^2} \quad (26)$$

$$u_c(rod) = \pm 0.925 \text{ mm}$$

$$u_c(sphere) = \pm 0.210 \text{ mm}$$

Based on the above calculations using equation (26), the uncertainty of the rod measurement is 0.925 mm and the uncertainty of the sphere diameter measurement is 0.210 mm. This can also be reported as an expanded uncertainty of 1.849 mm for the rod and 0.420 mm for the sphere diameter, both at a 95% confidence level, i.e. at a coverage factor of $k = 2$.

4.2.3 Discussion and Conclusion

The VDI/VDE standard specifies the following equation to be used when comparing the sphere spacing error (SD) with the maximum possible error (MPE) and accounting for the expanded uncertainty of the measurement (U) for the manufacture of the optical system:

$$|SD| \leq |MPE| - U \quad (27)$$

The same equation can be used to calculate the maximum possible error for the system in use by making the maximum possible error the subject of the above equation as follows:

$$|MPE| \geq |SD| + U \quad (28)$$

Table 10 below shows the summary of measurement results from the stereovision system. That is the sphere spacing error and expanded uncertainty for the distance between sphere 1 and sphere 3 as well as for the diameter of sphere 3. Then using equation (28), the maximum permissible error was calculated for each dimension and shown in Table 10.

Table 10: Summary of results for the stereovision system

Item	Rod (mm)	Sphere (mm)
Sphere spacing error	0.888	0.118
Expanded uncertainty	1.849	0.420
$\|\boldsymbol{MPE}\|$	**2.737**	**0.538**

It is understandable to regard the maximum possible errors calculated above as the maximum permissible errors of the developed stereovision system. This is because the most conservative uncertainty and spacing error of all the measurements was used when calculating the maximum possible errors. The VDI/VDE standard also specifies that for the user of the system, the following equation is applicable when comparing the sphere spacing errors with the limit (MPE):

$$|SD| \leq |MPE| + U \tag{29}$$

The VDI/VDE standard does not specify any reason for the difference in the two equations, equation (27) for the system manufacture and equation (29) for the system user. These are both used for comparing the sphere spacing error with the maximum possible error. It can be seen that the equation for the user allows for a bigger spacing error within the specified volume compared to the equation specified for the manufacturer. This in itself will help ensure that optical system manufacturers, manufacture accurate measurement systems.

Equation (29) was applied to all the sphere spacing errors in Table 7 and they all complied with the equation. Therefore, the verification test was considered successful. Furthermore, the results of the stereovision system were compared with results from the HP 3D scanner to check the conformance of the measurements. This is represented using the sketches below which are not drawn to scale.

Rod (Sphere 1 to 3):

- Stereovision system

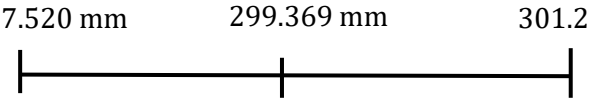

- HP Scanner

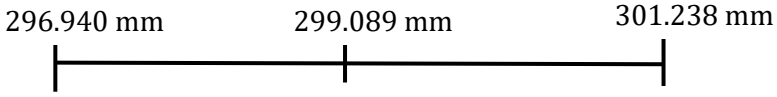

Sphere 4:

- Stereovision system

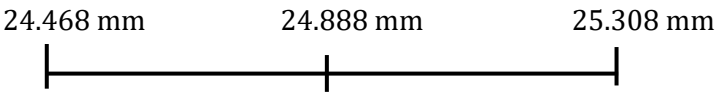

- HP Scanner

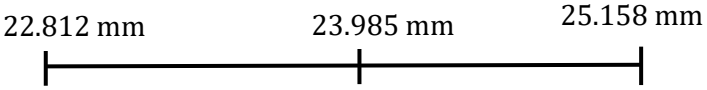

According to clause 2.3a of ILAC-G8:03/2009 on conformance to the specification which is mentioned in the GUM guide, it is clear that the calculated stereovision system uncertainty for the rod is in agreement with results from the HP 3D scanner system, i.e. results conform with each other. Therefore, based on the conformance results and the performance verification results, the stereovision system manufactured by the author can be used to further take measurements that are traceable using the VDI/VDE standard. For the rest of this report, the stereovision system will be used to refer to the hardware system developed by the author.

4.3 Task Related Calibration Based on the VCMM Technique

The second procedure after performance verification of the stereovision system when establishing traceable measurements is the task-related calibration of the system. As mentioned in the introduction to this section, this procedure employs the comparator principle where certain quantities are measured or calibrated to high accuracy. In addition to the comparator principle, the VCMM technique was applied in this procedure by the author and the following is a description of the steps followed by the VCMM Python programme which is based on the pyMulticam Python code [60].

Due to the complexity of the programme, this section was separated into two subsections. The first subsection describes the VCMM calibration code and includes theoretical experiments done to test the code. Then the main focus of the second subsection includes calculating all the uncertainty contributors affecting the calibration of the stereovision system. These uncertainty contributors are then incorporated into the VCMM programme, and then task related calibration of the stereovision system is performed.

4.3.1 VCMM Calibration Programme Development

The following steps describe a programme developed for the application of the VCMM technique on system calibration. This programme only allows artificial noise on the measurements from the tactile CMM and artificial noise on the image points from the cameras of the stereovision system. This noise allows for testing of how the developed VCMM programme behaves as more noise on the measurements is allowed. Later in the next section, the noise and uncertainty contributors to the measurements will be analysed in more detail and added to the VCMM programme instead of the artificial noise.

Programme Development

- *Step 1*: In [62], a smaller calibration plate was manufactured by machining grooves into a 3D plate and it is also shown in Figure 21. A bigger calibration plate was made by the author based on the small calibration plate as shown in Figure 21. The coordinates of the corners of each rectangle on the plate were then measured using a tactile CMM at NMISA. These coordinates can also be determined by measuring three planes that intersect at each corner and applying the law of error propagation to get the point uncertainty [62]. The calculated intersection of the three measured planes will be used as the fiducial points for the camera calibration. This method was not used due to the lack of enough data to apply the law of error propagation. Instead, the corner coordinates were measured using a tactile CMM and their uncertainties will be discussed later. A total of 96 points were measured in the small calibration plate and a total of 128 points were measured in the bigger calibration plate. These measured points are known as original world points. The tactile CMM is traceable to the laser standard at NMISA, thus the point measurements are traceable.

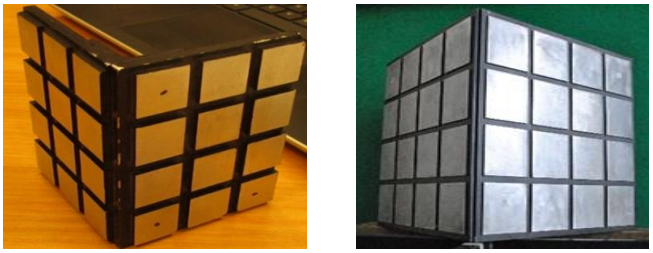

Figure 21: Small calibration plate (125x125x175 mm) on the left [62] **and the big calibration plate (350x350x350 mm) on the right**

- *Step 2*: A function that uses OpenCV was used to process the images. In this function, the edge detection algorithm within OpenCV was used to find the edges of the rectangles on the calibration plates above. Here, the contrast between the shiny surface and the black painted grooves was very useful. Lines were fitted to the detected edges and the intersection of the lines gave the image coordinates of the corners of the rectangles. The corners were detected quickly and matched to the fiducial points. In this description, "points" refer to the same thing as "corners".
- *Step 3*: The camera matrix was then calculated as well as lens distortion parameters. These were used to correct for lens distortion as specified by Hartley and Zisserman [62]. The program calculated new image points from the distortion parameters and the camera matrix. This was repeated for both cameras.
- *Step 4:* A Monte Carlo simulation was applied to repeat steps 1-3. Assuming a normal distribution of the measurements, artificial noise was added to both the image points and world points. The artificial noise is added as a standard deviation of the measurements in the simulation function. In the next section, the standard deviations used for the image points and world point needs to be a representation of real measurements. This will be discussed later. The effect of the number of iterations on the measurement results will also be discussed later.
- *Step 5:* Each output of the parameters calculated by the programme is stored by the programme as a representative sample of potential results for that specific parameter. Then the average and standard deviations of the distortion parameters and camera matrices are calculated.
- *Step 6:* The image points of the calibration object were triangulated using the data from *step 5* to get world points which were referred to as new world points. The deviation between the new world points and the original world points from the tactile CMM was also calculated.
- *Step 7*: The simulation was done several times and the new world points and the deviations from *step 6* were stored as a representative sample of results for each world point. Their averages were later calculated and used as final results for each point, i.e. the average of the sample for each new world point is the measurement for that world point and the average deviation is the uncertainty for that point.

In the statistical routine when the averages were calculated, 100% of the stored results were used to calculate the final results. All the above steps are shown in a flow diagram in Appendix C.2. It can be seen from the above VCMM programme steps that the VCMM gives uncertainty for point coordinates. This is not possible to get with the ISO or VDI/VDE performance verification standards and the VCMM offers a viable solution to calculating uncertainties of any geometric entity. This will be discussed later in this chapter.

4.3.2 Testing the VCMM Calibration Programme

After developing the VCMM programme, testing was done to verify that the programme meets the requirements which include functionality, performance, reliability, repeatability and usability. The following is a theoretical stereovision system shown in Figure 22 which was used to test the VCMM calibration programme described above. The theoretical stereovision system has two identical cameras translated a distance "*d*" from each other and facing the same direction, i.e. no rotation was allowed. A 3D calibration object of known world points was placed in between the cameras at a known distance "z". This theoretical stereovision system in Figure 22 was also coded in Python.

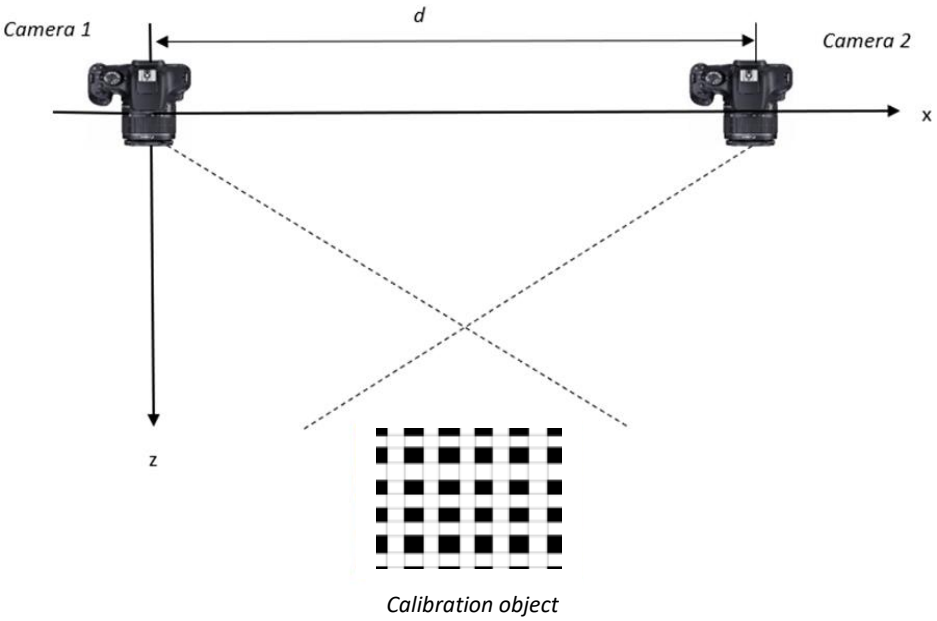

Figure 22: Theoretical stereovision system for testing the VCMM programme

In the theoretical system, it was necessary for the calibration object to always be visible to both cameras during this experiment. This ensured that any image point in a camera 1 picture always had a corresponding image point in a camera 2 picture. In Section 2.9, equation (2) was derived, i.e. the camera matrix equation. For both cameras in the theoretical system, K was the same and R was also the same since no rotation of the cameras was allowed. I was the identity matrix. C for camera 1 was a transpose of [0,0,0] and a transpose of [d,0,0] for camera 2. The following are camera matrices for both cameras based on the theoretical system where f is the focal length of a camera.

$$P_{camera\,1} = \begin{bmatrix} f & 0 & 0 & 0 \\ 0 & f & 0 & 0 \\ 0 & 0 & 1 & 0 \end{bmatrix} \tag{30}$$

$$P_{camera\,2} = \begin{bmatrix} f & 0 & 0 & -d \\ 0 & f & 0 & 0 \\ 0 & 0 & 1 & 0 \end{bmatrix} \tag{31}$$

Using the above camera matrices and the known world points of the calibration object, image points were calculated for both cameras using equation (3). These image points and world points were then used in the VCMM calibration programme to test the programme which also calculates the distortion parameters of the cameras including radial distortions in the cameras.

The VCMM programme was tested using the theoretical stereovision system. Allowing in both cameras, a focal length of 50 mm and 300 mm for d. During the first test, no artificial noise was allowed on the VCMM programme and it was anticipated that there would be no deviation between the original world points and the new triangulated world points, i.e. the uncertainty of the measurement would be zero.

But this was not the case, when testing was done there was a deviation between the world points leading to the measurements having an uncertainty. This uncertainty was due to the algorithms used on the VCMM programme and it is referred to as the algorithm error in this report. The algorithm error is mainly due to the algorithm used when the camera matrices are calculated and the algorithm used when world points are calculated through triangulation.

Calculation of the camera matrices was done using the Gold standard algorithm which is based on the least-squares algorithm and only requires a minimum of twelve image points and their corresponding world points to be implemented [63]. Triangulation was based on the Direct Linear Transform (DLT) algorithm. Both algorithms can be used to do any of the calculations on the VCMM as long as the requirements to use the algorithm are met, these requirements are well documented in literature [63].

The Gold Standard algorithm is considered the optimal algorithm and other algorithms results are assessed by how well they compare to the Gold Standard algorithm [63]. In [64], the Gold Standard and the DLT algorithms were used to calculate camera matrices of a Tsai grid [65] and it was shown that there was a slight improvement (in the order of one-thousandth of a pixel) of results when the Gold Standard algorithm was used. This is a very insignificant improvement and will have an insignificant effect on the measurement results from the VCMM system [66]. Therefore, any of the two algorithms is acceptable on the VCMM system since the choice of the algorithm has an insignificant effect on the system's measurement results.

Figure 23, which was simulated at zero artificial noise, shows the relationship between the algorithm error and the distance of the measured point from the calibration object's origin in each axes of the calibration object, i.e. a scatter plot diagram of all the points x coordinate against their corresponding x coordinate algorithm error. The same was done for all the other axes. It is clear from the results that the VCMM programme algorithm error increases as the distance from the origin of the calibration object increases.

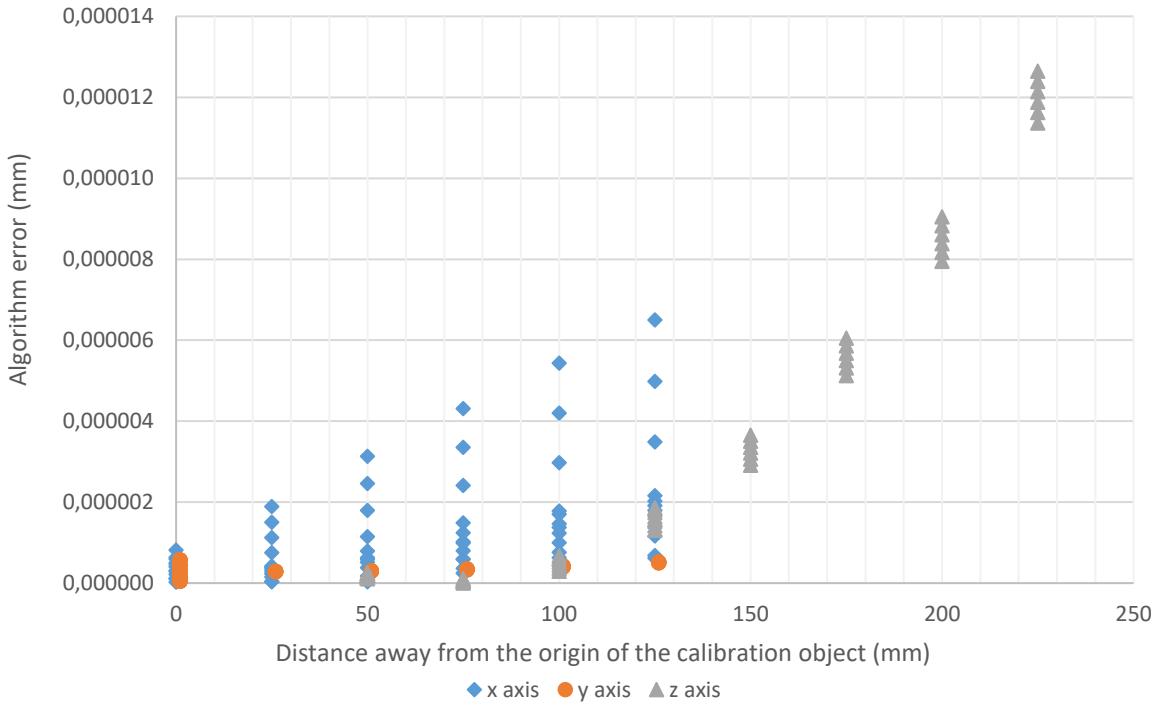

Figure 23: Algorithm error in the VCMM at zero artificial noise

The increase in the algorithm error as the measured distance increases can be seen clearly in the x axes and z axes. The y axes show a decrease in algorithm error as the distance away from the origin increases, which is the opposite of the behaviour shown by the other axes. Therefore, this VCMM behaviour was further investigated by looking at the setup of the theoretical system shown in Figure 22 from the side of camera 1 as shown in Figure 24 below, with O_s representing the origin of the system and O_w representing the origin of the calibration object.

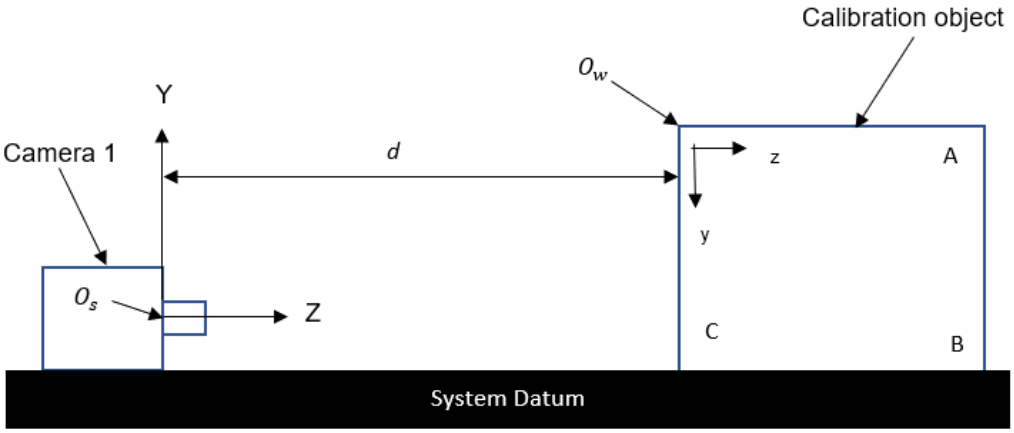

Figure 24: Side view of the theoretical system set up

In Figure 24, it can be seen that points away from the calibration object's origin in the z axes or the x axes (which is not visible in the figure but it's direction is perpendicular to this page) are also away from the cameras. Therefore, in addition to the conclusion made based on Figure 23 for the z and x axes, it can also be concluded that the uncertainty increases as the distance away from the cameras increases. In Figure 23, the y axes show a decrease in uncertainty as the distance from the calibration object's origin increases. But in Figure 24, it can be seen that moving away from the calibration object's origin in the y axes direction decreases the distance between the calibration object and the cameras. Therefore, the conclusion that the uncertainty increases as the distance away from the cameras increases is also valid for the y axes and it is visible in Figure 23.

This relationship between the measurement point and the cameras was anticipated. Points closer to the camera are clearer than points away from the camera when the viewing angle is kept constant [67]. This clear quality of these points is mostly due to their small focal depth (the distance of placement of the image plane relative to the lens) [68]. Table 11 below shows the maximum algorithm error in each axes direction when artificial noise is excluded. The algorithm error is inherently included in the final results of the VCMM and will not be further investigated when uncertainty contributors are investigated later in this chapter.

Table 11: Maximum algorithm errors in each axes

Axes	Maximum algorithm error (nm)
x	6.505
y	0.575
z	12.649

Many tests were performed on the VCMM with the image artificial noise and the world point artificial noise included. As anticipated, the uncertainty of the measurements increases as any of the artificial noises is increased. Another interesting test that was done with the VCMM calibration programme and the theoretical stereovision system, is the investigation of the effect of changing the camera focal length on the uncertainty of the measurements. For this investigation two points were selected; one closer to the cameras [0,26,50] mm and the other point further away from the cameras [125,101,50] mm. The image point artificial noise was kept constant at 0.1 pixels during the investigation and equation (32), which is based on the NMISA tactile CMM calibration certificate, was used for the world points artificial noise. These artificial noises will be discussed later in this chapter.

$$Wp_s = \frac{L+740}{400}\ \mu m \tag{32}$$

Where Wp_s is the world point artificial noise and L is the world point distance from the origin of the calibration object. The camera focal length was ranged between 18 mm and 50 mm. This focal length range was taken from the Nikon camera used in Section 4.2. The distance between the cameras was kept constant at 300 mm while the calibration object's origin was kept 50 mm away from the cameras. Figure 25 and Figure 26 below show the results of this investigation.

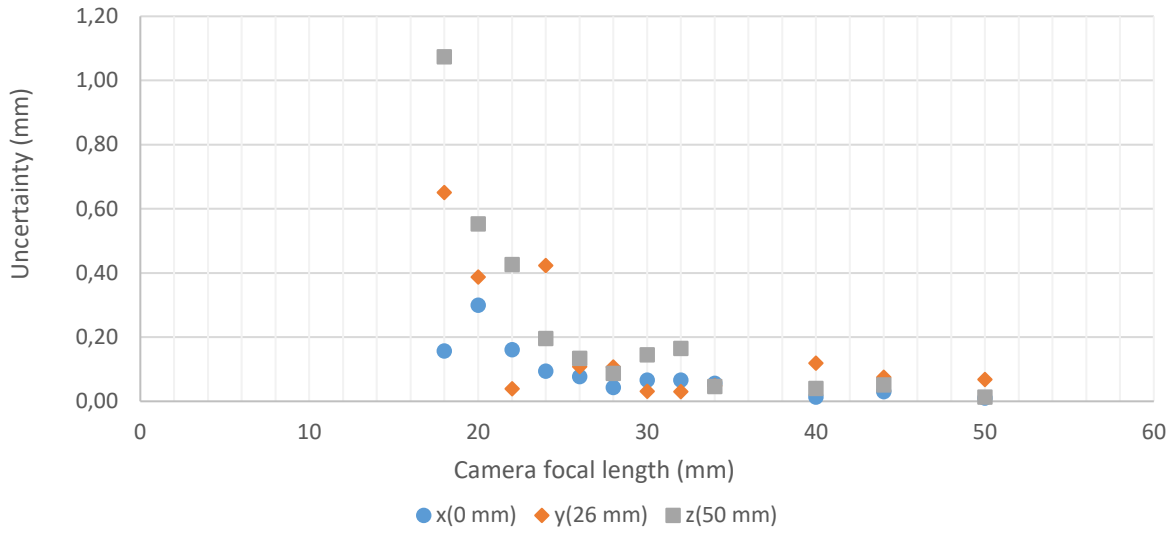

Figure 25: Effect of changing the focal length on the points closer to the origin

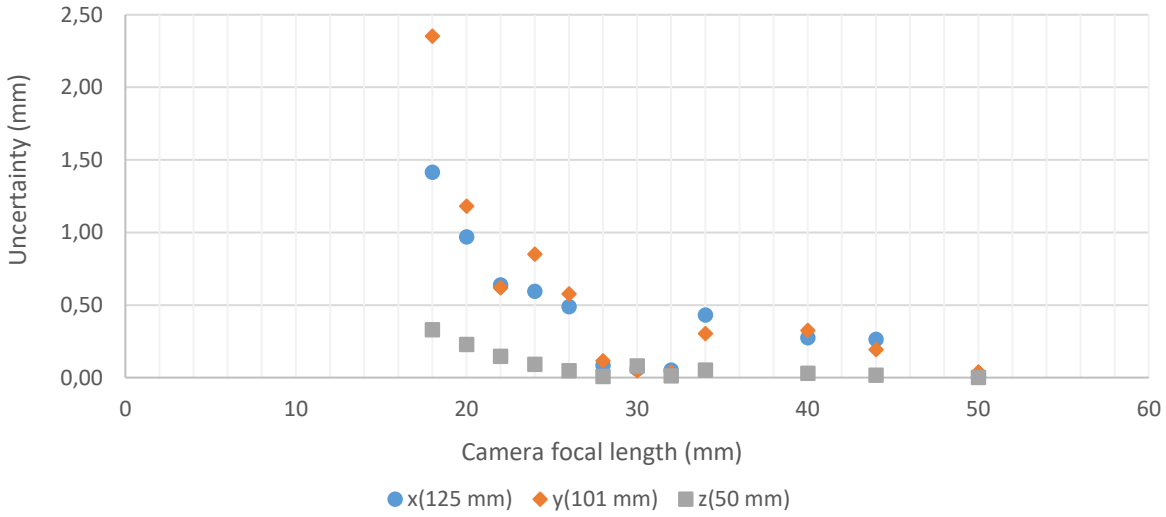

Figure 26: Effect of changing the focal length on points further away from the origin

As can be seen from Figure 25 and Figure 26, the system uncertainty decreases with an increase in focal length. This is expected since the linear pinhole camera model was used and everything on the stereovision system was kept the constant except for the focal length during this investigation. For the linear pinhole camera model, increasing the focal length causes a decrease in the viewing angle of the camera resulting in clear quality pictures since the sensor size remained the same [67]. Whereas when the focal length is decreased, the viewing angle increases for the same sensor size resulting in a more distorted object picture. Distortions are most predominant in the corners as demonstrated in Figure 25 and Figure 26 [67].

The VCMM has to be quick and simple, but at the same time sensitive to all important uncertainty influences, i.e. the artificial noises in this section. The sensitivity of the VCMM system to small changes in the noise allowed on the system was also tested. Table 12 shows the results of this investigation. For this investigation, point [125,1,225] mm was randomly chosen and the tests were performed at a focal length of 50 mm. When the VCMM sensitivity to image point noise was tested, the world point artificial noise was kept at zero. Whereas when the VCMM sensitivity to world point noise was tested, the image point artificial noise was kept at zero.

Table 12: Sensitivity of the VCMM system

Item	Sensitivity to image points(mm)		Sensitivity to world points(mm)	
Artificial noise	0.11 Pixels	0.10 Pixels	Wp_s	$Wp_s + 0.1(Wp_s)$
x	0.104	0.077	$1.874e^{-6}$	0.378
y	0.031	0.012	$0.686e^{-6}$	0.070
z	0.268	0.189	$4.223e^{-6}$	0.440

Many sensitivity tests were performed on the system and it can be seen from Table 12 above that the system is very sensitive to noise especially world point noise, i.e. a small change in the world point measurement noise results in a significant change in the measurement results.

In Section 4.3.4, the stereovision system developed in Section 4.2 will be calibrated using the VCMM programme which has been successfully developed and tested in this section. But first, before the system calibration is performed, it is important to ensure that the noises and uncertainty contributors used in the VCMM are good representations of a real measurement instead of using the artificial noises which were used in this subsection.

4.3.3 Uncertainty Contributors to the VCMM

In this subsection, uncertainty contributors to the VCMM programme are discussed in more detail before the VCMM is used with the stereovision system in the next section. The uncertainty of a measurement from the VCMM programme is essentially influenced by;

1) The uncertainty or noise of the calibrated world points
2) and the uncertainty or noise of the image points from the stereovision system

The uncertainty due to the algorithm error has already been discussed in Section 4.3.2. The above-mentioned uncertainty contributors are overall uncertainties of many uncertainty contributors to optical measurements discussed in Section 2.8.

1) Uncertainty or noise of the calibrated world points

The world points on the bigger calibration plate shown in Figure 21, were calibrated using the tactile CMM from NMISA as described in *step 1* of the VCMM programme in Section 4.3.1. The NMISA calibration certificate specifies equation (32) for the expanded uncertainty of measurements from their tactile CMM at a confidence level of 95%, i.e. coverage factor of 2. Since this expanded uncertainty is at a 95% confidence level, it can be further divided by 2 before it can be combined with other uncertainty contributors and used in the VCMM programme. Refer to the GUM guide on how uncertainty contributors are combined [69].

It is important to ensure that the uncertainties or noises used in the VCMM are a representation of real measurements. The world point expanded uncertainty calculated from equation (32) can be decreased significantly depending on the type of CMM used.

But it must be ensured that it does not go below the minimum practical limit of 24 nm at a 95% confidence level or 12 nm at a coverage factor of 1. This is the best recorded uncertainty achieved by a tactile CMM as reported in [70] and [71].

During the calibration of the stereovision system, environmental conditions were different from the condition when the tactile CMM was used to measure the calibration plate. But most of the differences in the environmental conditions, like the difference in humidity, results in an insignificant length uncertainty contribution since the material of the calibration plate is mild steel [72]. These insignificant uncertainty contributors were excluded in this analysis, but the difference in the measurement environment temperature will definitely have a significant influence on the uncertainty and it was included in the uncertainty analysis as well as the VCMM programme. This difference in temperature results in an uncertainty of the calibration object's linear temperature expansion coefficient and uncertainty due to the calibration plate's temperature deviation.

The linear temperature expansion of mild steel is $11.700e^{-6}\ \frac{\mathrm{m}}{\mathrm{m}}°\mathrm{C}^{-1}$ [58]. This leads to an estimated interval of $\pm 5.850e^{-6}\ \frac{\mathrm{m}}{\mathrm{m}}°\mathrm{C}^{-1}$ when a rectangular distribution is assumed. The calibration plate's linear temperature expansion coefficients uncertainty at this proposed rectangular distribution is $\frac{5.850e^{-6}}{\sqrt{3}} = 3.378\ \frac{\mathrm{m}}{\mathrm{m}}°\mathrm{C}^{-1}$. The laboratory temperature when the world points of the calibration plate were measured using a tactile CMM was 18.69 °C and when the stereovision system was used, a temperature of 21.50 °C was measured. Therefore, the temperature deviation in the laboratory is estimated to be ∓ 2.81 °C. The uncertainty due to the calibration plate's temperature deviation at proposed rectangular distribution is $\frac{2.81}{\sqrt{3}} = 1.62$ °C.

The two above uncertainty contributors are in temperature units. Sensitivity coefficients were used to convert them into the length units as described in the GUM guide [69]. For the calibration plate's linear temperature expansion coefficients uncertainty, the sensitivity coefficient was 2.8 $°\mathrm{C}\ L$, where L is the measured length. This resulted in $9.492e^{-6}\ L$ as an uncertainty. In the case of the uncertainty due to the calibration plate's temperature deviation, a sensitivity coefficient of $11.700e^{-6}\ °C^{-1}L$ was used. This resulted in an uncertainty of $1.898e^{-5}L$. Therefore, the total combined uncertainty of the world points that was used in the VCMM is:

$$World\ point\ uncertainty = \sqrt{\left(\frac{L+740}{800e^{6}}\right)^{2} + (9.492e^{-6}L)^{2} + (1.898e^{-5}L)^{2}} \qquad (33)$$

The length (L) in equation (33) above is in millimetres. This calculated world point uncertainty can be multiplied by a coverage factor of 2 to increase the uncertainty confidence level to 95%. The calculated expanded uncertainty will then be used in the VCMM as a standard deviation of the world points instead of artificial noise throughout the rest of this report as described in *step 4* of the VCMM programme in Section 4.3.1.

2) Uncertainty or noise of the image points from the stereovision system

The uncertainty of image points from the real stereovision system has many uncertainty contributors. In Section 2.9, the effect of temperature on image measurements uncertainty was discussed. Uncertainty due to focal depth and uncertainty due to circle of confusion (this is an optical spot caused by a cone of light rays from a lens not coming to a perfect focus when imaging a point source) is discussed in [73].

In Section 2.9, an analytical expression based on the GUM guide of uncertainty characterizing the results of image processing software was derived which can be used for the uncertainty of measurements from the VCMM. But the expression is difficult to use due to the fact that it requires a lot of tests to be done based on the stereovision system, it does not incorporate all the image measurement uncertainty contributors and performing the tests is beyond the scope of this project.

Alternatively, a more practical noise of 0.200 pixels at a 95% confidence level on the VCMM programme was allowed. This is based on stereovision image measurement experiments performed in [71]. Assuming a rectangular distribution of this noise, this results in an interval of ±0.100 pixels. This is then further divided by $\sqrt{3}$ to get an uncertainty of 0.058 pixels for the image points.

For the standard deviation of image points on the VCMM as described in *step 4* of the VCMM programme in Section 4.3.1, the uncertainty of the image points is multiplied by 2 to get an expanded uncertainty of 0.116 pixels. This increases the confidence level on the image point measurements to 95%. The calculated image point measurement expanded uncertainty will be used throughout the rest of this report instead of using the image point artificial noise.

4.3.4 Task Related Calibration Results

The bigger calibration plate shown in Figure 21 was used for this task related calibration of the stereovision system using the VCMM. Setup details of the stereovision system are shown in Figure 27.

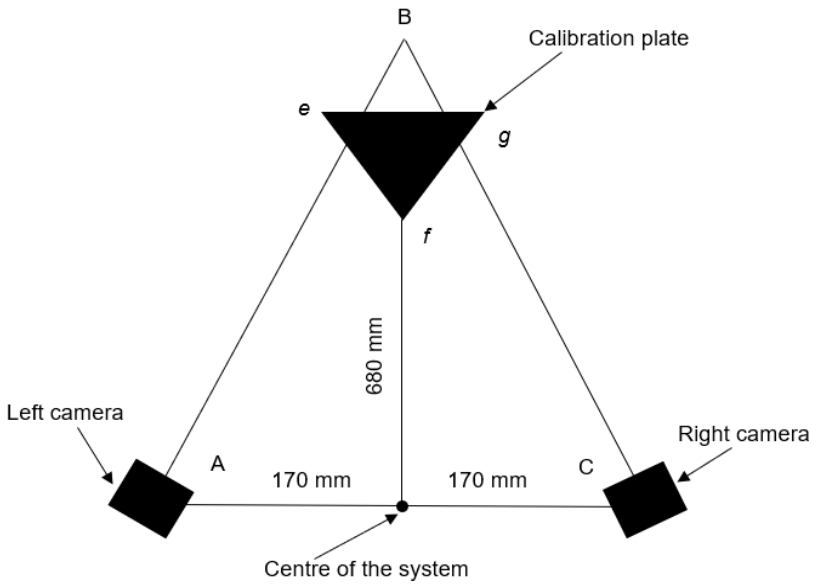

Figure 27: System setup during calibration

The cameras were placed 170 mm away from the centre of the system and the closest point of the calibration plate was placed 680 mm away from the centre of the system. The angle between the cameras, that is angle $A\widehat{B}C$, was approximately 60 degrees. The system was used to take the calibration plate measurements as described in Section 4.2.1.

The first test that was done using the VCMM was a convergence test. This is where the effect of the number of iterations on the measurement results was investigated. Based on the central limit theorem of statistics [74], it was anticipated that as the number of iterations increases, the measurement results will show convergence. Five points were chosen on the calibration plate as shown in Table 13 for the convergence test.

Table 13: Point selected from the calibration plate

Point	x – coordinate (mm)	y – coordinate (mm)	z – coordinate (mm)
1	16.002	339.518	-2.825
2	100.370	94.781	-1.379
3	184.818	11.161	0.392
4	-2.236	94.931	90.667
5	-2.395	95.239	344.624

The convergence test was performed for all the axes of the system. The following Figure 28 shows the VCMM measurement uncertainty convergence after different iterations for only the x axes. The other axes were not reported since they have a convergence behaviour similar to the x axes.

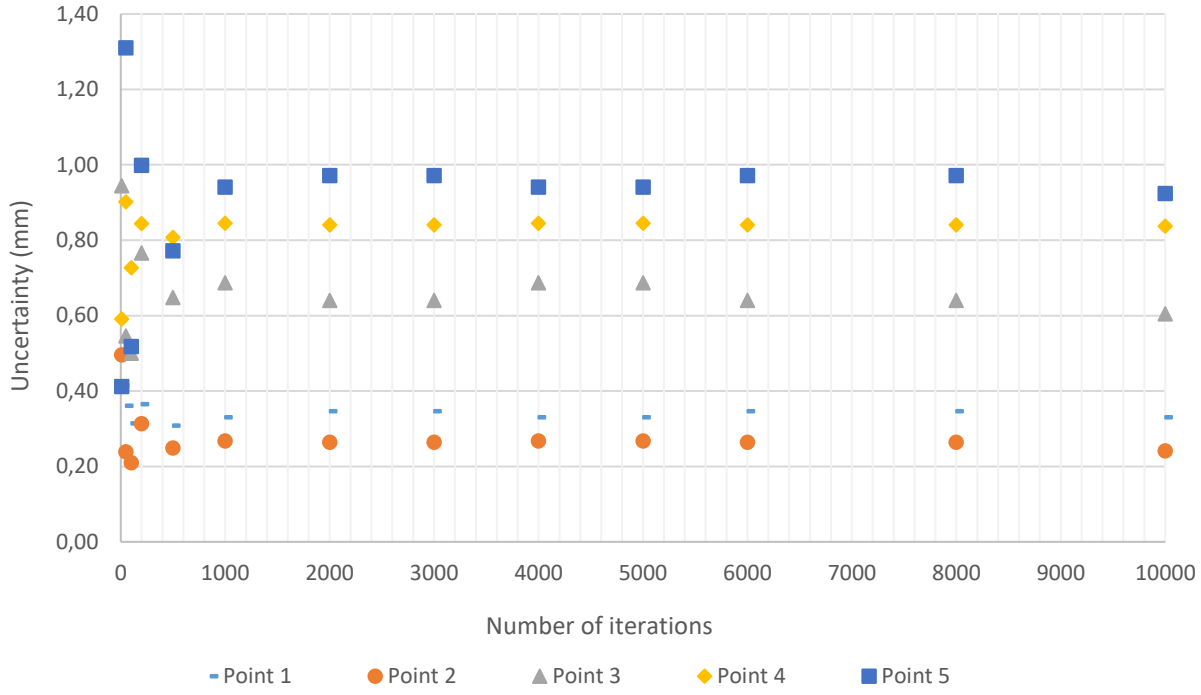

Figure 28: VCMM convergence in the x axes

The convergence of measurement results is shown in Figure 28. From the data points collected, it is clear that the VCMM system convergence was achieved after a thousand iterations. From this convergence analysis, it can be concluded that a thousand iterations or more are necessary on the VCMM when performing measurements. All the remaining tests in this chapter will be done at a thousand iterations.

In Section 4.3.2, it was concluded that points closer to the cameras have less uncertainty than points further away from the camera. This behaviour was mostly due to the focal depth since a theoretical system was used. In this section, the same behaviour is anticipated. But the behaviour will not only be due to focal depth. The circle of confusion (the optical spot caused by a cone of light rays from a lens not coming to a perfect focus when imaging a point source), depth of field (the distance between the nearest and the furthest objects that are in acceptably sharp focus in an image) and aperture also have a significant contribution on the system behaviour [68].

It was also anticipated that the quality of the image will decrease as the distance away from the camera increases. The following calibration plate image in Figure 29 was taken using the right-hand side camera of the stereovision system developed in Section 4.2. In the figure, a few sections were selected and cropped to check the quality of the image in different sections.

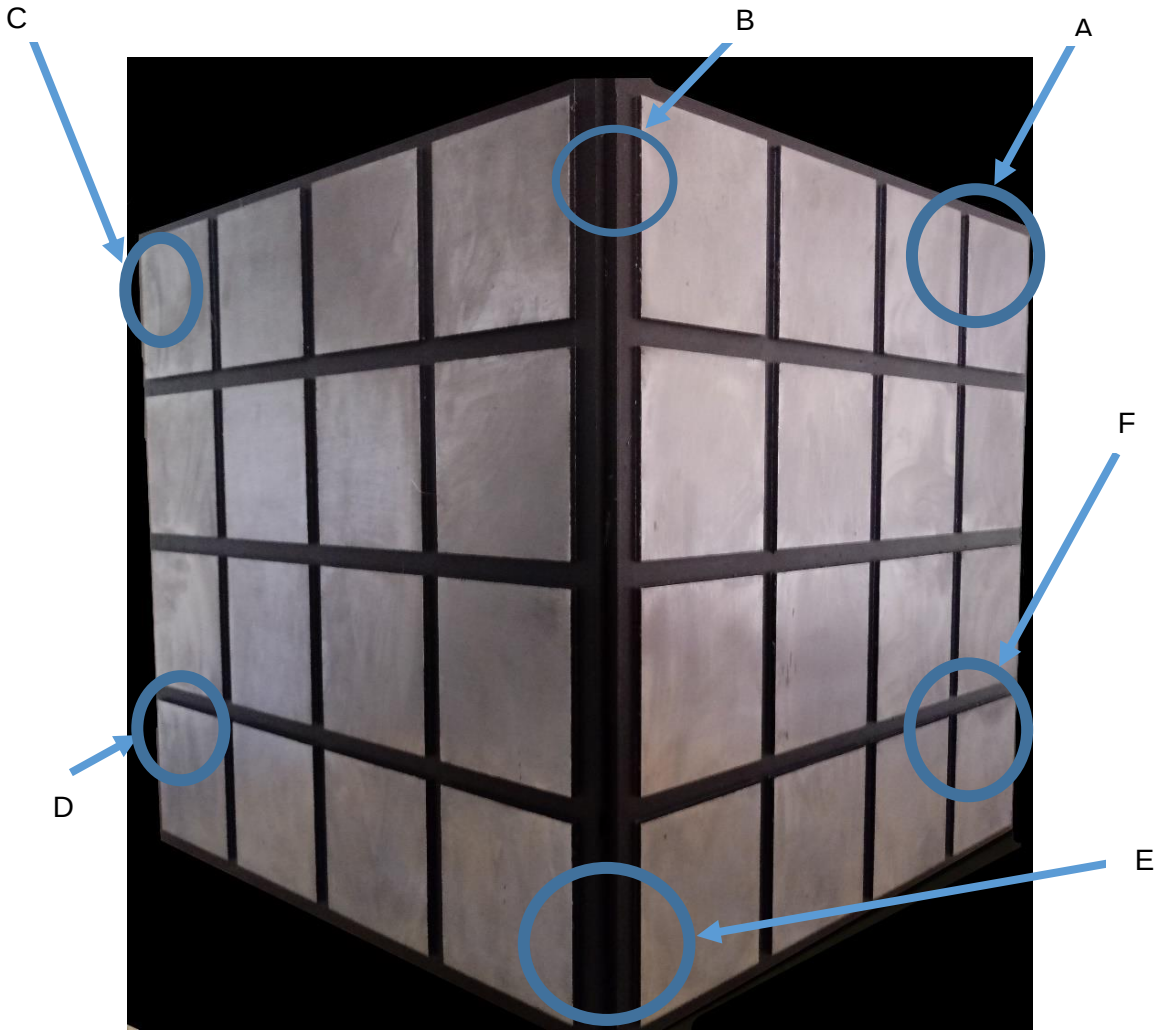

Figure 29: Calibration plate picture from the VCMM

The image in Figure 29 was viewed using Python and OpenCV. Figure 30 below shows the cropped images of each section. Cropping of the images was done using Microsoft Word and it was ensured that the picture sizes are equal.

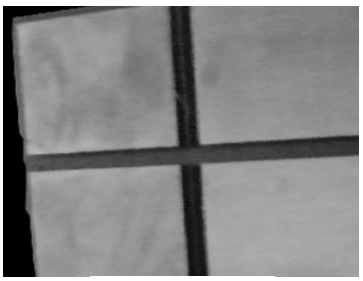

Section C

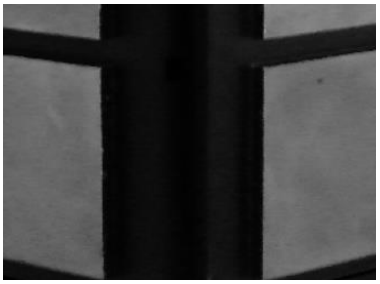

Section E

Figure 30: Cropped images of the different sections

In Figure 29 and Figure 30, the closest section to the camera is section E and section C is the furthest from the camera. In section E the image is sharper than in section C. This holds for all the other sections on the image. More sections of the image are shown in Appendix D. This difference in image quality is another reason for anticipating the real stereovision system measurements to behave similar to the theoretical system measurements performed in Section 4.3.2, i.e. points closer to the cameras have less uncertainty than points further away from the camera. In both the theoretical system and the stereovision system, the VCMM was used.

Figure 31, Figure 32 and Figure 33 show the results of the stereovision system calibration measurements from the VCMM. The calculated expanded uncertainties from Section 4.3.3 were used as standard deviations of the measurements in the simulation function instead of using the artificial noises as described in Section 4.3.1. These figures plot the measurement uncertainty for each coordinate of the calibration plate. Each axes is plotted separately, e.g. Figure 31 only shows the x axes values.

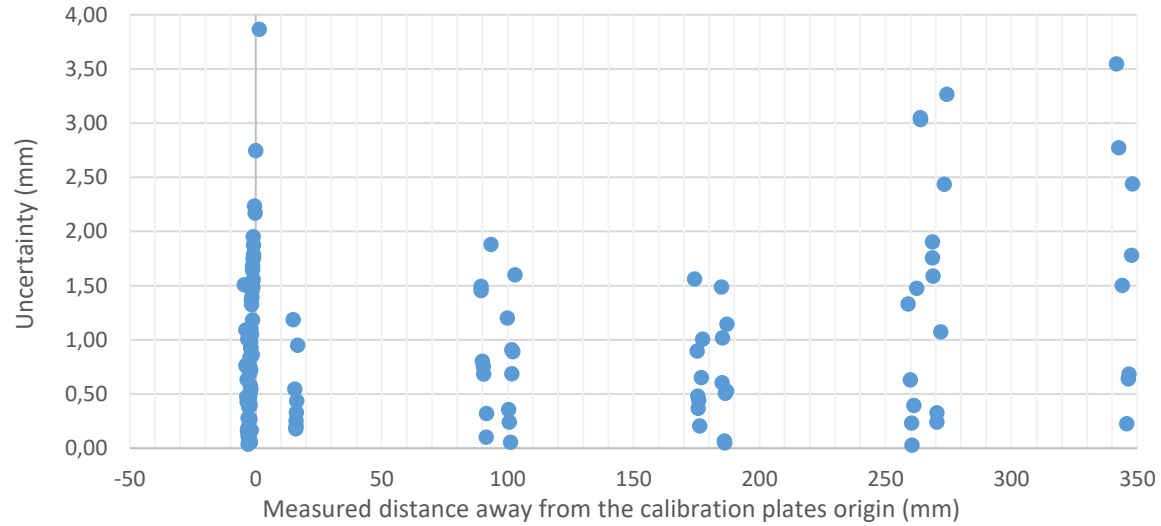

Figure 31: Coordinate's x axes uncertainty from the VCMM

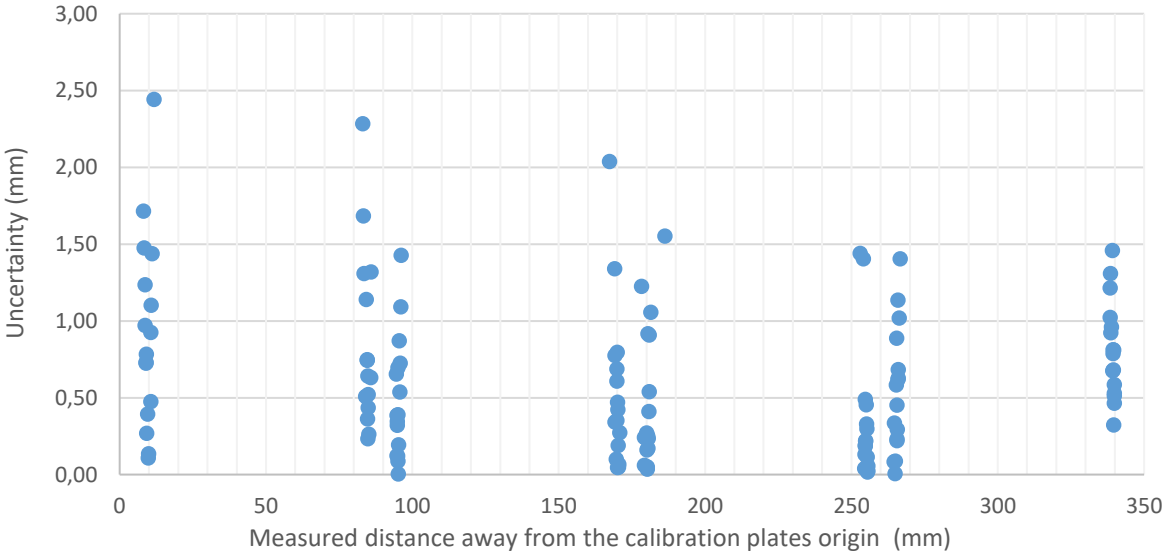

Figure 32: Coordinate's y axes uncertainty from the VCMM

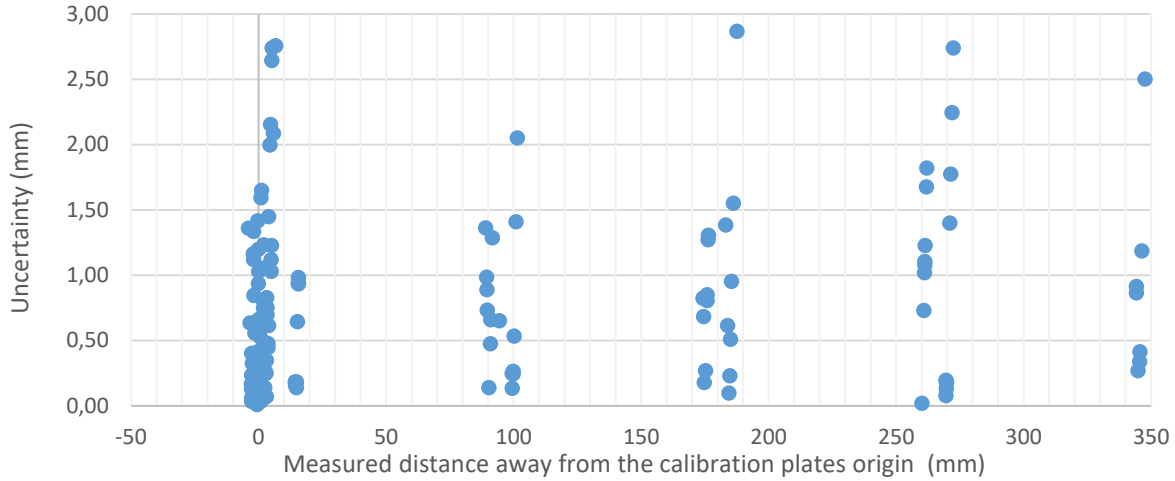

Figure 33: Coordinate's z axes uncertainty from the VCMM

The view of the stereovision system and calibration plate setup used for these tests is similar to the side view shown in Figure 24. Therefore, the stereovision system calibration measurement results using the VCMM show the anticipated behaviour resulting from the uncertainty that increases as the distance away from the cameras increases. This system behaviour was also explained in Section 4.3.2. Figure 24 was used to further explain the behaviour shown by the y axes in Figure 32.

The difference between the measurements done on the stereovision system in this section and the theoretical system which was used in Section 4.3.2, is that the theoretical system uses perfect images. Whereas, the quality of images from the stereovision system is influenced by many factors. These factors have already been described in this section when convergence tests were performed. Figure 29 and Figure 30 were used to further show the effect of the quality of images from the stereovision system on the VCMM measurements. Also, the noise values used in this case are a representation of a real measurement as described in Section 4.3.3 compared to the artificial noise values that were used when the theoretical system was tested in Section 4.3.2.

It can also be noticed that some point measurements in the x axes and the z axes have an uncertainty that is more than the stereovision system's maximum permissible error of 2.737 mm (as calculated in Section 4.2.3). The large measurement uncertainty can either be due to a bad point measurement from the NMISA tactile CMM or bad quality of that specific point on the stereovision system image. Figure 34 and Figure 35 show a scatter plot of the top view of the calibration plate measurements from the NMISA tactile CMM, i.e. the figures show a scatter plot of the x axes and z axes of each side of the calibration plate.

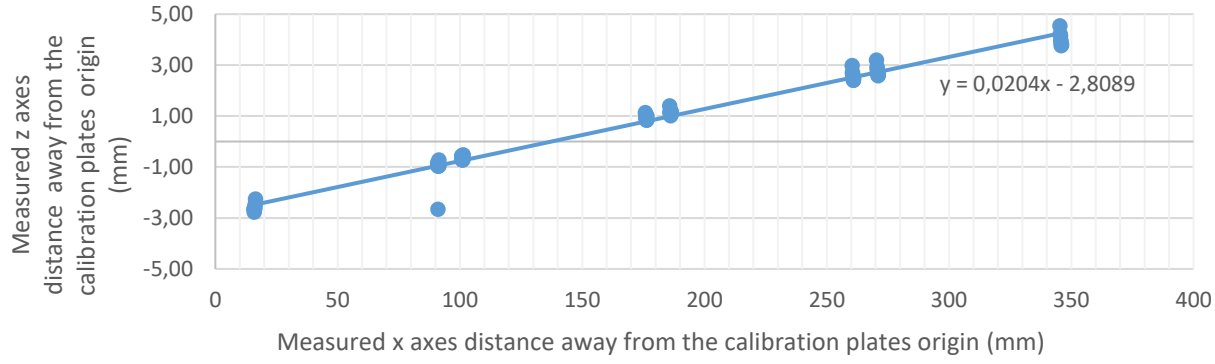

Figure 34: Top view of the right-side distance measurements of the calibration plate

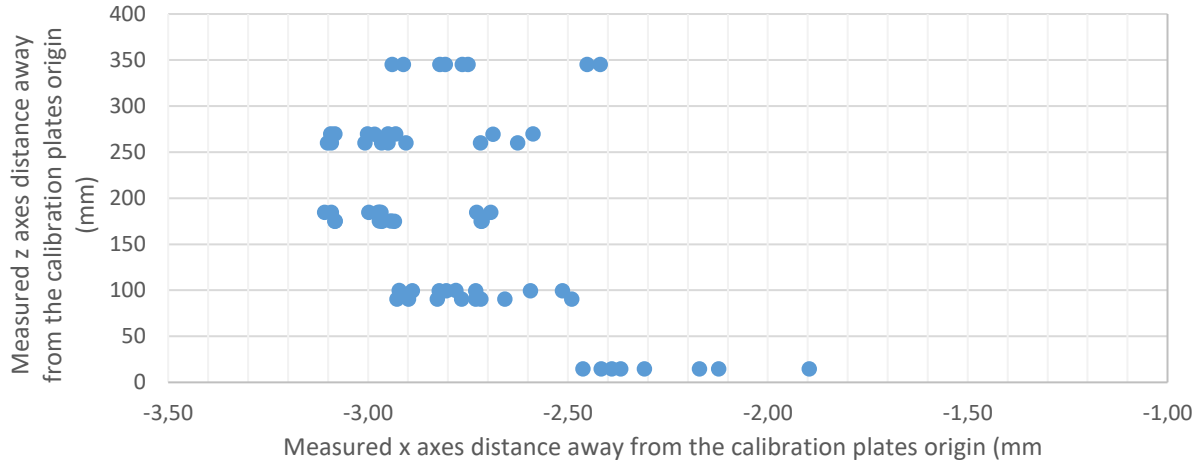

Figure 35: Top view of the left side of the calibration plate

In Figure 34 it can be seen that the right side of the 3D calibration plate is at an angle of 1.169 degrees from the anticipated horizontal position and there is a point measurement that is far away from other points measurements. This point measurement was one of the point measurements with a large uncertainty and it is referred to as an outlier in this report. The outlier is considered as a bad measurement from the NMISA tactile CMM and will be discussed later in this chapter. In Figure 35 a straight line was anticipated but instead, the left side of the plate is curved. Both of these calibration plate deformations do not have a significant effect on the uncertainty of the measurements to account for the large measurement uncertainties shown in Figure 31 and Figure 33 except for the one outlier which will be discussed later.

The large measurement uncertainties from the VCMM can only be due to the accuracy of the point measurements from the NMISA tactile CMM, of which one obvious point has been found already in Figure 34 as an outlier, and the accuracy of the image points which depends on the image quality as explained earlier in this section. These large measurement uncertainties were further investigated by plotting the uncertainties of the measurements as shown in Figure 36 and Figure 37. Figure 36 shows the xy plane of the 3D calibration plate which is referred to as the right-hand side in this report and Figure 37 shows the zy plane which is referred to as the left-hand side of the 3D calibration plate.

In each figure, the measured point coordinates from the VCMM were plotted. Then for each point measurement, four additional measurements were calculated and plotted based on the point measurement and its uncertainty from the VCMM. The following equations were used to calculate the additional four points measurements from the VCMM results:

$$Point_1(x,y) = (x_m + u_{x_m}, y_m) \tag{34}$$

$$Point_2(x,y) = (x_m - u_{x_m}, y_m) \tag{35}$$

$$Point_3(x,y) = (x_m, y_m + u_{y_m}) \tag{36}$$

$$Point_4(x,y) = (x_m, y_m + u_{y_m}) \tag{37}$$

Where $Point_n(x,y)$ is the additional point measurement based on the VCMM results, x_m and y_m are the measurements for each point from the VCMM, x_m is replaced with z_m when these calculations are done for the zy plane. u_{x_m} and u_{y_m} are the uncertainties of the point measurements from the VCMM, in the case of the zy plane u_{z_m} is used instead of u_{x_m}. In both figures, the origin is the same as the origin of the 3D calibration plate.

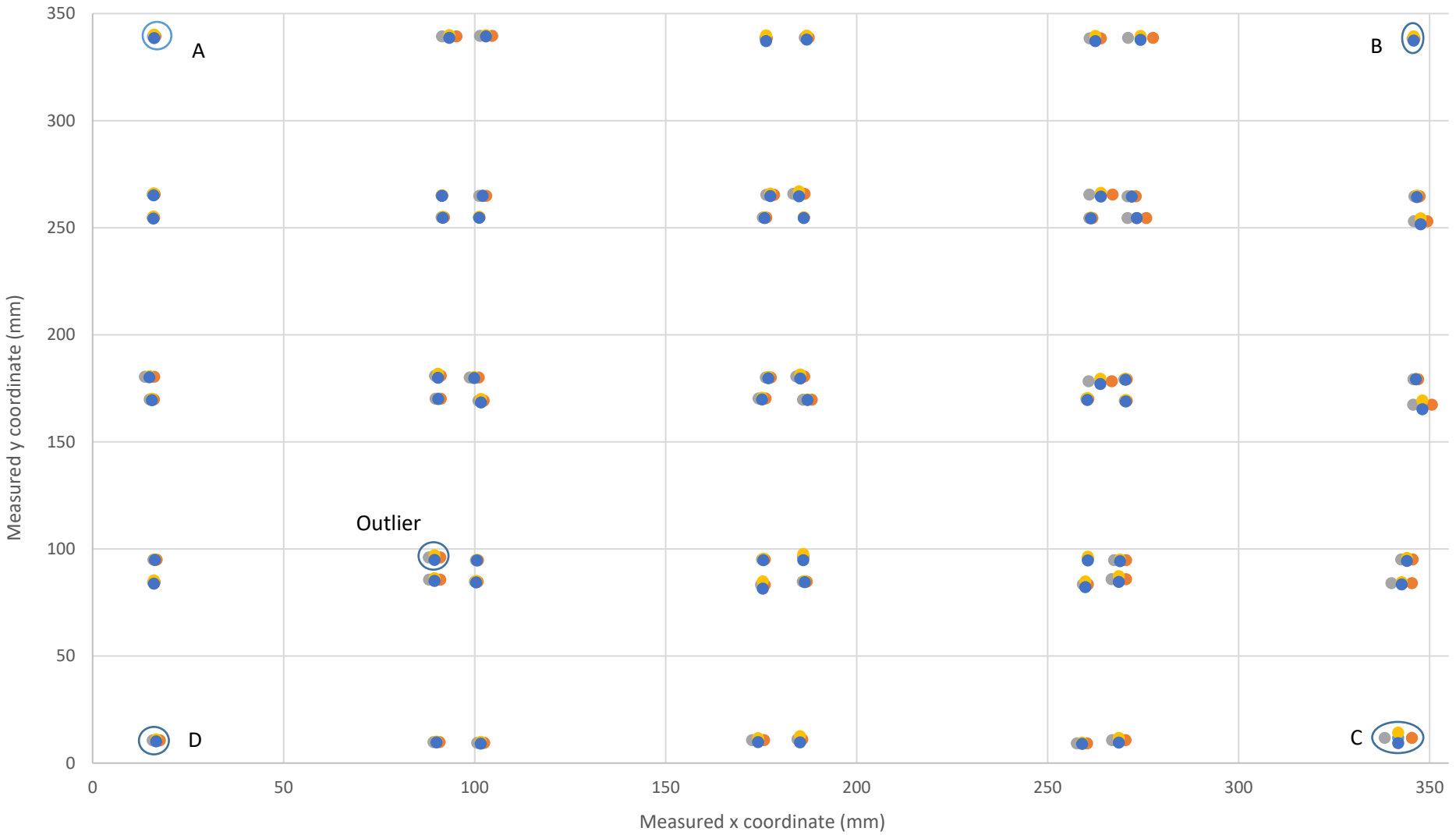

Figure 36: Uncertainty behaviour on the right side of the 3D calibration plate

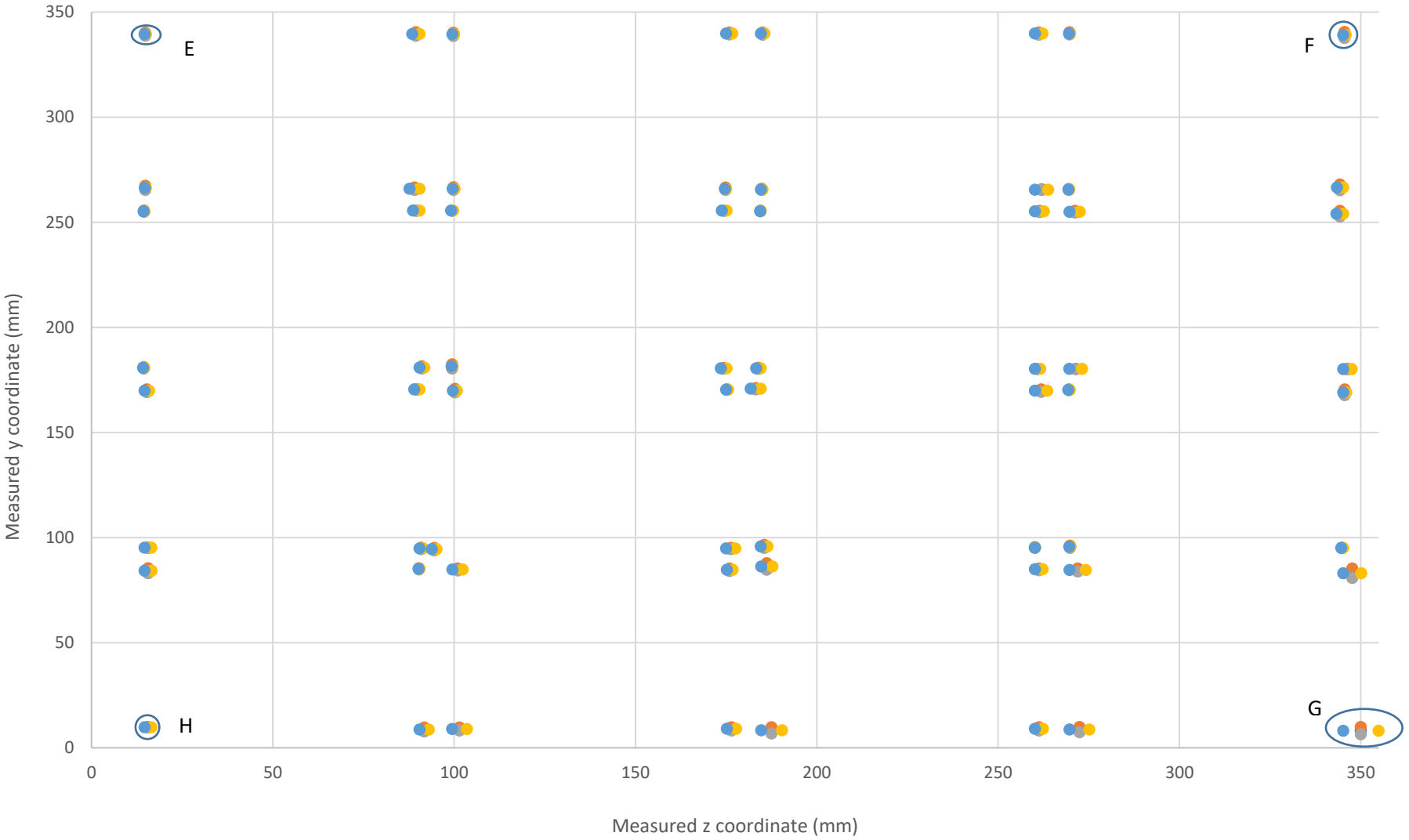

Figure 37: Uncertainty behaviour on the left side of the 3D calibration plate

In both Figure 36 and Figure 37, the anticipated behaviour of the measurement uncertainty increasing as the measured point distance away from the cameras increases can be seen. In Figure 36, point A is the closest point to the cameras, and point C is further away from the cameras. In Figure 37, point E is the closest point to the cameras and point G is further away from the cameras. From the above analysis, it can be seen that only one point has a large uncertainty due to the accuracy of the point measurements from the NMISA tactile CMM, i.e. the outlier shown in Figure 36. Therefore, it can be concluded that the rest of the large measurement uncertainties are due to the accuracy of the image points which depends on the image quality as explained earlier in this section.

The best way to deal with the large measurement uncertainties from the VCMM is to perform the measurements again, this time around ensuring that both the tactile CMM measurement and the image point measurements are accurate. Image point measurement accuracy can be improved by using cameras that have a better resolution than the cameras used in the stereovision system shown in Figure 19. Another method of dealing with big uncertainties is to remove the points with big uncertainties and recalibrate the system. The second method will be discussed later in this section.

In the introduction to this chapter, it was mentioned that task related calibration employs the comparator principle. Here certain quantities are measured or calibrated to high accuracy. The measured quantity is then compared with a calibrated standard of similar form and dimension. In this case, the comparison was done by comparing the deviation of the VCMM measurements from tactile CMM measurements with the maximum permissible error of 2.737 mm calculated in Section 4.2 during performance verification of the stereovision system.

In the case where the deviation is bigger than the maximum permissible error, the first option is to remeasure the point and do the calibration again. The beauty of using the VCMM for the system calibration, referred to as VCMM calibration in this section, is that there are a lot of points that are calibrated within the volume. Therefore, the VCMM calibration allows for the removal of some of the points that were measured badly instead of doing the whole measurement from scratch. In this case, only eight of the hundred and twenty-eight points exceeded the maximum permissible error and were removed during the calibration. This includes the outlier that was discovered earlier in this section. Figure 38, Figure 39 and Figure 40 show the final calibration measurements of the stereovision system using the VCMM after some of the points with a bigger uncertainty were removed from the VCMM calibration.

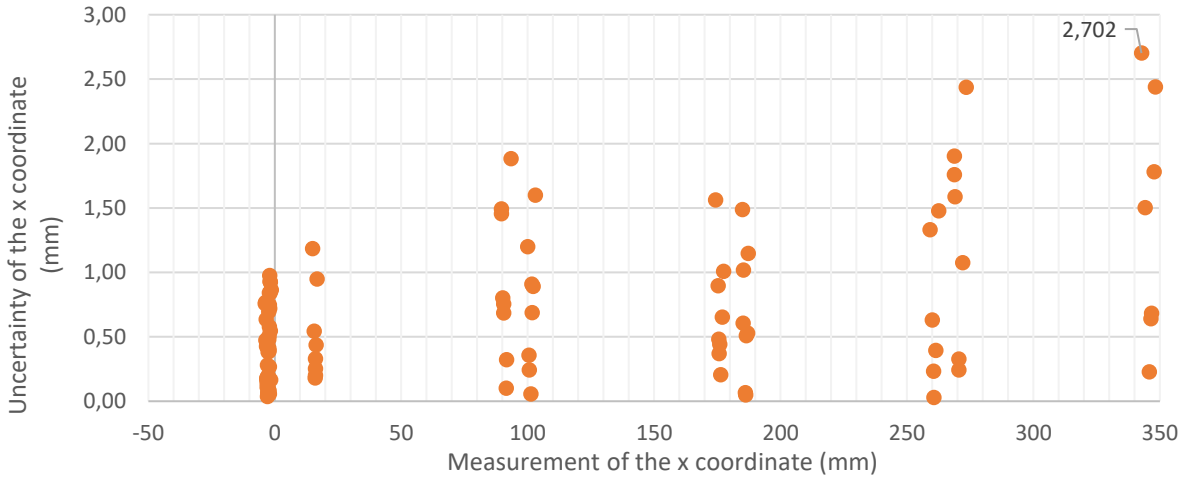

Figure 38: Final x coordinate calibration measurement

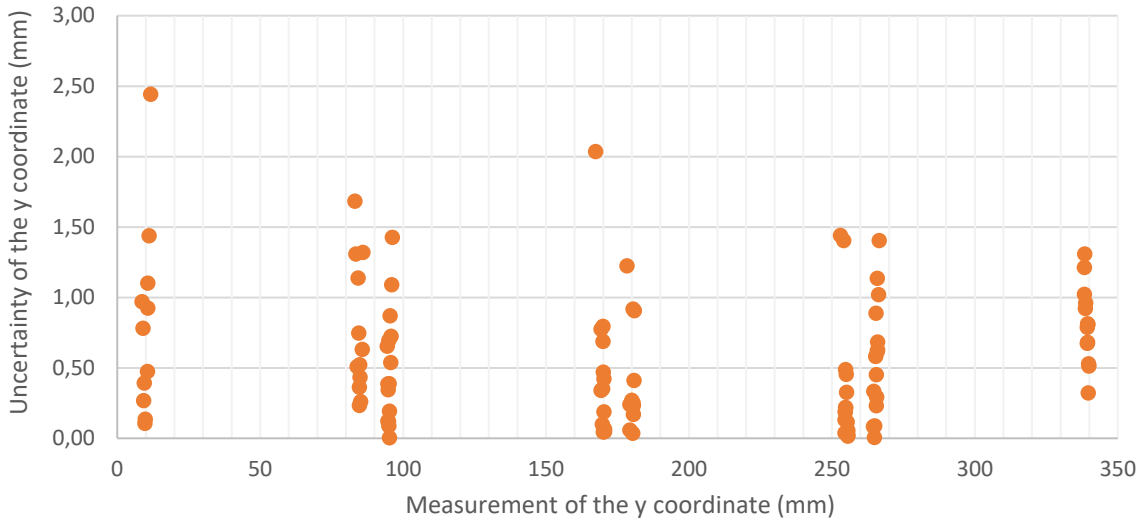

Figure 39: Final y coordinate calibration measurement

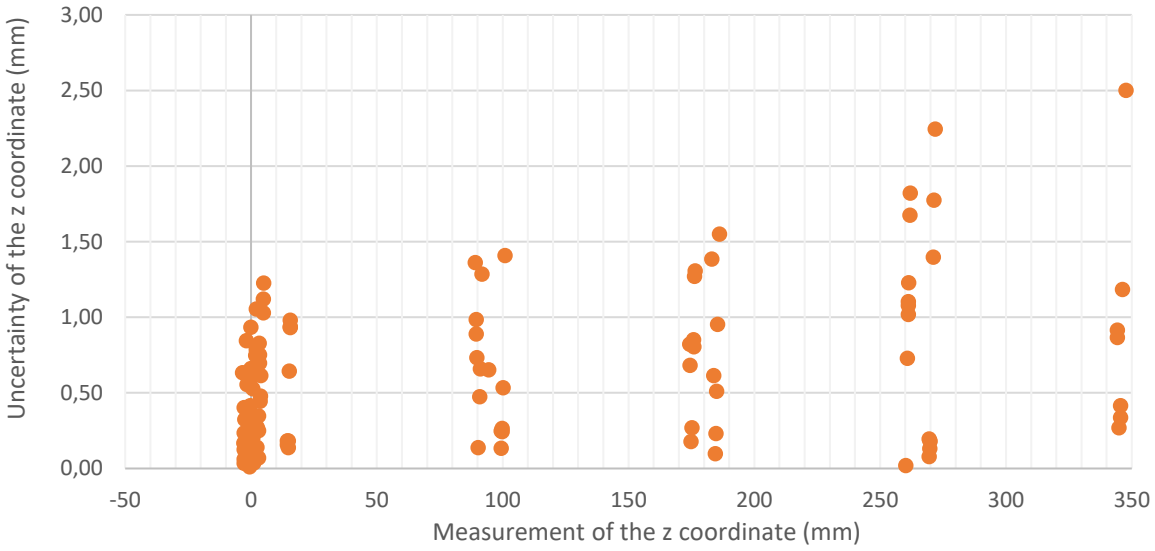

Figure 40: Final z coordinate calibration measurement

Up to this point in this chapter, the performance verification of the developed stereovision system has been done successfully and the developed VCMM was successfully used to perform the task related calibration of the stereovision system. The VCMM inherently adds the algorithm errors on the measurements. It was also ensured that there is a 95% confidence level in both the NMISA tactile CMM measurements as well as their corresponding image point measurements. Also, 100% of the stored Monte Carlo simulation results were used to calculate the final measurement results for each coordinate as described in Section 4.3.1.

Based on all these mentioned reasons and the GUM guide on the combination of uncertainty contributors [69], it is understandable to have more than 95% confidence level on the measurements from the developed VCMM system, i.e. the measurements have a coverage factor of 2. Therefore, the stereovision system has been successfully verified for its performance and calibrated and can be used to take measurements. The process of measurements and simulation done on the VCMM is regarded as calibration of the stereovision system since it generates valid uncertainties for all the measured points of the 3D calibration plate.

4.4 Measurement of the Tetrahedron Artefact Based on the VCMM Programme

In this section, the stereovision system will be used to measure a tetrahedron artefact shown in Figure 15. The VCMM will be used to estimate the measurement uncertainties for each measured dimension. The decision whether the VCMM still calculates the "correct" measurement uncertainty can be determined by comparing VCMM measurement results of the tetrahedron artefact with the calibrated values which were measured in Section 4.3.4. This will be further investigated in this section by further comparing the VCMM measurement results with measurements from the HP 3D scanner used to measure the tetrahedron artefact in Section 3.3.

The beauty of using a VCMM is that it gives an uncertainty of a point in 3D space. This allows for the achievement of full traceability of measurements from the optical CMMs. This is due to the fact that the point measurement and the uncertainty can be propagated to any type of shape or surface function including freeform surfaces. This will also be demonstrated in this section.

Another advantage of having an uncertainty of a 3D point on the selected volume is that the user of the VCMM can see how the point measurement uncertainties are distributed within the volume. The user is then able to place the workpiece on the part of the work volume where there are smaller measurement uncertainties. For example, based on the calibration done in Section 4.3.4, a workpiece must be placed closer to *f* in Figure 27. This is the side of the stereovision system calibrated volume closer to the cameras. The initial VCMM programme used during the stereovision system calibration described in Section 4.3.1 was modified as described in the following steps to be able to give the tetrahedron artefact dimensional measurements with their uncertainties as outputs of the VCMM programme:

- *Step 1:* The calibration plate was replaced with the object to be measured, i.e. the tetrahedron artefact.
- *Step 2:* Many image points of the tetrahedron artefact that lie on the intended tetrahedron spheres were calculated as described in *steps 2* and *3* in Section 4.2.1. In this case sphere 1 and sphere 3 were only calculated since they were the only spheres used when the HP 3D scanner was used to take measurements.
- *Step 3*: These image points and their standard deviation are added to the VCMM programme using the Monte Carlo simulation function. The image point standard deviation has already been calculated in Section 4.3.3.
- *Step 4*: Allow for the VCMM calibration programme as described in Section 4.3.1.
- *Step 5*: The sphere image points from *step 3* and camera matrices calculated in *step 4* during calibration were used to triangulate and get the corresponding world points that lie on the sphere. Since in step 3, there are many sphere image points added to the VCMM. Many sphere world points are calculated simultaneously in this step.
- *Step 6:* A least-squares sphere fit Python code developed in Section 4.2.1 is used to calculate each sphere centre, each sphere diameter and the distance between two selected spheres using equation (19) and (20).
- *Step 7:* This is where the law of propagation of error is used [75]. This is a mathematical derived way of combining the multiple uncertainties of the variables that make up a function in order to get an accurate measurement uncertainty of the function. The VCMM can calculate the uncertainty of each and every variable that is part of the function, i.e. the uncertainty of the x y and z coordinate of each point in the 3D space.

Using the law of propagation of error, the following functions for the uncertainties of equation (21), which calculates the sphere radius, and equation (22), which calculates the distance between two sphere centres, were calculated:

$$U_{(21)} = \sqrt{\frac{\left(U_x^2+U_{x_i}^2\right).(x-x_i)^2+\left(U_y^2+U_{y_i}^2\right).(y-y_i)^2+\left(U_z^2+U_{z_i}^2\right).(z-z_i)^2}{\left(\sqrt{(x-x_i)^2+(y-y_i)^2+(z-z_i)^2}\right)^2}} \tag{38}$$

$$U_{(22)} = \sqrt{\frac{\left(U_{x_2}^2+U_{x_1}^2\right).(x_2-x_1)^2+\left(U_{y_2}^2+U_{y_1}^2\right).(y_2-y_1)^2+\left(U_{z_2}^2+U_{z_1}^2\right).(z_2-z_1)^2}{\left(\sqrt{(x_2-x_1)^2+(y_2-y_1)^2+(z_2-z_1)^2}\right)^2}} \tag{39}$$

$U_{(21)}$ is the uncertainty of the sphere radius and $U_{(22)}$ is the uncertainty of the distance between two sphere centres. In both equations, the variables used were described in Section 4.2.1 and U_i is an expanded uncertainty of variable i, e.g. U_{x_2} is the expanded uncertainty of x_2. In Section 2.7, it was seen that freeform surfaces are generally described as functions using polynomials, neural networks, non-uniform rational basic splines and other mathematical methods depending on the form of the artefact. After the surface has been described mathematically, the law of error propagation can be applied similar to equation (21) and (22) to get the function uncertainties which is an uncertainty of the freeform surface.

Some freeform surfaces are difficult to describe or estimate as a function. Since the VCMM calculates a point in 3D space with its uncertainty, a lot of points that lie on the surface of the freeform shape can be measured using the VCMM with their uncertainty in that way calibrating for the form of that complex artefact as shown in Figure 41 [76]. Therefore, full traceability of freeform surfaces can be achieved with optical CMMs using the VCMM technique.

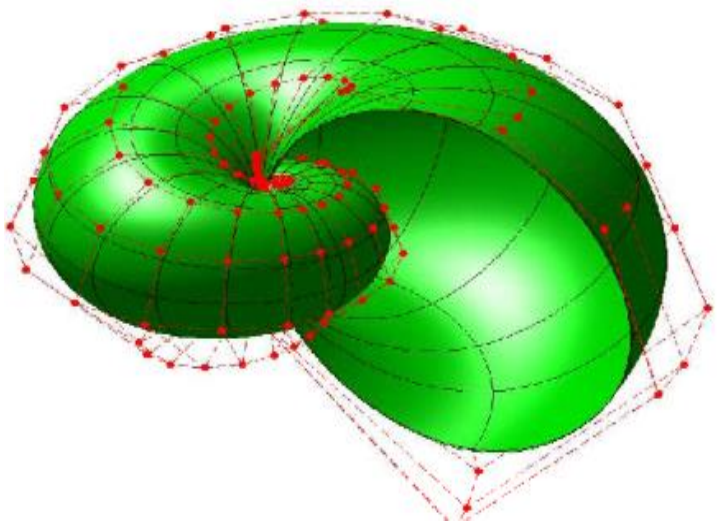

Figure 41: Example of a freeform surface [76]

- *Step 8:* All the above steps were repeated at least 1000 times and the sphere radius and the distance between two spheres were stored as a representative sample of results for the artefact measurements. Later the sample averages were calculated and used as final measurement results.

Based on the above steps, it can be seen that any type of shape can be measured using the VCMM. The following Table 14 shows the tetrahedron artefact measurement results from the tactile CMM as well as both the VCMM and the HP 3D scanner for sphere 3 and the distance between sphere 1 and sphere 3. When the stereovision system was used, the tetrahedron artefact's intended spheres, i.e. sphere 1 and sphere 3, were placed as close as possible to the cameras within the calibrated volume.

Table 14: VCMM simulation measurement results of a tetrahedron artefact

Item	Tactile CMM (mm)		HP 3D Scanner (mm)		VCMM (mm)	
	Measurement	Uncertainty	Measurement	Uncertainty	Measurement	Uncertainty
Sphere 3	25.006	0.002	23.985	1.173	25.276	0.687
Sphere 1 - 3	300.257	0.003	299.089	2.149	299.145	1.475

In Table 14 it can be seen that the VCMM is more accurate than the HP 3D scanner. In this chapter, the VCMM technique has been successfully applied in optical CMM measurements to achieve full traceability of measurements in these systems. Full traceability of freeform surface measurements has also been theoretically demonstrated which is not possible with other methods discussed in the literature review of this report. Performance verification using the VDI/VDE standard was also demonstrated in this chapter.

Chapter 5: Conclusions and Recommendations

The main objectives of this research were to investigate the traceability of measurements in optical coordinate measuring machines in various South African industries and to develop a virtual optical coordinate measuring machine to establish traceability. The research background and literature review showed that the application of the VCMM technology in optical CMMs can go part of the way in solving the traceability challenge. This technique will even allow traceable measurements to be done in complex freeform artefacts.

In Section 2.6, a survey was done to investigate the distribution of different types of CMMs in the South African industry, especially optical CMMs. The survey indicated a significant uptake of optical CMM systems in the country and a need for an acceptable national standard in order to support the activities of the companies already using optical CMMs.

In Section 2.10, challenges in optical CMMs measurements were investigated and possible solutions were given to mitigate the uncertainty contribution of each challenge. In the literature review, a Virtual CMM is shown as a viable approach for determining measurement uncertainty and achieving full traceability in optical measurement systems. Therefore, a framework for developing a Virtual CMM to establish traceability of optical measurements is described in Section 4.3.1.

The optical VCMM was developed and successful measurements of a tetrahedron artefact were taken using a tactile CMM, an HP 3D scanner and the developed optical VCMM system. The results were all in agreement with the optical VCMM having an uncertainty of 1.475 mm for the measured distance of 299.145 mm and an uncertainty of 0.687 mm for a diameter of 25.276 mm. The confidence level in both measurements is 95% and the VCMM was more accurate than the HP 3D scanner. It was also successfully demonstrated how freeform surfaces can be measured using the VCMM in theory.

This research is a valuable contribution towards the South African metrology industry and the International Standardisation Organisation (ISO) in trying to achieve traceability of optical CMM measurements and overcoming the many challenges faced by the users of optical CMMs. In the future, the uncertainty achieved from the optical VCMM system can be improved significantly by investing more time in developing a more robust stereovision system including the calibration plate. This can be done by taking more accurate tactile CMM measurements and image points of the calibration plate and calculating the noise of image points and also include all the possible uncertainty contributors on the VCMM.

Appendix A: CMM Standards

An internationally recognized standard allows for better communication between users and manufacturers [7]. To better understand the standards applicable to the different coordinate measuring systems (CMM), the CMMs are separated by their measurement range distances as follows:

1. The nano/micro range (<10 mm)
2. The close range (10 mm – 2 m)
3. The mid to long-range (>2 m)

A.1. Nano Range

In this range, the ISO-TC 213 standard has a series of documents for the practitioner, these documents are related to profile measurement on a surface and they are summarized in the ISO 25178 (GPS): Surface Texture Standards [7]. Determination of surface texture is done using either a series of profiles or area measurements. A comprehensive documentary specification standard B46.1 which includes some area analyses has also been published by the ASME [77]. Assurance is given by the ISO 25178 standard that measurement in this range are traceable since it provides a measurement standard (ISO 25178-70), a means for calibrating the deviation of the instrument (ISO 25178-600), a way to calculate area surface texture measurements (ISO 25178-71) and a method for calculating the uncertainties associated with the measurements [78].

A.2. Close Range

The available standards and test methods in this range are used to measure the spatial accuracy of close-range 3D optical imaging systems. These standards are mostly utilized in the assessment of the accuracy of an indication of size, e.g. probing error, sphere spacing error, flatness, length and measurement error [79].

Form is usually evaluated as part of a probing error for spheres and flat surfaces. In CMM systems, the parameter probing error is defined as the three-dimensional behaviour of the entire CMM system in a very small measured volume [79]. Differentiation is generally made between the probing error form and probing error size in the VDI/VDE 2630-1.3 standard, where probing error size (PS) refers to the difference between the measured diameter and the reference diameter.

$$PS = D - D_{ref} \tag{40}$$

Whereas probing error form (PF) refers to the difference between the maximum and the minimum distance of the measured surface points from the centre of the sphere.

$$PF = R_{max} - R_{min} \tag{41}$$

Figure 42 below shows the sphere diameter and the maximum and minimum distance of a measured surface point from the centre of the sphere.

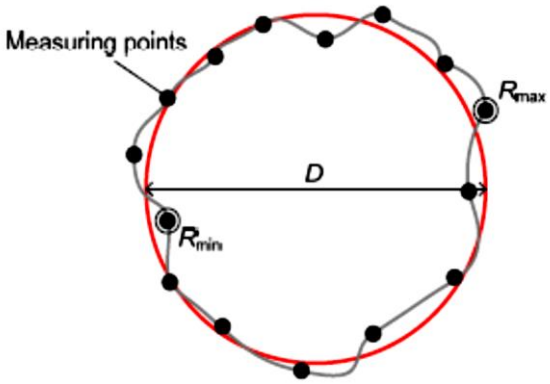

Figure 42: Measurement of the sphere diameter (D), the minimum distance from the sphere centre (R_{min}), and the maximum distance from the sphere centre (R_{max}). A best fit method was used for the compensating element, i.e. the circle in this figure [79]

Currently, the national guideline and international standards in this range of 3D imaging systems only cover the basic shapes, i.e. shapes that are not complex [7]. The German VDI/VDE standard has been very active in defining standards for coordinate metrology especially coordinate measuring machines (CMMs) equipped with optical probing (2D and 3D) capability. The VDI/VDE 2617 Part 6.2 (2005) standard (the guideline for the application of ISO 10360 to coordinate measuring machines with optical distance sensors) proposed a revision to the ISO 10360-2 standard, which is for tests specific to coordinate measuring machines that have been equipped with an optical distance sensor (ODS) including both triangulation based and interferometry based optical sensors that can acquire a single coordinate, a set of coordinates on a line, and a complete area composed of 3D coordinates [7].

Recommendations made in the VDI/VDE 2617 standard are closely followed by the VDI/VDE 2634 Part 1-3 standard. But the VDI/VDE 2634 standard is more specific on the type of CMM which includes mobile measurement systems. Part 2 and Part 3 are most valuable to manufacturers and users of optical 3D imaging systems since these two parts of the guidelines verify system compliance with the required performance specifications. The verification of system compliance is done through acceptance tests performed by the manufacturers and reverification tests performed by the users. This ensures the traceability of measurements in these systems is achieved. Part 2 is concerned with single view optical systems based on area scanning and Part 3 addresses multiple view systems [7].

Area scanning is based on triangulation methods which also include fringe projection, moiré techniques and photogrammetry or scanning systems with area-based measuring capabilities. More details are available in the VDI/VDE documentary standards. For all types of measurement systems, testing is done in normal modes of operation and conditions [7]. Operating mode refers to the configuration options of the system and conditions of operation, i.e. external influences on the system.

ISO 14253-1 [80] must be utilized for the valuation of conformity and non-conformity of measurements with specifications and ISO 23165 gives the instructions for the estimation of testing uncertainty [81]. The VDI/VDE 2634 guideline describes a method of measuring the reference artefact that is used to define a spatial length or simple forms (sphere or plane) to high accuracy.

Currently, the VDI/VDE 2634 standard and the ISO 10360 standard are used in the CMM industry. But the VDI/VDE 2634 standard seems to be the most developed standard for ensuring that measurements from non-contact 3D scanners are traceable and it also caters to optical CMMs which are not included in the ISO 10360 standard. The ISO 10360 standard is mostly used in discrete point systems as shown in Figure 43. Whereas, the VDI/VDE 2634 standard can be used for both discrete and scanning systems but mostly used for scanning systems.

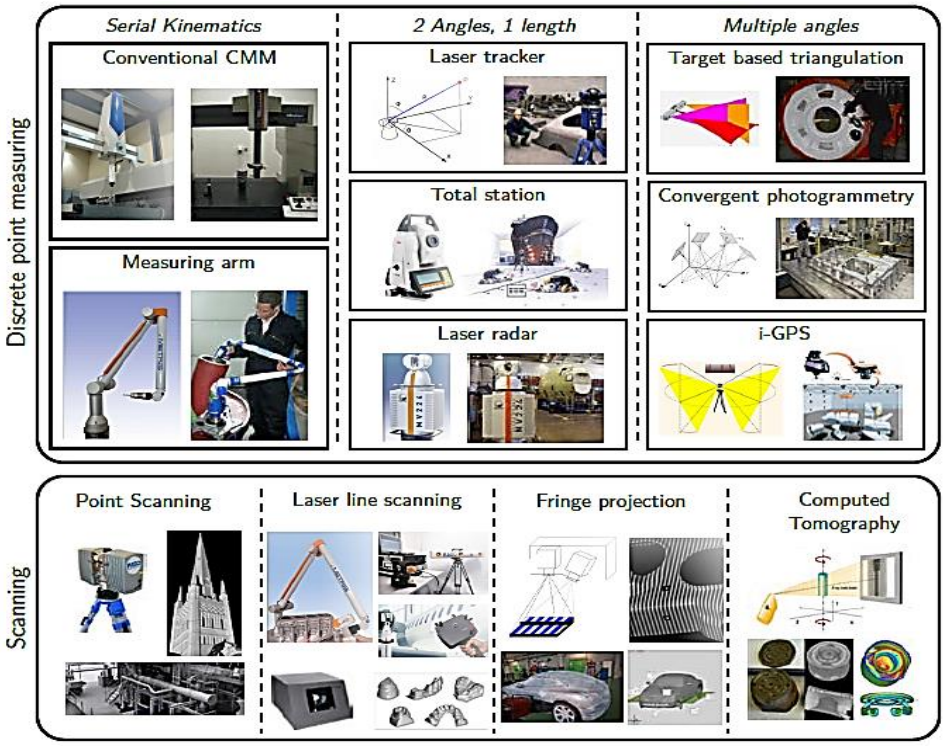

Figure 43: Classification of common coordinate measuring systems [42]

Part 1 of the VDI/VDE 2634 standard describes the practical acceptance and reverification methods for the evaluation of the accuracy of a non-contact 3D measuring system with point by point probing. The definition of the length measurement error parameter in this standard is similar to ISO 10360-2 and the probing error is considered in the determination of the length measurement error. Methods and artefacts for the testing of non-contact 3D measuring systems are described in this part of the VDI standard. The methods are equally suited for the acceptance of 3D measuring systems and the reverification of a non-contact 3D measuring systems.

Whereas Part 2 of the standard was developed in strict accordance with the requirements and recommendations of the guideline VDI 1000 which describe systems for surface probing. Additionally, the flatness measurement error is defined using rectangular parallelepiped artefacts and a sphere artefact for sphere spacing error.

Lastly, Part 3 of the standard gives practical acceptance tests and reverification procedures to assess the accuracy of imaging non-contact 3D measuring systems (optical CMMs) providing area-based sampling. Part 3 applies to the measurement of 3D objects using multiple images.

Due to the complexity of the verification of non-contact measurement systems, guides such as the VDI/VDE 2634 series [20] describe methods to demonstrate their capability using test artefacts with features such as spheres, ball-bars and planes. However, the VDI/VDE guide does not extend to fully address performance verification when freeform surfaces (complex and natural shapes) are to be measured using optical CMMs [20]. This will be further discussed later in this report.

To verify most parts of the measurement volume, the verification artefact needs to be measured in numerous positions within the measuring volume. The VDI/VDE 2634 standard states that at least three arbitrary positions need to be chosen for the measurements, but it is recommended to use five to seven positions. For multiple view scanning systems, the total number of scans resulting from at least five different sensor positions for at least three artefact positions is a minimum. Therefore, the number of measurements required can dramatically increase in number from typically 15 to as many as 40 datasets. Thus, this type of verification approach can be extremely time consuming and can result in high cost. Despite being the most developed standard, the VDI/VDE 2634 series still needs to be improved since the standard does not cover performance verification of freeform surface measuring systems and the standard does not set a limit to the number of points scanned on the artefact [70], i.e. it does not take into consideration the nature of the point cloud [82].

In 2013 ISO/TC 213 published a documentary standard ISO 10360-8 describing acceptance and reverification tests for CMMs with optical distance sensors [83]. The optical distance sensors (ODS) include both single point measuring sensors and area measuring sensors, e.g. laser point scanners and laser line scanners. Co-axial measurements with interferometry and confocal based systems are also covered. Unlike off axes measurement systems like triangulation-based systems, co-axial measurement systems provide 3D data along a single axis. One technical objective that is covered in this part of the ISO 10360 is the testing of errors of the optical distance sensor in the sensor local volume of measurement. These tests should ensure direct traceability to the unit length when the CMM is used in similar length measurement situations. The ISO 10360-8 specifies that the performance requirements can be assigned by the manufacturer or the user of the CMM.

Then it further specifies the manner of execution of the acceptance and reverification tests to demonstrate the stated requirements, rules for verifying conformance and applications for which the acceptance and reverification tests can be used. The acceptance test looks at the performance of a CMM with optical distance sensors and those equipped with area measuring sensors. Data rejection and repeated measurements are well explained in the document. Reverification tests and interim checks need to be part of a user's quality assurance system [7].

The ISO 10360 standard does not explicitly apply to optical systems [84]. However, ISO 10360-2 may be applied by mutual agreement on such systems and the standard series has been improved and it is still being improved to also cater to optical CMMs.

Whereas on the other hand the VDI/VDE 2634 is mostly used in optical systems. There are similarities between ISO 10360 and VDI/VDE 2634 testing methodologies, but there are some important changes in the way the tests are implemented. There are several other standards and documentation not mentioned here pertaining to 3D imaging. Figure 3 in Chapter 1 shows the standards that are applicable to all the different types of CMMs. The figure also shows the artefact dimensions that are traceable when using each standard.

A.3. Mid to Long Range

There are two different approaches to the acceptance and reverification of optical 3D imaging systems performance characteristics for the mid to long range category. One approach originates from the surveying world and is based on field testing. The other approach results from efforts to validate systems for industrial and construction applications in a more controlled environment using reference instruments to ensure measurement traceability. In any case, these standards describe methods to evaluate the performance of a single detector laser-based scanning system based on the principle of time of flight. These systems mostly perform hemispherical scanning [7]. The technical committee 172 of the International Standardisation Organisation (ISO) concerned with geodetic and surveying instruments has successfully developed ISO 17123-9 on terrestrial laser scanners and ISO 16331-2 also on terrestrial laser scanners [85].

In 2006, the American Society for Testing and Materials (ASTM) Committee E57 was established to develop standards for the performance of 3D imaging systems under the mid to long range [86]. The following standards have been published by the committee:

- In 2014, they published the E2919-14 standard focusing on standard test methods for evaluating the performance of systems that measure static six degrees of freedom.
- In 2015, they published the E2938-15 standard focusing on standard test methods for evaluating the relative range measurement performance of 3D imaging systems in the medium range.
- In 2016, they developed the E3064-16 standard focusing on standard test methods for evaluating the performance of optical tracking systems that measure six degrees of freedom.
- In 2017, E3124-17 standards focusing on standard test methods for measuring system latency performance of optical tracking systems that measure six degrees of freedom
- In 2017, E3125-17 standards focusing on standard test methods for evaluating the point to point distance measurement performance of spherical coordinate 3D imaging systems in the medium range.

These standards are specifically for the test methods for evaluating the performance of 3D imaging systems with each standard focusing on a different 3D imaging system. The ASTM E57 committee has been very active in preparing and promoting documentary standards [87]. The ASTM E57 committee has currently no activity in the other ranges of CMMs [7].

The reason for having a different standard for each class of 3D measuring systems is that the committee realized that error sources relevant for one class of 3D imaging systems may not apply to another class of 3D imaging systems [29]. This leads to different working teams within the committee thus the different standards.

Appendix B: Survey Questions

The following are the survey questions that were used in the online platform to achieve the purpose of the survey described in Section 2.6.

1. What type of Coordinate measuring machine(s) do you manufacture or distribute?
2. How many of each of the CMMs do you manufacture per year?
3. How many of each CMM type did you sell in the past 10 years to South African companies/individuals?
4. What is the accuracy of your manufactured machines (please indicate accuracy and machine/s)?
5. If you also do work on CMMs, what type of work is it?
6. If you also do work on CMMs, what accuracy do you require from your system?
7. If you also do work on CMMs, what is the typical size (major dimension) of the components you measure?
8. How often does the CMMs you distribute have to be calibrated (for each type of CMM you use)?
9. Do you provide an accredited calibration service? If so, which standard are you using?
10. What other challenges do you have with regards to using the CMM?
11. Do you think the traceability of measurements is important when using a CMM?

Appendix C: Developed Programs

C.1. Flow Diagram of Taking Measurements from the Stereovision System

The flow diagram below in Figure 44 illustrates the steps of the programme that takes measurements from the stereovision system. These steps are described in Section 4.2.1.

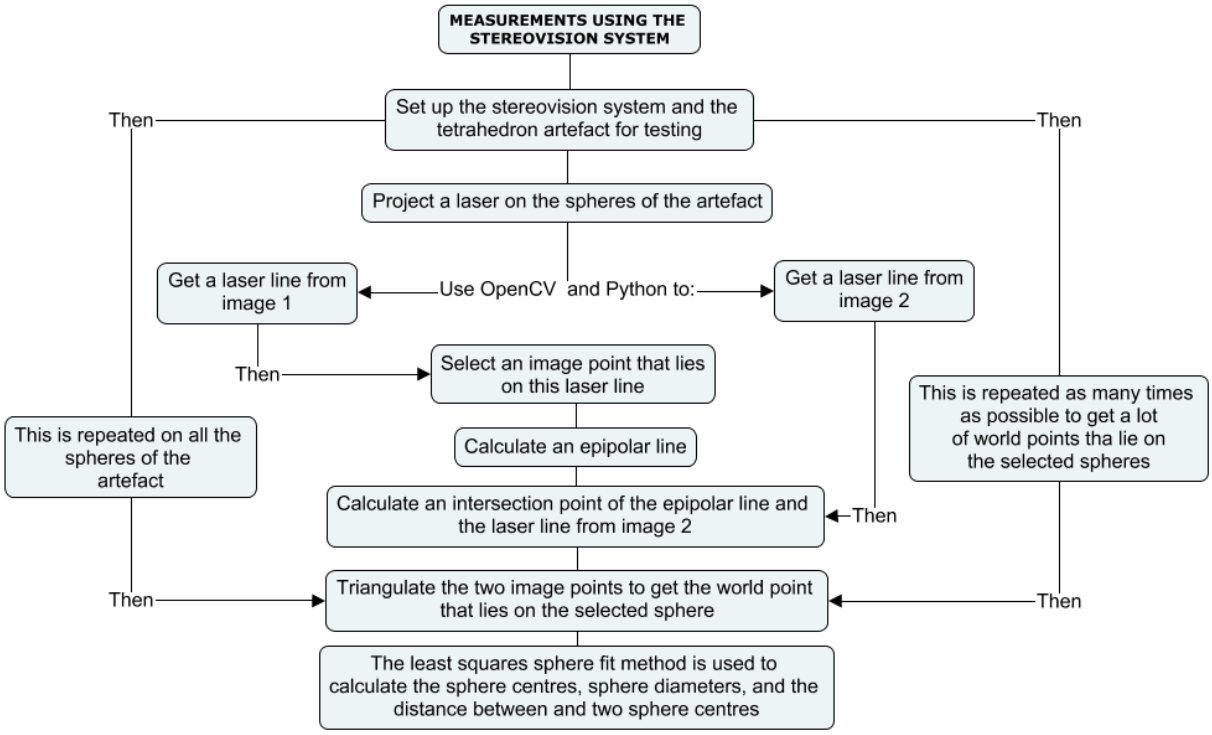

Figure 44: Flow diagram of taking measurements from the stereovision system

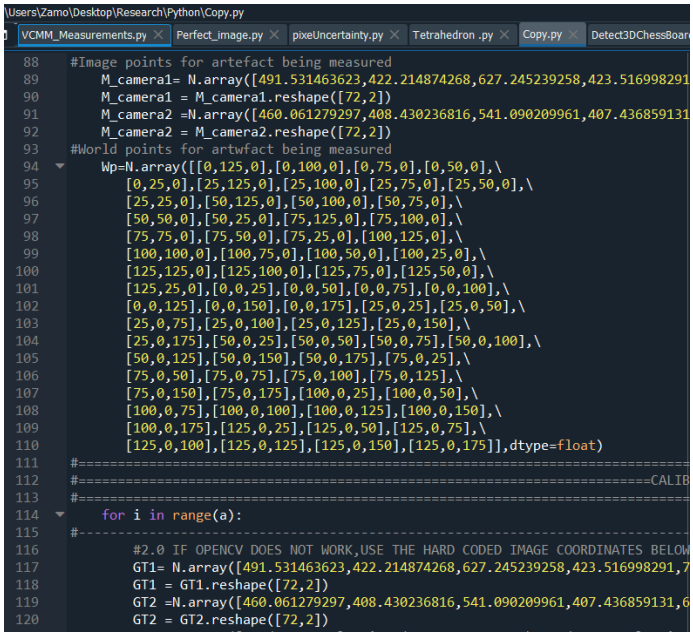

Figure 45: Section of the Python code for taking measurements from the stereovision system

C.2. Flow Diagram of the VCMM Calibration Programme

The flow diagram below in Figure 46 illustrates the steps of the VCMM calibration programme

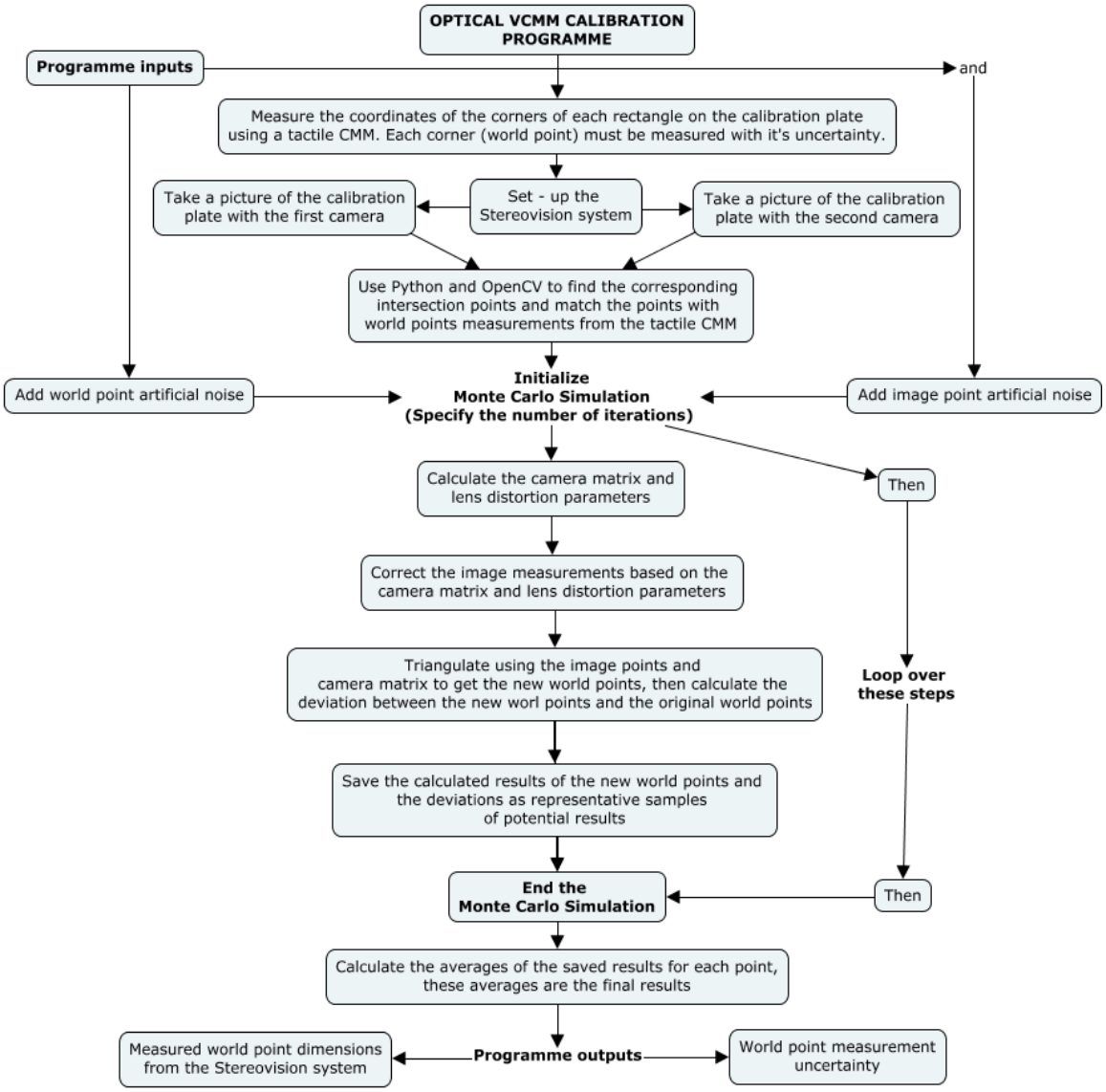

Figure 46:Flow diagram of the VCMM calibration programme

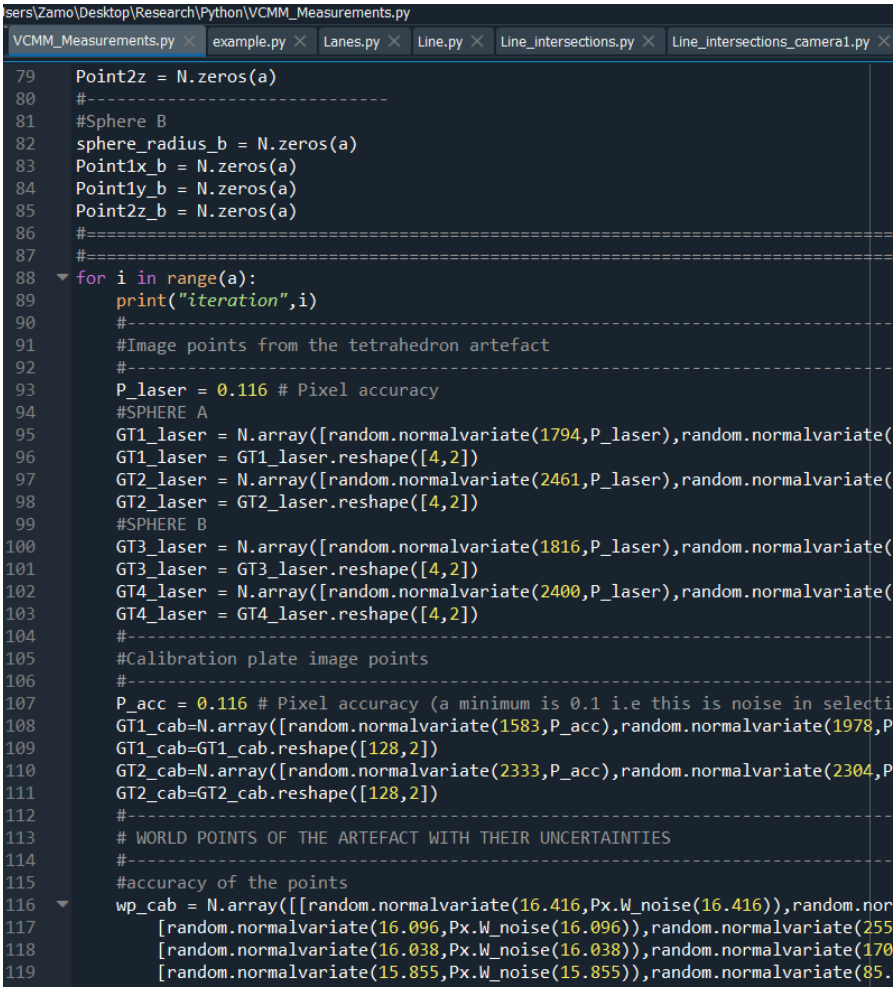

Figure 47:Section of the Python code of the VCMM calibration programme

Appendix D: Cropped Image Sections

The image in Figure 29 was viewed using Python and OpenCV, the following Figure 48 shows the cropped images of each section. Cropping of the images was done using Microsoft Word and it was ensured that the picture sizes are equal.

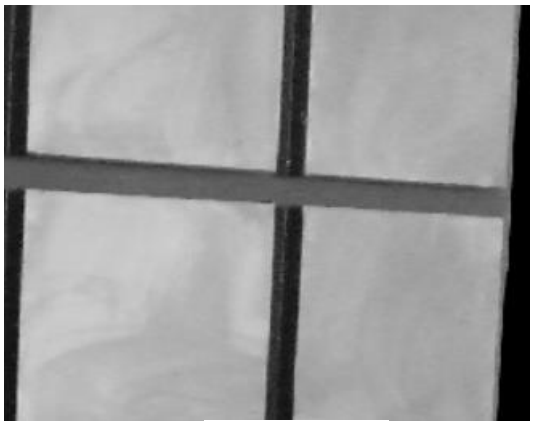

Section A

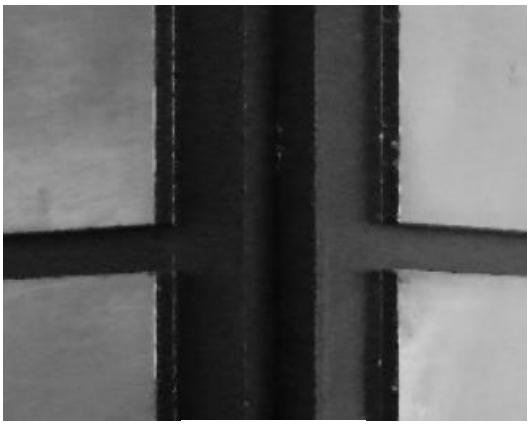

Section B

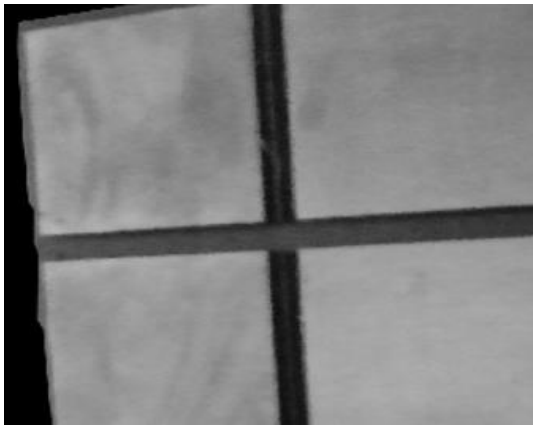

Section C

Section D

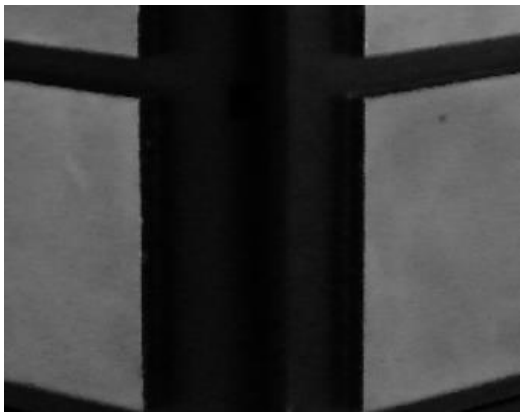

Section E

Section F

Figure 48: Cropped images of the different sections

References

[1] NMISA, National Metrology Institute Of South Africa Mission and Vision, [Online]. Available: http://www.nmisa.org/the-nmisa/Pages/VisionMission.aspx. [Accessed 14 February 2018].

[2] ISO/IEC(99): International Vocabulary of Metrology - *Basic and General Concepts and Associated terms,* 2007.

[3] V. Mousavi, M. Khosravi, M. Ahmadi, N. Noori, S. Haghshenas, A. Hosseininaveh and M. Varshosaz, *The performance evaluation of a multi image 3D reconstruction software with different sensors,* Measurements, vol. 9, no. 120, pp. 1-10, May 2018.

[4] P. Cauchick-Miguel, T. King and J. Davis, *CMM Verification: a survey,* Measurement, vol. 17, no. 1, pp. 1-16, January 1996.

[5] NMISA, *NMISA Traceability chart*, NMISA Length Department, Pretoria, South Africa, July 2018.

[6] H. Schwenke , M. Franke, J. Hannaford and H. Nkunzmann, *Error mapping of CMMs and machine tools by a single tracking interferometer,* CIRP Annals, vol. 54, no. 1, pp. 475-478, 2005.

[7] J.A. Beraldin, D. Mackinnon and L. Cournoyer, *Progress report on standards development*, 17th International Congress of Metrology(13003) on Metrological characterization of 3D imaging systems, National Research Council of Canada(Ottawa), EDP Sciences, 2015.

[8] Z. Luthuli, K. Schreve and O.A. Kruger, *Traceability challenges for optical length metrology*, Stellenbosch, Stellenbosch University Department of Mechanical and Mechatronic Engineering, South Africa, 2018.

[9] M. Trenk, M. Franke and Dr H. Schwenke, *The "Virtual CMM" a software tool for uncertainty evaluation - practical application in an accredidited calibration lab*, 38116 Braunschweig Germany, Physikalisch - Technische Bundesanstalt , Department of Coordinate Metrology, 2012.

[10] NSAI, National Standards Authority of Ireland, [Online]. Available: https://www.nsai.ie/Location.aspx. [Accessed 05 April 2018].

[11] J.A. Bosch, *Coordinate Measuring Machines and Systems*, Introduction to Metrology, New York, Marcel Dekker Inc., 1995, pp. 1-5.

[12] OASIS. [Online]. Available: http://www.oasisalignment.com/blog/what-is-metrology-anyway/. [Accessed 12 April 2018].

[13] R.J. Hocken and P.H. Pereira, *Coordinate Measuring Machines and Systems*, Engineering and Technology , Boca Raton, CRC Press, 2011, pp. 60-80.

[14] Gaugehow, [Online]. Available: https://gaugehow.com/2019/05/19/what-is-cmm-and-types-of-coordinate-measuring-machine/. [Accessed 19 10 2020].

[15] R.J. Hocken and P.H. Pereira, *Coordinate Measuring Machines and Systems*, Manufacturing Engineering and Material Processing, Boca Raton, CRC Press, 2011, pp. 50-52.

[16] BIPM, Bureau International des Poids et Measures, [Online]. Available: https://kcdb.bipm.org/appendixc/. [Accessed Friday October 2019].

[17] Willrich precision instruments, [Online]. Available: https://willrich.com/product/renishaw-revo-vision-probe-rvp/. [Accessed Friday October 2019].

[18] ISO 10360-4: Geometrical Product Specifications(GPS), *Acceptance and reverification tests for coordinate measuring machines(CMM) used in scanning measuring mode,* 2000.

[19] L.Z. JI, *Design of Optical Triangulation Devices,* Optics and Laser Technology, vol. 21, no. 5, pp. 335-338, 1989.

[20] VDE/VDI 2634 -1: German standard - Optical 3D measuring systems, *Imaging systems with point by point probing,* 2002.

[21] J.F. Larue, M. Viala, D. Brown and C. Mony, *Dynamic Referencing in 3D Optical Metrology for Higher Accuracy in Shop Floor Conditions*, Creaform, France, 2016.

[22] Creaform, Portable 3D Measurement solutions, [Online]. Available: https://www.creaform3d.com/en/metrology-solutions/c-link-functionality. [Accessed 29 July 2019].

[23] Melexis, Application note : Time of flight(AUH), [Online]. Available: http://www.wpgkorea.com/report/REPORT_4835_7.pdf. [Accessed 13 Sepetember 2018].

[24] Renishaw. [Online]. Available: http://www.renishaw.com/en/interferometry-explained--7854. [Accessed 7 September 2018].

[25] K. Creath and J.C. Wyant, *Moire and Fringe projection techniques*, Optical Shop Testing Second Edition, New York, John Wiley & Sons Inc, 1992, pp. 653-683.

[26] ISO 9001: Quality Management System Requirements, 2008.

[27] ISO/IEC 17025: General requirements for the competence of testing and calibration laboratories, 2005.

[28] ISO 14253-1: Geometrical Product Specifications(GPS), Inspection by measurement of workpiece and measuring equipment, *Decision rules for proving conformance or non-conformance with specifications,* 1998.

[29] B. Muralikrishnan, P. Rachakonda, M. Shilling, V. Lee, C. Blackburn, D. Sawyer, G. Cheok and L. Cournoyer, ASTM E57.02 : Instrument Runoff at NIST, *Part 1 : Background Information and Key Findings*, U.S. Department of Commerce, May 2016.

[30] K. Busch, H. Kunzmann and F. Waldele, *Calibration of coordinate measuring machines,* Precision Engineering, vol. 7, no. 3, pp. 139-144, July 1985.

[31] N. Pears, Y. Lui and P. Buntin(Ed), *3D imaging analysis and application*, Verlag London, Springer, 2012.

[32] P. Muller, *Coordinate Metrology by Traceable Computed Tomography*, Denmark, Technical University of Denmark, 2012, pp. 24-25.

[33] ISO/IEC - Part 3: Guide to the expression of uncertainty in measurements, 1995.

[34] M.J. Baldwin, D.K. Summerhays, A.D. Campbell and P.R. Henke, *Application of Simulation Software to Coordinate Measurement Uncertainty Evaluations*, Volcano, Metrosage, January 2004, pp. 40-52.

[35] Bureau International des Poids et Measures(BIPM), The internation System of Units(SI), [Online]. Available: https://www.bipm.org/en/about-us/. [Accessed 29 June 2019].

[36] B. Acko, M. McCarthy, F. Haertig and B. Buchmeister, *Standards for testing freeform measurement capability of optical and tactile coordinate measuring machines,* Measuring Science and Technology, vol. 23, no. 9, pp. 3-6, 25 July 2012.

[37] E. Trapet, E. Savior and L.D. Chiffre, *New advances in traceability of CMMs for almost the entire range of industrial dimensional metrology needs,* CIRP Annals, vol. 53, no. 1, pp. 433-438, 2004.

[38] O.A. Kruger, *Personal communication on the number of CMMs recorded by NMISA that are in the South African Industry,* Stellenbosch, 2018.

[39] JIS B 7440: Japanese Industrial Standard, *Test Code for Accuracy of Coordinate Measuring Machines*, Tokyo, Japanise Standards Association, 1987.

[40] F.Z. Fang, X.D. Zhang, A. Weckenmann, G.X. Zhang and C. Evans, *Manufacturing and measurement of freeform optics,* CIRP Annals - Manufacturing Technology, vol. 62, no. 2, pp. 823-846, 2013.

[41] D.F. Elkott, H.A. Elmaraghy and W.H. Elmaraghy, *Automatic sampling for CMM inspection planning of freeform surfaces,* International Journal of Production Research, vol. 40, no. 11, pp. 2653-2676, 2002.

[42] N.V. Gestel, *Determining measuremet uncertainties of feature measurements on 1 cmm,* pp. 5-6, Katholieke Universiteit Leuven - Faculteit Ingenieurswetenschappen, September 2011.

[43] J. Sladek and A. Gaska, *Evaluation of coordinate measurement uncertainty with use of virtual machine model based on Monte Carlo Method,* Measurement, vol. 45, no. 6, pp. 1564-1575, July 2012.

[44] ISO/TS 15530 - 3: Geometrical Product Specifications(GPS) - Coordinate measuring machines(CMM), *Technique for determining the uncertainty of Measurement - Use of calibrated workpieces or standards,* 2004.

[45] J. Sladek, A. Gaska, M. Olszewska, R. Kupiec and M. Krawczyk, *Virtual Coordinate Measuring Machine Built Using Lasertracer System and Spherical Standard,* Metrology and Measurement Systems, vol. XX, no. 1, pp. 77-86, 2013.

[46] J.A Beraldin, *Basic theory on surface measurement uncertainty of 3D imaging systems*, SPIE Digital Library, California, Institute for Information Technology, 19 January 2009.

[47] ISO 15530 - 4: Geometric Product Specifications - Coordinate measuring machines(CMM), *Technique for determining the uncertainty of measurement-Evaluating task specific measurement uncertainty using simulation,* 2008.

[48] VDI/VDE 2617 - 6 - 1: Accuracy of coordinate measuring machines - Characteristics and their testing, *Coordinate measuring machines with optical probing - Code of practice for the application of DIN EN ISO 10360 to coordinate measuring machines with optical sensors for lateral,* 2007.

[49] K. Ostrowska, A. Gaska, R. Kupiec, K. Gromczak, P. Wojakowski and J. Sladek, *Comparison of accuracy of virtual articulated coordinate measuring machine based on different metrological models,* Measurement, vol. 133, pp. 262-270, February 2019.

[50] NIST uncertainty machine, National Institute of Standards and Technology, [Online]. Available: https://uncertainty.nist.gov/. [Accessed Saturday, October 2019].

[51] R. Hartley and A. Zisserman, *Multiple View Geometry in Computer Vision,* Cambridge, Cambridge University Press, 2003.

[52] J.I. Gonzalez, J.C. Gamez, C.G. Artal and A.M.N. Cabrera, *Stability study of camera calibration methods*, Granada Espana, VI Workshop en Agentes Fisicos, 2005.

[53] K. Irie, I.M. Woodhead, A.E. McKinnon and K. Unsworth, *Measured Effects of Temperature on Illumination Independent Camera Noise*, 24th International Conference Image and Vision Computing, New Zealand, Lincon University, Department of Applied Computing, 2009.

[54] J. Nakurama, *Image Sensors and Signal Processing for Digital Still Cameras*, CRC Press, New York, United States of America, 2006.

[55] M.D. Santo, C. Liguori and A. Pietrosanto, *Uncertainty Characterization in Image Based Measurements: A preliminary Discussion,* IEEE Transactions on Instrumentation and Measurement, vol. 49, no. 5, pp. 1101-1107, October 2000.

[56] HP Official site, [Online]. Available: https://www8.hp.com/us/en/campaign/3Dscanner/overview.html. [Accessed 12 August 2019].

[57] B. Acko, *Uncertainty of measurements in Optical CMM technology*, Email correspondences regarding the SOP - 36 procedure, 2019.

[58] The Engineering ToolBox, [Online]. Available: https://www.engineeringtoolbox.com/docs/documents/816/psychrometric_chart_29inHg.pdf. [Accessed 28 July 2019].

[59] M. Jekel, Least Squares Sphere Fit, [Online]. Available: https://jekel.me/2015/Least-Squares-Sphere-Fit/. [Accessed 20 October 2018].

[60] K. Schreve, *pyMultiCam User Guide*, Department of Mechanical Engineering, Stellenbosch University, South Africa, 3 October 2012.

[61] B. Henning and K. Schreve, *Laser Based Stereovision Measurement of Aspherical Mirrors*, Stellenbosch University, Department of Mechanical and Mechatronic Engineering, South Africa, 2012.

[62] K. Schreve, *Edge Scanning and Swept Surface Approximation in Reverse Engineering*, University of Stellenbosch, Department of Mechanical Engineering, South Africa, 2001.

[63] R. Hartley and A. Zisserman, *Estimation - 2D Projective Transformation*, Multiple View Geometry in Computer Vision Second Edition, Cambridge, Cambridge university press, 2003, pp. 88-92.

[64] R. Hartley and A. Zisserman, *Computation of the Camera Matrix*, Multiple View Geometry in Computer Vision Second Edition, Cambridge, Cambridge University Press, 2003, p. 182.

[65] S. Huybrechts and S.W. Tsai, *Analysis and behaviour of grid structures,* Computer science and Technology, vol. 56, no. 9, pp. 1001-1015, 1996.

[66] K. Takita, T. Aoki, Y. Sasaki, T. Higuchi and K. Kobayashi, *High Accuracy Subpixel Image Registration Based on Phase only correction,* IEICE Transactions on fundamentals of electronics, communications, and computer science, Vols. E86-A, no. 8, pp. 1925-1934, 2003.

[67] A. Robinson, *Crime Scene Photography*, Focus, Depth of field and Lenses, Washington, The George Washington University, August 2016, p. 206.

[68] T. Scheuermann, *Advanced Depth of Field*, ATI Research, 3D Application Research Group, 2004.

[69] BIPM, [Online]. Available: https://www.bipm.org/utils/common/documents/jcgm/JCGM_100_2008_E.pdf. [Accessed 26 February 2020].

[70] K. Schreve, *Error Distribution of a 3D Vision Based Measurement System*, Department of Mechanical Engineering, Stellenbosch University, South Africa, pp. 1-12, 2010.

[71] K. Schreve, *How accurate can a stereovision measurement be?*, Stellenbosch University, Department of Mechanical Engineering, South Africa, 2012.

[72] J. Lancaster, *A review of the influence of environmental humidity and water on friction, lubrication and water,* Tribology International, vol. 23, no. 6, pp. 371-389, 1990.

[73] J. Goransson and A. Karlsson, Practical Post Process Depth of Field, [Online]. Available: http://www.cse.chalmers.se/edu/year/2011/course/TDA361/Advanced%20Computer%20Graphics/Practical_Post-Process_Depth_Of_Field.pdf. [Accessed 05 April 2020].

[74] Y. Shang, *A central limit theorem for randomly indexed m-dependent random variables,* Filomat, vol. 26, no. 4, pp. 713-717, 2012.

[75] Chemistry Libretext, [Online]. Available: https://chem.libretexts.org/Bookshelves/Analytical_Chemistry/Supplemental_Modules_(Analytical_Chemistry)/Quantifying_Nature/Significant_Digits/Propagation_of_Error. [Accessed 08 April 2020].

[76] Research gate, [Online]. Available: https://www.researchgate.net/figure/Physical-mesh-and-control-points-for-a-cubic-NURBS-surface_fig2_265853615. [Accessed 08 04 2020].

[77] ASME B46.1: Standard by ASME International - *Surface texture , Surface Roughness , Waviness and Lay,* 2009.

[78] C.L. Giusca and R.K. Leach, *Calibration of the metrological characteristics of imaging confocal microscopes (ICMs)*, Measurement Good Practice Guide No.128 National Physical Laboratory, United Kingdom(Teddington), National physical Laboratory Engineering and Measurement Division, 2012, pp. 1-13.

[79] J. Hiller, S. Kasperl, T. Schon, S. Schropfer and D. Weiss, *Comparison of probing error in dimensional measurements by means of 3D computed tomography with circular and helical sampling*, Second International Symposium on NDT in Aerospace, Germany, Oberkochen, 2010.

[80] ISO 14253-1: Geometric Product Specification (GPS), *Inspection by measurement of workpieces and measuring equipments - Decision rules for proving conformity or non conformity with specifications,* 1998.

[81] ISO 23165: Geometric Product Specification (GPS), *Guideline for the evaluation of coordinate measuring machine(CMM) test uncertainty,* 2006.

[82] F. Remondino, *Videometrics, Range Imaging, Range Applications XII and Automated Visual Inspection*, Proceedings of a meeting held At SPIE Optical Metrology, Munich Germany, 16-17 May 2013.

[83] ISO 10360-8: Acceptance and reverification tests for coordinate measuring machines(CMM) with optical distance sensors, 2013.

[84] D. Flack, CMM Verification Good Practice Guide No.42, National Physical Laboratory, [Online]. Available: https://www.npl.co.uk/special-pages/guides/gpg42_cmmv. [Accessed Friday October 2019].

[85] R. Gottwald, *Field Procedures for Testing Terrestrial Laser Scanners(TLS), A Contribution to the Future ISO Standard*, TS 2D - Calibration of Instruments, Switzerland, January 2008.

[86] G.S. Cheok, A.M. Lytle and K.S. Saidi, ASTM E57 3D Imaging Systems Committee, SPIE, [Online]. Available: https://www.spiedigitallibrary.org/conference-proceedings-of-spie/6950/69500J/ASTM-E57-3D-imaging-systems-committee-an-update/10.1117/12.791929.short?SSO=1. [Accessed 05 September 2018].

[87] ASTM(E57 E2544 - 11a): Standard Terminology for 3D Imaging Systems - *Commitee E57 on 3D Imaging Systems* , ASTM International, 2017.